ELSEVIER

Physica D 148 (2001) 49–96

PHYSICA D

www.elsevier.com/locate/physd

Bifurcation to fully nonlinear synchronized structures in slowly varying media

Benoît Pier*, Patrick Huerre, Jean-Marc Chomaz

Laboratoire d'Hydrodynamique (LadHyX), CNRS–École polytechnique, F-91128 Palaiseau Cedex, France

Received 9 December 1999; received in revised form 5 July 2000; accepted 17 July 2000
Communicated by S. Fauve

Abstract

The selection of fully nonlinear extended oscillating states is analyzed in the context of one-dimensional nonlinear evolution equations with slowly spatially varying coefficients on a doubly infinite domain. Two types of synchronized structures referred to as *steep* and *soft* global modes are shown to exist. Steep global modes are characterized by the presence of a sharp stationary front at a marginally absolutely unstable station and their frequency is determined by the corresponding linear absolute frequency, as in Dee–Langer propagating fronts. Soft global modes exhibit slowly varying amplitude and wave number over the entire domain and their frequency is determined by the application of a saddle point condition to the local nonlinear dispersion relation. The two selection criteria are compared and shown to be mutually exclusive. The onset of global instability first gives rise to a steep global mode via a saddle-node bifurcation as soon as local linear absolute instability is reached somewhere in the medium. As a result, such self-sustained structures may be observed while the medium is still globally stable in a strictly linear approximation. Soft global modes only occur further above global onset and for sufficiently weak advection. The entire bifurcation scenario and state diagram are described in terms of three characteristic control parameters. The complete spatial structure of nonlinear global modes is analytically obtained in the framework of WKBJ approximations. © 2001 Elsevier Science B.V. All rights reserved.

PACS: 47.20.Ft; 47.20.Ky; 47.54.+r; 03.40.Kf

Keywords: Hydrodynamic stability; Frequency selection; Nonlinear global modes

1. Introduction

It is now well established that spatially developing open shear flows may be divided into two classes: some flows are very sensitive to inflow conditions and essentially behave as *noise amplifiers*, others display intrinsic dynamics and may be interpreted as *global oscillators* [20–22]. The present paper is concerned with the latter class of systems and examines in detail the synchronized self-sustained structures which they can support. In previous studies, we have demonstrated the existence of nonlinear *soft global modes* [33] and *steep global modes* [34]. The objective of the present investigation is to analyze the bifurcation scenarios which lead from the basic state to either of these

* Corresponding author. Present address: Department of Applied Mathematics and Theoretical Physics, University of Cambridge, Silver Street, Cambridge CB3 9EW, UK.

0167-2789/01/$ – see front matter © 2001 Elsevier Science B.V. All rights reserved.
PII: S0167-2789(00)00146-9

fully nonlinear structures as the global control parameters are varied. The analysis is carried out in the context of one-dimensional evolution models with spatially varying coefficients in order to account for the streamwise development of the basic state.

A variety of physical systems give rise to intrinsic self-sustained oscillations: mixing layers with strong enough counterflow [46], low-density jets [29,44], cylinder wakes [27,38,45], wakes behind blunt-edged plates [18,19], thin aerofoil wakes [49], Taylor–Couette flow between concentric spheres [43], Taylor–Couette flow between circular cylinders with throughflow [5], Rayleigh–Bénard convection with throughflow [31], baroclinically unstable atmospheric flows [17,37], sunspot cycles [1,28], etc. Many of these flows display a spatially varying basic state, and hence a spatial dependence of the local instability characteristics. The goal of a global analysis is to obtain in a self-consistent manner a spatially extended structure made up of wave trains governed by the local properties of the medium and tuned at an overall global frequency ω_{g}. The unknown global frequency ω_{g} is to be derived from a nonlinear eigenvalue problem consisting of the evolution equation and associated boundary conditions. The associated eigenfunction yields the spatial structure of the corresponding self-sustained oscillations. The resolution of the eigenvalue problem is typically undertaken under the hypothesis of slow spatial variations whereby the underlying basic state evolves slowly over a typical instability length scale. In this framework, the main objective of the global mode analysis is to derive *global* frequency selection criteria from the *local* dispersion relation prevailing at each streamwise station.

Linear global mode analyses are now fairly complete. Chomaz et al. [7] demonstrated that the complex global frequency is determined by a saddle point (equivalently a double turning point) condition applied to the local linear dispersion relation for the linear complex Ginzburg–Landau equation with spatially varying coefficients. This criterion had previously been discovered and implemented by Soward and Jones [43] to describe oscillating states in Taylor–Couette flow between concentric spheres. According to Monkewitz et al. [30], the same criterion also holds for the Navier–Stokes equations linearized about an arbitrary slowly varying basic flow. More recently, Le Dizès et al. [25] reexamined the case of the spatially varying linear complex Ginzburg–Landau equation and demonstrated the existence of another family of linear global modes with two simple turning points. The causal nature of these linear global modes has been established for the same model by Hunt and Crighton [23]: the exact linear impulse response does converge, for large time, to the most unstable linear global mode. The validity of the linear saddle point criterion has been fully confirmed in the direct numerical simulations of the Kármán vortex street behind a blunt-edged plate by Hammond and Redekopp [19].

Paradoxically, the weakly nonlinear extension of these concepts is fraught with difficulties, as emphasized by Chomaz et al. [6] and Le Dizès et al. [24]: the Landau constant pertaining to the Hopf bifurcation near global mode onset does not display a well-defined sign as the WKBJ spatial inhomogeneity parameter is decreased. Furthermore, the weakly nonlinear formulation is only valid in an exponentially small vicinity of threshold.

To obviate such weakly nonlinear studies, it appears natural to resort to a fully nonlinear approach where fluctuations are of order unity. Such a line of thought has been consistently pursued since the early 1990s in the framework of nonlinear Ginzburg–Landau type models. The classical absolute/convective instability concepts introduced in a linear context by Bers [3] and Briggs [4] have been generalized to the fully nonlinear regime by Chomaz [8]. The absolute/convective nature of the nonlinear dynamics is then directly related to the propagation direction of the front separating the basic state from the bifurcated state [16,39–41]. The properties of fully nonlinear global modes on a semi-infinite domain governed by Ginzburg–Landau type equations with constant coefficients have been thoroughly studied by Couairon and Chomaz [10,12,13]. In this case, a nonlinear global mode is obtained when an upstream travelling front is halted in its motion by the upstream boundary point. This event occurs whenever the medium is nonlinearly absolutely unstable in the sense of Chomaz [8]. The reader is referred to Chomaz and Couairon [9] and Tobias et al. [47] for a corresponding analysis of the finite interval problem.

Corresponding fully nonlinear analyses have been performed for the complex Ginzburg–Landau equation with *spatially varying coefficients in infinite media*. Two varieties of nonlinear global modes have been identified. Soft global modes, obtained by Pier and Huerre [33], obey a saddle point frequency selection criterion applied to the local nonlinear dispersion relation. This criterion is formally analogous to its linear counterpart. The associated spatial eigenfunction structure displays smoothly varying amplitude and wave number over the entire domain. By contrast, according to the preliminary results reported by Pier et al. [34], steep global modes are governed by a marginal linear instability criterion: the steep global frequency is imposed by the real absolute frequency [3] prevailing at the transition station between local linear convective and absolute instability. This criterion is akin to the linear front velocity selection principle put forward by Dee and Langer [16]: for a wide class of systems, the speed of the front separating the basic state from the bifurcated state is such that in the co-moving frame the medium is marginally linearly absolutely unstable. The steep global spatial structure displays a stationary sharp front at the transition station with a sudden jump in wave number. In all other regions, the amplitude and wave number are slowly varying. Similar steep self-sustained structures have been numerically identified and analytically determined in amplitude evolution models pertaining to solar and stellar magnetic activity cycles by Bassom et al. [1] and Meunier et al. [28]. The properties of nonlinear global modes governed by the real Ginzburg–Landau equation in a semi-infinite domain with combined distributed spatial inhomogeneity have been obtained by Couairon [11] and Couairon and Chomaz [14]. Predicted scaling laws for the amplitude and position of the maximum very favorably compare with experimental and numerical observations of bluff-body wakes.

The purpose of the present study is two-fold: first, we wish to map out the domains of existence of soft or steep global modes in an appropriate control parameter space and to characterize the associated bifurcations. Secondly, we present the detailed asymptotic structure of the various layers and regions which make up their spatial distribution.

Consider a system governed by a one-dimensional nonlinear partial differential equation that is first-order in time of the form

$$\frac{\partial \psi}{\partial t} = \mathcal{F}(\partial_x; X)[\psi], \tag{1}$$

where x and t represent space and time coordinates, respectively, and X a slow space variable to be defined shortly. The basic state is assumed to be $\psi = 0$, and the function $\psi(x, t)$ represents the fluctuations riding on the basic state. In regions of finite amplitude, ψ is governed by the full nonlinear operator $\mathcal{F}$. In small amplitude regions, ψ is a perturbation governed by Eq. (1) linearized around the basic state, i.e.,

$$\frac{\partial \psi}{\partial t} = \mathcal{L}(\partial_x; X)[\psi]. \tag{2}$$

A crucial assumption of the present investigation is the slow spatial development of the medium as exemplified by the introduction of the slow spatial variable X in the operators $\mathcal{F}$ and $\mathcal{L}$. The weak non-uniformity hypothesis is fulfilled if the ratio $\epsilon = \lambda/L$ between the typical instability length scale λ and the inhomogeneity length scale L is small. As a result of this scale separation, the weak variations of the medium instability properties may be described through the slow variable

$$X = \epsilon x \quad \text{with } \epsilon \ll 1. \tag{3}$$

If the slow space variable X is frozen, system (1) becomes a PDE in x and t with constant coefficients which captures the local properties prevailing at that station X. In order to construct a global mode it is necessary to "piece together" local wave trains at different X by explicitly accounting for the weak coupling between local and global properties via relation (3).

The outline of this paper is as follows. The essential concepts necessary to carry out this study are introduced in Sections 2 and 3. Local instability properties where X is frozen are summarized in Section 2. Emphasis is

given to the relationship between causality and the spatial response to a localized harmonic forcing (Section 2.3). In this framework, stationary fronts are shown to naturally arise as the limiting spatial response of the system in the absence of forcing when the medium is marginally absolutely unstable (Section 2.4). Variations of the local instability properties over the entire X-domain are analyzed in Section 3. More specifically, the distribution over X of linear spatial branches (Section 3.2) and nonlinear spatial branches (Section 3.3) is investigated as the global frequency is varied.

Section 4 is concerned with the determination of the leading-order approximation to the global frequency and spatial distribution of fully nonlinear synchronized states governed by (1). It contains the essential results concerning the structure of steep global modes (Section 4.2), the nature of their bifurcation from the basic state (Sections 4.3–4.5), the structure of soft global modes (Section 4.6), and finally the respective domains of existence of steep and soft global modes (Sections 4.7 and 4.8) in control parameter space.

Section 5 is devoted to the complete higher-order asymptotic analysis of the various regions and layers which make up the spatial structure of global modes (cf. Fig. 15). Higher-order corrections to the global frequencies are then obtained. The results are derived in the general context of system (1) by following a methodology analogous to that previously used by Bassom et al. [1] and Pier and Huerre [33].

All the results in principle apply to any nonlinear system governed by an equation of the form (1). However, in order to obtain explicit results and to validate them by direct numerical simulations, we repeatedly use as an illustrative example the complex Ginzburg–Landau (CGL) equation

$$\mathrm{i}\frac{\partial\psi}{\partial t} = \left(\omega_0(X) + \frac{1}{2}\omega_{kk}(X)k_0(X)^2\right)\psi + \mathrm{i}\omega_{kk}(X)k_0(X)\frac{\partial\psi}{\partial x} - \frac{1}{2}\omega_{kk}(X)\frac{\partial^2\psi}{\partial x^2} + \gamma(X)|\psi|^2\psi \tag{4}$$

for a complex function $\psi(x,t)$. For convenience, the CGL equation is written here as derived from the Taylor expansion of the dispersion relation around $k_0(X)$ in the same manner as [20]. The precise meaning of all the quantities appearing in (4) is discussed in detail in Section 2. The complex X-dependent coefficients $\omega_0(X)$ and $k_0(X)$ denote the usual local absolute frequency and wave number, respectively, while $\omega_{kk}(X)$ is the second derivative of the linear dispersion relation with respect to the wave number k. The complex Landau "constant" $\gamma(X)$ is chosen so that nonlinearities are stabilizing everywhere (supercritical bifurcation), i.e., $\gamma_\mathrm{i}(X) \equiv \mathrm{Im}\,\gamma(X) < 0$ for all X. In the entire paper, the field $\psi(x,t)$ is assumed to be advected in the positive x-direction everywhere to mimic the dynamics of open flows. As demonstrated in Section 4.8, this assumption is equivalent to $k_{0,\mathrm{i}}(X) < 0$ for all X. Thus, the increasing and decreasing x-directions will be referred to as "downstream" and "upstream", respectively. The Ginzburg–Landau model (4) has been shown to successfully describe a large range of pattern formation phenomena [15,26,32]. Here this idealized representation of spatially developing flows is invoked as a specific example. Similar conclusions may be shown to hold for real flows governed by the Navier–Stokes equations [35,36].

2. Local instability properties

Under the assumption that the governing equation only depends on space through the slow variable X, local characteristics of the medium are recovered by freezing X in (1) and studying the corresponding strictly uniform medium. In the sequel, "local" always refers to properties of spatially uniform systems obtained by extending the medium at a specific downstream station X towards $x = \pm\infty$. At this local level of analysis, X and x are then considered to be independent: the fast component x is involved in spatial differentiation whereas X plays the part of an independent control parameter. The rigorous asymptotic analysis re-establishing the link between x and X via (3) in terms of WKBJ approximations [2] is postponed to Section 5.

In this section, the properties of infinite spatially uniform media governed by an equation of the form

$$\frac{\partial \psi}{\partial t} = \mathcal{F}(\partial_x)[\psi] \tag{5}$$

are reviewed. The results are applicable to any nonlinear operator $\mathcal{F}(\partial_x) = \mathcal{F}(\partial_x; X_0)$ derived from (1) for some fixed location $X = X_0$. Explicit forms are obtained for the uniform CGL equation

$$\mathrm{i}\frac{\partial \psi}{\partial t} = \left(\omega_0 + \frac{1}{2}\omega_{kk}k_0^2\right)\psi + \mathrm{i}\omega_{kk}k_0\frac{\partial \psi}{\partial x} - \frac{1}{2}\omega_{kk}\frac{\partial^2 \psi}{\partial x^2} + \gamma|\psi|^2\psi. \tag{6}$$

The linear properties dictating the dynamics of small amplitude perturbations are routinely obtained. The main assumption used throughout the study is that (5) admits a continuous family of nonlinear travelling waves. This is guaranteed as long as the nonlinearities are supercritically stabilizing, as demonstrated below.

Small amplitude perturbations are governed by the counterpart of (5) linearized around $\psi = 0$,

$$\frac{\partial \psi}{\partial t} = \mathcal{L}(\partial_x)[\psi]. \tag{7}$$

Any perturbation is a superposition of elementary waves $\mathrm{e}^{\mathrm{i}(kx-\omega t)}$ where the complex wave number k and frequency ω satisfy the linear dispersion relation

$$\omega = \Omega^{\mathrm{l}}(k) \equiv \mathrm{i}\mathcal{L}(\mathrm{i}k). \tag{8}$$

For Eq. (6), it takes the simple form

$$\omega = \omega_0 + \tfrac{1}{2}\omega_{kk}(k - k_0)^2, \tag{9}$$

where it is assumed that $\omega_{kk,\mathrm{i}} \equiv \mathrm{Im}\,\omega_{kk} < 0$ in order to enforce causality (see Section 2.3).

Dispersion relation (8) governs all linear properties of the system. Three situations are of particular interest: the temporal evolution problem, the impulse response, and the spatial response problem.

2.1. Temporal evolution and nonlinear dispersion relation

A spatially harmonic perturbation $\psi(x, t = 0) = A\,\mathrm{e}^{\mathrm{i}kx} + \text{c.c.}$ of real wave number k and small amplitude $A \ll 1$ initially evolves according to the linear dispersion relation (8). Its linear temporal growth rate is $\Omega^{\mathrm{l}}_{\mathrm{i}}(k) \equiv \mathrm{Im}\,\Omega^{\mathrm{l}}(k)$. Two typical variations of $\Omega^{\mathrm{l}}_{\mathrm{r}}$ and $\Omega^{\mathrm{l}}_{\mathrm{i}}$ with k are sketched by solid lines in Fig. 1. Whenever $\Omega^{\mathrm{l}}_{\mathrm{i}}(k) > 0$, the wave is temporally amplified and eventually governed by the full nonlinear equation (5). Assume that stabilizing nonlinearities lead to a fully nonlinear travelling wave of the form

$$\psi(x, t) = \Psi(kx - \omega t; k), \tag{10}$$

where ω is a real frequency and the function $\Psi(\theta; k)$ is 2π periodic in θ. This one-parameter family of nonlinear solutions parameterized by k is characterized by the nonlinear dispersion relation

$$\omega = \Omega^{\mathrm{nl}}(k), \tag{11}$$

represented by the dashed curves in Fig. 1a and c. The travelling waves (10) and dispersion relation (11) are the nonlinear counterparts of the linear normal modes $\mathrm{e}^{\mathrm{i}(kx-\omega t)}$ and dispersion relation (8). Since the medium is assumed to be supercritical, nonlinear solutions $\Psi(\theta; k)$ only exist in the unstable wave number range defined by $\Omega^{\mathrm{l}}_{\mathrm{i}}(k) > 0$.

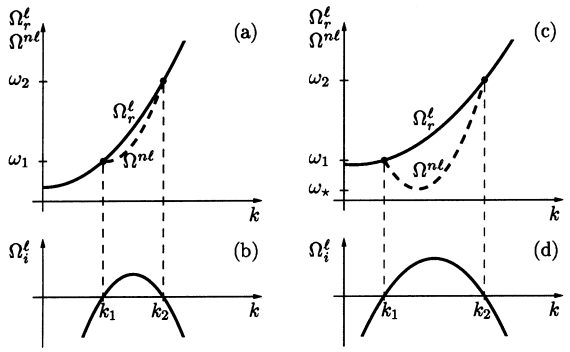

Fig. 1. Linear and nonlinear temporal branches of the CGL equation. (b), (d) Temporal growth rate $\Omega_{\rm i}^{\rm l}(k)$ as a function of the real wave number. Unstable wave numbers lie in the range $k_1 < k < k_2$. (a), (c) The nonlinear temporal branch $\Omega^{\rm nl}(k)$ (dashed curves) is defined in the unstable wave number range and is connected to the $\Omega_{\rm r}^{\rm l}(k)$ curve (solid lines) at the neutrally stable boundaries where $\omega_1 = \Omega^{\rm l}(k_1) = \Omega^{\rm nl}(k_1)$ and $\omega_2 = \Omega^{\rm l}(k_2) = \Omega^{\rm nl}(k_2)$. The nonlinear branch may be (a) monotonous or (c) exhibit an extremum, at $\omega_\star$.

As the boundaries of this range are approached, the linear growth rate vanishes as well as the nonlinear saturation amplitude of $\Psi(\theta; k)$. In the neutrally stable limit, the nonlinear frequency equals the linear real frequency,

$$\Omega^{\rm nl}(k) = \Omega^{\rm l}(k) \quad \text{when} \quad \Omega_{\rm i}^{\rm l}(k) = 0 \tag{12}$$

(see Fig. 1). In weakly unstable media, the unstable wave number range is small and in general the nonlinear frequency is a monotonous function of the wave number (Fig. 1a). Further above threshold, the unstable wave number range increases and the nonlinear temporal branch $\Omega^{\rm nl}(k)$ may exhibit an extremum $\omega_\star$ (Fig. 1c). As a result, one value of ω may be associated to two distinct wave numbers as further discussed in Section 2.3.

In general, the functions Ψ as well as $\Omega^{\rm nl}$ cannot be calculated analytically. They are obtained by performing a numerical simulation in a spatially periodic interval of wavelength $2\pi/k$ [35,36]. In the particular case of the CGL equation (6), nonlinear solutions are explicitly obtained as finite amplitude harmonic waves,

$$\psi(x,t) = R(k)\exp\{{\rm i}[kx - \Omega^{\rm nl}(k)t]\},$$

with

$$\Omega^{\rm nl}(k) = \frac{{\rm Im}(\gamma^\star \Omega^{\rm l}(k))}{{\rm Im}\,\gamma^\star}, \qquad R^2(k) = \frac{{\rm Im}(\Omega^{\rm l}(k))}{{\rm Im}\,\gamma^\star},$$

where the superscript $\star$ denotes the complex conjugate. Recall that the condition of stabilizing nonlinearities implies $\gamma_{\rm i} < 0$.

2.2. Impulse response and absolute instability

Unstable systems may be further characterized by studying their response to an impulsive localized perturbation [3,4,20–22]: in an unstable medium, at least one growing wave packet develops from the impulse location. If the growing wave packet moves away from its source and eventually leaves the medium unperturbed, the instability is said to be *convective*. If, by contrast, the instability grows in place and invades the system both upstream and downstream, the instability is said to be *absolute*. The convective or absolute nature of the instability depends on the absolute frequency ω_0 associated with the absolute wave number k_0 defined by a zero group velocity condition as

$$\omega_0 = \Omega^{\rm l}(k_0), \qquad \frac{{\rm d}\Omega^{\rm l}}{{\rm d}k}(k_0) = 0. \tag{13}$$

The medium is absolutely unstable (AU) if $\omega_{0,\mathrm{i}} > 0$, convectively unstable (CU) if $\omega_{0,\mathrm{i}} < 0$. The form (6) in which the CGL equation has been cast explicitly puts forward its dependence on ω_0 and k_0.

2.3. Spatial response and causality

Consider the response of the medium to a localized time-harmonic excitation. The response to a forcing of real frequency ω_f and amplitude A_f, switched on at $t = 0$, is governed by the signaling problem

$$\frac{\partial \psi}{\partial t} = \mathcal{F}(\partial_x)[\psi] + A_\mathrm{f}\delta(x)H(t)\,\mathrm{e}^{-\mathrm{i}\omega_\mathrm{f} t} + \text{c.c.} \tag{14}$$

with H denoting the Heaviside unit step function and δ the Dirac delta function.

For small amplitude forcing ($A_\mathrm{f} \ll 1$), the response in the neighborhood of the forcing location is governed by the linear spatial problem with $\mathcal{F}$ replaced by $\mathcal{L}$ in (14). Switching on the forcing at $t = 0$ produces a transient wave packet together with the steady-state response at the forcing frequency. Whenever the medium is stable or convectively unstable, transients decay or move away out of the system, and the longtime response is established at the forcing frequency. When the medium is absolutely unstable, switch-on transients overwhelm the response at the forcing frequency and the signaling problem (14) is ill-posed [3,4]. Hence, we only consider the spatial problem (14) for at most CU systems. The steady-state linear response is made up of normal modes $\mathrm{e}^{\mathrm{i}(kx-\omega_\mathrm{f} t)}$ satisfying $\omega_\mathrm{f} = \Omega^\mathrm{l}(k)$. For a given ω_f, this linear dispersion relation in general admits several solutions $k^\mathrm{l}_m(\omega_\mathrm{f})$ indexed by m, the number of which very much depends on the particular form of $\Omega^\mathrm{l}(k)$.

Causality requires that $\psi = 0$ for all $t < 0$. Using a residue calculation in the complex ω-plane to solve (14) with $\mathcal{F}$ replaced by $\mathcal{L}$, and assuming that temporal growth rates are bounded ($\max\{\Omega^\mathrm{l}_\mathrm{i}(k),\, k \text{ real}\}$ finite), it is readily shown [3,4,20] that the spatial branches k^l_m either pertain to the downstream ($x > 0$) or to the upstream ($x < 0$) response to forcing. The downstream (upstream) branches are denoted by $k^{\mathrm{l}+}_m$ ($k^{\mathrm{l}-}_m$). For a given real forcing frequency the distribution of the spatial branches $k^\mathrm{l}_m(\omega)$ into $+$ or $-$ branches is derived, according to classical arguments [3,4], from an examination of the complete linear dispersion relation $\Omega^\mathrm{l}(k)$ in the entire complex k-plane. In the sequel, spatial branches are said to be causal $+$ or causal $-$ branches according to whether they prevail downstream ($x > 0$) or upstream ($x < 0$) of the forcing location. Hence, causality always refers to the spatial response to a localized harmonic forcing.

For simplicity assume that $\Omega^\mathrm{l}(k)$ exhibits a single second-order branch point ω_0 with only two spatial branches $k^{\mathrm{l}+}$ and $k^{\mathrm{l}-}$, as in the case of the CGL dispersion relation (9) where

$$k^{\mathrm{l}\pm}(\omega) = k_0 \pm \sqrt{2\frac{\omega - \omega_0}{\omega_{kk}}}. \tag{15}$$

The spatial growth rate of the response depends on $k^\mathrm{l}_\mathrm{i} \equiv \mathrm{Im}\, k^\mathrm{l}$. The downstream response decays for frequencies such that $k^{\mathrm{l}+}_\mathrm{i}(\omega) > 0$; upstream decay occurs when $k^{\mathrm{l}-}_\mathrm{i}(\omega) < 0$. This is always the case for stable media (Fig. 2a). Whenever a linear spatial $k^{\mathrm{l}+}(\omega)$ branch is amplified, nonlinear terms have to be taken into account at some distance from the source, however small the forcing amplitude. When the response reaches finite amplitude, nonlinear saturation prevents further amplification and leads to a nonlinear travelling wave at the excitation frequency for some real wave number k^nl (Fig. 2b). Since the nonlinear wave train is asymptotically reached far downstream of the source, it is denoted as $k^{\mathrm{nl}+}(\omega)$. This nonlinear wave train would also be obtained in a temporal evolution problem at the same wave number. Thus, the forcing frequency ω_f and the nonlinear response wave number $k^{\mathrm{nl}+}$ again satisfy the nonlinear dispersion relation (11). Hence, nonlinear spatial branches $k^{\mathrm{nl}\pm}(\omega)$ may formally be obtained by solving (11) for a given frequency. Following the convention of the "front community" [42], the superscripts $+$ and $-$ in this formal definition are assigned according to the sign of the "nonlinear group velocity" $\mathrm{d}\Omega^\mathrm{nl}/\mathrm{d}k$. In

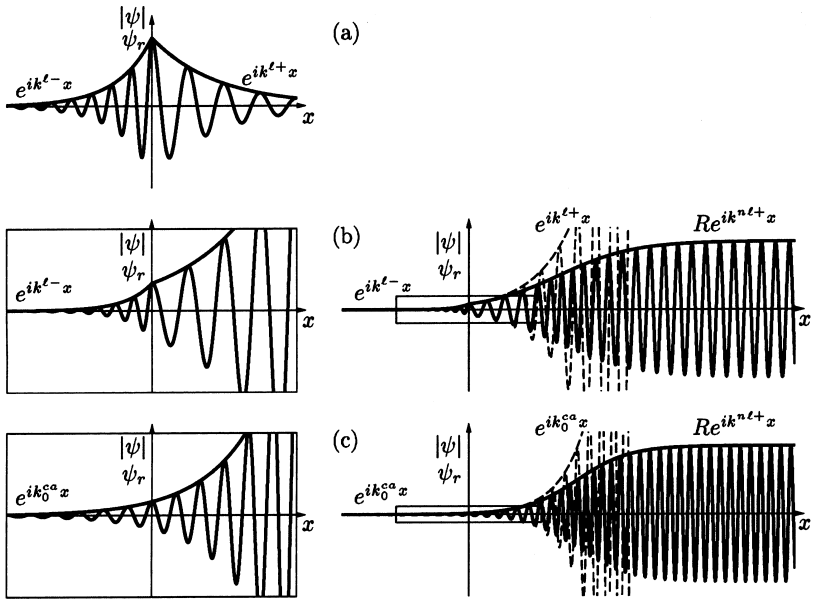

Fig. 2. Response to time harmonic forcing applied at $x = 0$. (a) Upstream and downstream decaying response in a stable or CU medium. (b) Linearly amplified downstream response and nonlinearly saturated solution in a CU medium. (c) Stationary front in a marginally absolutely unstable medium. Note that slope discontinuity at the forcing location has vanished. Dashed lines indicate exponentially growing branches in the linear approximation.

the situation of Fig. 1a, only $k^{\mathrm{nl}+}(\omega)$ exists for $\omega_1 < \omega < \omega_2$, whereas both nonlinear spatial branches appear for the situation in Fig. 1c: $k^{\mathrm{nl}+}(\omega)$ for $\omega_\star < \omega < \omega_2$ and $k^{\mathrm{nl}-}(\omega)$ for $\omega_\star < \omega < \omega_1$. These definitions of $k^{\mathrm{nl}+}(\omega)$ and $k^{\mathrm{nl}-}(\omega)$ branches apply to CU as well as AU systems. We stress, however, that only those branches accessible via a spatial response problem in a CU medium have causal meaning. In particular, due to the choice of a basic advection towards $x = +\infty$, only the downstream response may be spatially amplified, and the $k^{\mathrm{nl}-}(\omega)$ branch is never accessible via a forcing problem.

2.4. Stationary fronts as spatial response without forcing

Many studies [16,39–42] have been devoted to the derivation of selection criteria for propagating fronts connecting an unstable $\psi = 0$ state to a fully nonlinear saturated state in a uniform medium. In situations where the front velocity is linearly selected [16,40], the front moves towards its decaying edge in AU media, towards its finite-amplitude edge in CU media. A stationary front is then precisely obtained when the medium is exactly at the CU/AU transition. The same stationary front solution may be recovered in the context of the spatial response to time-harmonic forcing as discussed below.

Consider the signaling problem (14) in a uniform medium

$$\frac{\partial \psi}{\partial t} = \mathcal{F}(\partial_x; X)[\psi] + A_{\mathrm{f}}\delta(x)H(t)\,\mathrm{e}^{-\mathrm{i}\omega_{\mathrm{f}}t} + \text{c.c.}, \tag{16}$$

where the frozen slow scale X has been explicitly introduced as an external control parameter. Let us examine how the response to a localized forcing of frequency ω_{f} varies with the parameter X which controls the instability properties of the medium. Assume that the medium is stable or CU for $X < X^{\mathrm{ca}}$ and marginally AU at $X = X^{\mathrm{ca}}$, i.e., $\omega_{0,\mathrm{i}}(X) < 0$ for $X < X^{\mathrm{ca}}$ and $\omega_0^{\mathrm{ca}} \equiv \omega_0(X^{\mathrm{ca}})$ real. Let $k_0^{\mathrm{ca}} \equiv k_0(X^{\mathrm{ca}})$ denote the complex absolute wave

number at the CU/AU transition. Since basic advection is assumed to be in the positive x-direction, $k_{0,\mathrm{i}}^{\mathrm{ca}} < 0$, as shown in Section 4.8.

Let us use as an illustrative example the CGL equation (4) with forcing as in (16). Upon making use of the associated linear dispersion relation Ω^{l} given by (9) and invoking continuity of the solution at $x = 0$, the exact longtime linear response is obtained as

$$\psi(x,t) = \frac{2A_{\mathrm{f}}}{\omega_{kk}(X)} \frac{\exp\{\mathrm{i}[k^{\mathrm{l}\pm}(X,\omega_{\mathrm{f}})x - \omega_{\mathrm{f}}t]\}}{k^{\mathrm{l}+}(X,\omega_{\mathrm{f}}) - k^{\mathrm{l}-}(X,\omega_{\mathrm{f}})} + \text{c.c.} \tag{17}$$

The $\mathrm{e}^{\mathrm{i}k^{\mathrm{l}+}x}$ and $\mathrm{e}^{\mathrm{i}k^{\mathrm{l}-}x}$ branches naturally pertain to the regions $x > 0$ and $x < 0$, respectively. In order to obtain a normalized response such that $\max|\psi(0,t)| = \alpha$, the forcing amplitude is adjusted to the level

$$A_{\mathrm{f}}(X,\omega_{\mathrm{f}}) = \tfrac{1}{4}\alpha\omega_{kk}(X)[k^{\mathrm{l}+}(X,\omega_{\mathrm{f}}) - k^{\mathrm{l}-}(X,\omega_{\mathrm{f}})]. \tag{18}$$

If $\alpha \ll 1$, the linear response is guaranteed to remain valid in a neighborhood of $x = 0$ even though the response may reach a finite amplitude further downstream.

If the medium is stable for large $X < 0$, both upstream and downstream parts of the response decay, i.e., $k_{\mathrm{i}}^{\mathrm{l}+}(X,\omega_{\mathrm{f}}) > 0$ and $k_{\mathrm{i}}^{\mathrm{l}-}(X,\omega_{\mathrm{f}}) < 0$ for large $X < 0$ (cf. Fig. 2a). As the control parameter X and forcing frequency ω_{f} are varied continuously to approach the limit $X^{\mathrm{ca}}, \omega_0^{\mathrm{ca}}$, the downstream response $k^{\mathrm{l}+}$ is eventually amplified, whereas the upstream branch $k^{\mathrm{l}-}$ still decays (Fig. 2b). Indeed, by definition of ω_0^{ca} (see also (15)) both spatial branches meet at $X = X^{\mathrm{ca}}$ and $\omega_{\mathrm{f}} = \omega_0^{\mathrm{ca}}$, i.e.,

$$k^{\mathrm{l}+}(X^{\mathrm{ca}},\omega_0^{\mathrm{ca}}) = k^{\mathrm{l}-}(X^{\mathrm{ca}},\omega_0^{\mathrm{ca}}) = k_0^{\mathrm{ca}}.$$

Since $k_{0,\mathrm{i}}^{\mathrm{ca}} < 0$, it is therefore guaranteed that $k_{\mathrm{i}}^{\mathrm{l}+}(X,\omega_{\mathrm{f}})$ changes sign and becomes negative as (X,ω_{f}) approach $(X^{\mathrm{ca}},\omega_0^{\mathrm{ca}})$, while $k_{\mathrm{i}}^{\mathrm{l}-}(X,\omega_{\mathrm{f}})$ does not. In such a regime, the downstream growing response $\alpha\exp[\mathrm{i}k^{\mathrm{l}+}(X,\omega_{\mathrm{f}})x]$ reaches a finite amplitude at $x \sim \ln\alpha/k_{\mathrm{i}}^{\mathrm{l}+} > 0$. At this station, the linearly growing wave $k^{\mathrm{l}+}(X,\omega_{\mathrm{f}})$ gives way to its nonlinear counterpart $k^{\mathrm{nl}+}(X,\omega_{\mathrm{f}})$.

In the stable or convectively unstable regime ($X < X^{\mathrm{ca}}$), both the spatial growth rate and wave number are discontinuous at $x = 0$, i.e., $k^{\mathrm{l}+} \neq k^{\mathrm{l}-}$. The forcing location is then a singular point of the total response (Fig. 2a and b). When $(X,\omega_{\mathrm{f}}) \to (X^{\mathrm{ca}},\omega_0^{\mathrm{ca}})$, the medium approaches absolute instability and both branches $k^{\mathrm{l}+}(X,\omega_{\mathrm{f}})$ and $k^{\mathrm{l}-}(X,\omega_{\mathrm{f}})$ tend towards k_0^{ca}. Thus, in this process, the slope discontinuity in the response at $x = 0$ smoothes out. Moreover, according to (18), the forcing amplitude $A_{\mathrm{f}}(X,\omega_{\mathrm{f}})$ required to maintain the normalization condition $\max|\psi(0,t)| = \alpha$ vanishes. Thus, in the marginally AU regime $X = X^{\mathrm{ca}}$, a smooth stationary front of frequency $\omega_{\mathrm{f}} = \omega_0^{\mathrm{ca}}$ prevails without any forcing (Fig. 2c). This front directly connects the upstream linear $k^{\mathrm{l}-}$ branch to the downstream nonlinear $k^{\mathrm{nl}+}$ branch. As mentioned in Section 2.3, the $+$ and $-$ notations have causal meaning only in CU systems. The previous argument indicates that, in a marginally AU system, the two branches on both sides of a front are still determined by causal considerations through a continuation procedure from the CU side. From the above discussion, a stationary front in a spatially uniform system is obtained for zero amplitude forcing whenever the medium becomes marginally AU and the forcing frequency equals the corresponding real absolute frequency ω_0^{ca}. This strategy may be implemented numerically to obtain front-like structures not only in the context of one-dimensional evolution equations (16) but also in more complex systems, e.g., wake flows governed by the Navier–Stokes equations [35,36].

3. Spatial variations of local instability properties

The previous results derived for spatially uniform media also yield the local linear and nonlinear instability characteristics of weakly nonuniform media, provided that the control parameter X now be interpreted as the slow

streamwise coordinate. The respective dispersion relations at each station X read

$$\omega = \Omega^{\mathrm{l}}(k, X), \quad \omega \text{ and } k \text{ complex}, \tag{19}$$

$$\omega = \Omega^{\mathrm{nl}}(k, X), \quad \omega \text{ and } k \text{ real}. \tag{20}$$

The local linear dispersion relation pertains to any complex wave number whereas the local nonlinear dispersion relation is defined only for real wave numbers associated with a positive temporal growth rate $\Omega_{\mathrm{i}}^{\mathrm{l}}(k, X) > 0$. In strictly uniform media, linear normal modes are sought in the form $\psi = A \exp\{\mathrm{i}[k^{\mathrm{l}}(\omega)x - \omega t]\} + \text{c.c.}$ In weakly nonuniform media, such modes are replaced by

$$\psi = A(X) \exp\left(\frac{\mathrm{i}}{\epsilon}\int^{X} k^{\mathrm{l}}(u, \omega)\,\mathrm{d}u - \mathrm{i}\omega t\right) + \text{c.c.} \tag{21}$$

As demonstrated in the classical WKBJ procedure carried out in Section 5, the local linear wave number $k^{\mathrm{l}}(X, \omega)$ necessarily satisfies the local linear dispersion relation (19). In strictly uniform media, nonlinear travelling waves are sought in the form $\Psi[k^{\mathrm{nl}}(\omega)x - \omega t; k^{\mathrm{nl}}(\omega)]$ (10). In weakly nonuniform media, such travelling waves are replaced by slowly modulated wave packets of the form

$$\psi \sim \Psi\left(\frac{1}{\epsilon}\int^{X} k^{\mathrm{nl}}(u, \omega)\,\mathrm{d}u - \omega t + \Theta(X); k^{\mathrm{nl}}(X, \omega), X\right), \tag{22}$$

where the local nonlinear wave number $k^{\mathrm{nl}}(X, \omega)$ satisfies the nonlinear local dispersion relation (20). The slowly varying functions $A(X)$ and $\Theta(X)$ appearing in (21) and (22), respectively, are obtained in the complete asymptotic analysis (Section 5).

The objective of this section is then to study the changing topology of linear complex k^{l} and nonlinear real k^{nl} spatial branches as the global real frequency is varied. The globally synchronized structures obtained in Sections 4 and 5 crucially depend on these spatial branches.

3.1. Instability domains

Let us first introduce the regions of local convective or absolute instability in physical X-space and determine the domain of existence of nonlinear wave trains in (X, k)-space. The local absolute frequency $\omega_0(X)$ and wave number $k_0(X)$ are derived from the local linear dispersion relation (19) as in (13). The local convective or absolute nature of the medium is determined by the sign of $\omega_{0,\mathrm{i}}(X)$. In a typical situation of interest, absolute instability occurs in a central finite domain. For definiteness, consider $\omega_0(X)$ to be of the parabolic form sketched in the complex ω-plane in Fig. 3a: $\omega_{0,\mathrm{i}}(X)$ is an increasing–decreasing function of X with a single maximum $\omega_{0,\mathrm{i}}^{\max}$ reached at $X = X^{\max}$.

Whenever $\omega_{0,\mathrm{i}}^{\max} > 0$, there exists a finite *AU domain*, $X^{\mathrm{ca}} < X < X^{\mathrm{ac}}$, defined as the region where $\omega_{0,\mathrm{i}}(X) > 0$. Its boundaries X^{ca} and X^{ac} are the stations where the local absolute frequency is real, $\omega_0^{\mathrm{ca}} \equiv \omega_0(X^{\mathrm{ca}})$ and $\omega_0^{\mathrm{ac}} \equiv \omega_0(X^{\mathrm{ac}})$, respectively.

The domain of local instability, characterized by unstable real wave numbers, $\Omega_{\mathrm{i}}^{\mathrm{l}}(k, X) > 0$, defines the *nonlinear balloon* in the (X, k)-plane (Fig. 3b). In the X-direction, the balloon extends beyond the AU domain to the stations of linear neutral stability, denoted X^{sc} and X^{cs}. At each unstable location, the nonlinear balloon extends in the k-direction over the local unstable wave number range. Note that, due to causality, large wave numbers are always temporally decaying; thus, the nonlinear balloon is necessarily bounded in the k-direction.

A typical system, therefore, displays the following structure: a central AU domain $X^{\mathrm{ca}} < X < X^{\mathrm{ac}}$ of finite extent, surrounded by two CU regions $X^{\mathrm{sc}} < X < X^{\mathrm{ca}}$ and $X^{\mathrm{ac}} < X < X^{\mathrm{cs}}$, which in turn are embedded in

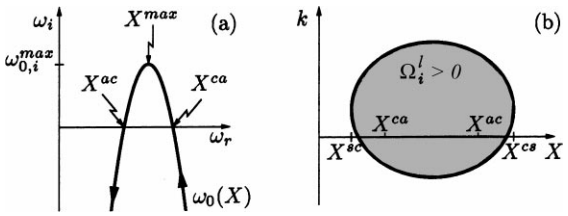

Fig. 3. (a) Locus of the local absolute frequency $\omega_0(X)$ in the complex frequency plane for $-\infty < X < +\infty$. The AU interval $X^{ca} < X < X^{ac}$ is associated with $\omega_{0,i}(X) > 0$. (b) Nonlinear balloon of the CGL equation in the (X, k)-plane defined by $\Omega_i^l(k, X) > 0$ and bounded by the curve of neutral stability $\Omega_i^l(k, X) = 0$. In the X-direction the balloon spans the domain of local linear instability $X^{sc} < X < X^{cs}$ and extends beyond the AU interval.

two semi-infinite stable regions extending to $X = \pm\infty$. As mentioned in Section 4.1, one may relax the stability requirement at $X = \pm\infty$ and the medium may remain CU to $X = \pm\infty$.

3.2. Linear spatial branches

The loci of linear spatial branches $k^l(X, \omega)$ as functions of X is now qualitatively discussed in the complex k-plane for different values of the complex frequency ω. Such an analysis will illustrate the relationship between the behavior of linear spatial branches and the local CU/AU properties of the medium. Linear spatial branches $k^l(X, \omega)$ are obtained by solving the local linear dispersion relation (19) for a given frequency ω. In the case of the CGL equation (4) they read

$$k^{l\pm}(X, \omega) = k_0(X) \pm \sqrt{2\frac{\omega - \omega_0(X)}{\omega_{kk}(X)}}. \tag{23}$$

In Section 2.3, the choice of the $+$ and $-$ branches was shown to be dictated by causality for real frequencies in stable or CU media. The fate of spatial branches in the AU range $X^{ca} < X < X^{ac}$ is now examined for different frequencies in the complex ω-plane, as illustrated for the CGL equation in Fig. 4.

As a result of causality [3,4], the spatial branches $k^{l\pm}(X, \omega)$ do not cross the k_r-axis in the complex k-plane for large enough $\omega_i > 0$. For such frequencies far above the absolute frequency curve $\{\omega_0(X)\}$ (cf. Fig. 4a), the k^{l+} (k^{l-}) branch is globally defined as the one located in the upper (lower) half k-plane for all real X. The $k^{l\pm}(X, \omega)$ branches continuously deform as ω is varied. They may cross the k_r-axis for finite values of X (Fig. 4b–d), but remain in the same half k-plane for $X \to \pm\infty$. As ω is kept above the curve $\{\omega_0(X)\}$ (denoted by $\omega \succ \{\omega_0(X)\}$), no branch switching may occur (Fig. 4b–d) as readily seen by inspection of Eq. (23). This property yields definitions of the $k^{l\pm}$ branches that remain uniformly valid in X, for all complex frequencies $\omega \succ \{\omega_0(X)\}$, even though the medium may be locally AU.

When $\omega \in \{\omega_0(X)\}$, say $\omega = \omega_0(X_0)$, the two $k^{l\pm}$ branches pinch at $k_0(X_0)$ for $X = X_0$ (Fig. 4e illustrates the case of particular interest where $X_0 = X^{ca}$). For frequencies $\omega \prec \{\omega_0(X)\}$ below the absolute frequency curve, the continuous k^l curves connect the upper and lower half k-planes as X is varied from $-\infty$ to $+\infty$ (Fig. 4f). Global $k^{l\pm}$ branches can no longer be defined, but the $+$ and $-$ superscripts may still be assigned according to causality in the distinct $X < X^{ca}$ and $X > X^{ac}$ regions represented by thick lines in Fig. 4. For $\omega \prec \{\omega_0(X)\}$ (Fig. 4f), the k^{l-} branch for $X < X^{ca}$ is connected to the k^{l+} branch in the region $X > X^{ac}$, across the AU domain (part of the curve being represented by a thin line).

These considerations apply in particular to real ω. For frequencies outside the ω_0^{ca}–ω_0^{ac} interval, i.e., $\omega \succ \{\omega_0(X)\}$, the k^{l+} and k^{l-} branches are globally defined, although causality considerations do not apply in the central AU

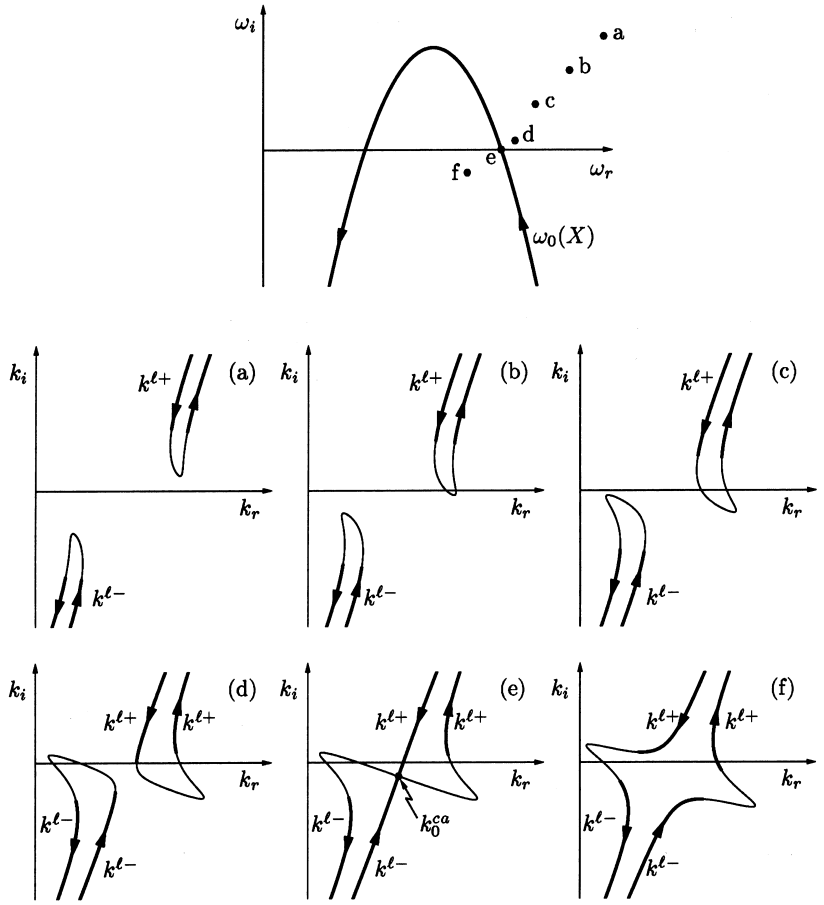

Fig. 4. (a–f) Loci of linear spatial branches $k^{\mathrm{l}}(X,\omega)$ of CGL equation in the complex k-plane for frequencies ω indicated in the complex frequency plane on top sketch. Arrows on the curves indicate direction of increasing X. Thick lines pertain to the stable or CU regions $X < X^{\mathrm{ca}}$ and $X > X^{\mathrm{ac}}$, thin lines to the central AU region $X^{\mathrm{ca}} < X < X^{\mathrm{ac}}$. (a–d) For frequencies $\omega \succ \{\omega_0(X)\}$, the spatial branches $k^{\mathrm{l}\pm}(X)$ remain distinct and are located in the same half k-plane for $X \to \pm\infty$, but they may cross the k_{r}-axis for finite values of X. As the frequency approaches the $\omega_0(X)$ curve, the spatial branches move closer to each other. (e) For a frequency located on the $\omega_0(X)$ curve, here $\omega = \omega_0(X^{\mathrm{ca}})$, pinching occurs at the corresponding absolute wave number, here at $k = k_0^{\mathrm{ca}}$, when $X = X^{\mathrm{ca}}$. (f) When $\omega \prec \{\omega_0(X)\}$, the continuous curves connect the upper and lower half k-planes as $X \to \pm\infty$. Definition as $k^{\mathrm{l}\pm}$ branches still holds in the distinct CU domains $X < X^{\mathrm{ca}}$ and $X > X^{\mathrm{ac}}$, but not in the central AU region.

domain. For frequencies in the ω_0^{ca}–ω_0^{ac} interval, i.e., $\omega \prec \{\omega_0(X)\}$, the $k^{\mathrm{l}+}$ and $k^{\mathrm{l}-}$ branches turn one into the other across the AU domain.

3.3. Nonlinear spatial branches

The goal of this section is to describe synthetically the qualitative properties of the nonlinear spatial branches $k^{\mathrm{nl}}(X,\omega)$ as functions of X for different values of the real frequency ω. Finite amplitude waves are governed by the nonlinear dispersion relation (20). Fig. 5 illustrates its properties in the case of the CGL equation, by projecting the surface defined as $\omega = \Omega^{\mathrm{nl}}(k, X)$ in the (X, k, ω)-space onto the (X, k)-plane. Nonlinear spatial branches $k^{\mathrm{nl}}(X,\omega)$ for a given real frequency ω are obtained as the level contours $\Omega^{\mathrm{nl}}(k, X) = \mathrm{C}^{\mathrm{st}}$ indicated by long dashed lines.

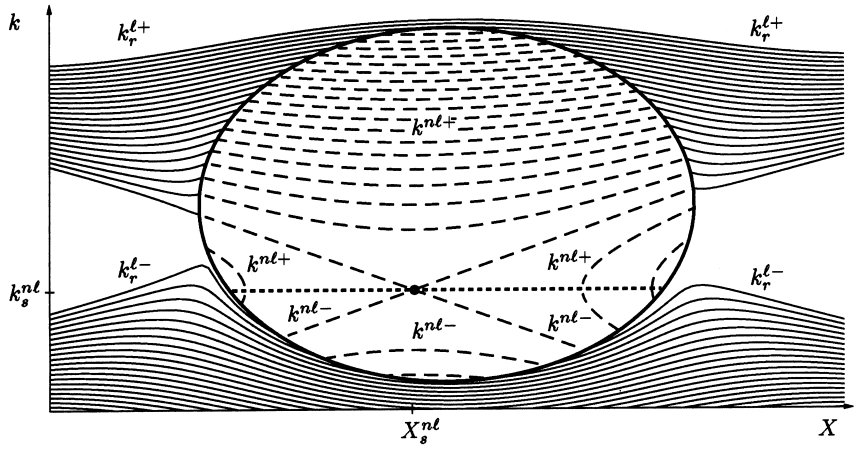

Fig. 5. Projection of the CGL nonlinear dispersion relation surface $\omega = \Omega^{\mathrm{nl}}(k, X)$ on the (X, k)-plane. Nonlinear spatial branches $k^{\mathrm{nl}+}(X, \omega)$ and $k^{\mathrm{nl}-}(X, \omega)$ represented by constant frequency level curves (dashed lines) live within the nonlinear balloon bounded by the neutral stability boundary (thick solid line). Nonlinear spatial branches display a saddle structure and, by convention, $k^{\mathrm{nl}+}$ and $k^{\mathrm{nl}-}$ refer to the upper and lower regions on either side of the steepest descent curve (thick dotted line) emerging from the saddle point $X_{\mathrm{s}}^{\mathrm{nl}}, k_{\mathrm{s}}^{\mathrm{nl}}$ (solid dot) corresponding to the frequency $\omega_{\mathrm{s}}^{\mathrm{nl}}$. The real parts $k_{\mathrm{r}}^{\mathrm{l}\pm}$ of the linear spatial branches (thin solid lines) are also shown outside the nonlinear balloon for the same frequencies as the nonlinear branches. Note their continuous connection at the neutral stability boundary.

Nonlinear wave trains only exist inside the nonlinear balloon of the (X, k)-plane, defined by $\Omega_{\mathrm{i}}^{\mathrm{l}}(k, X) > 0$ (see Fig. 3b). Its neutrally stable boundary characterized by $\Omega_{\mathrm{i}}^{\mathrm{l}}(k, X) = 0$ is represented by the thick closed curve in Fig. 5. Since the nonlinear dispersion relation $\omega = \Omega^{\mathrm{nl}}(k, X)$ is always a single-valued function of k, the mapping in the (X, k)-plane is one-to-one and all the nonlinear solutions are contained inside the neutral stability boundary. By contrast, $k^{\mathrm{nl}}(X, \omega)$ is not ensured to be a single-valued function of ω. We have deliberately chosen a configuration displaying this double-valuedness, which is made manifest here by the saddle point structure in the dashed contour levels $\Omega^{\mathrm{nl}}(k, X) = \mathrm{C}^{\mathrm{st}}$. Following the definition adopted in Section 2.3, the nonlinear spatial branches are labeled $k^{\mathrm{nl}+}$ and $k^{\mathrm{nl}-}$ according to the sign of the "nonlinear group velocity" $\partial\Omega^{\mathrm{nl}}/\partial k$. Accordingly, the $k^{\mathrm{nl}+}$ and $k^{\mathrm{nl}-}$ domains of Fig. 5 are precisely connected via the steepest descent curve (short dashed line) emerging from the saddle point (solid dot).

In order to emphasize the relationship between linear and nonlinear branches, the linear spatial branches $k^{\mathrm{l}\pm}(X, \omega)$ have also been displayed by thin solid lines in Fig. 5 through their real part $k_{\mathrm{r}}^{\mathrm{l}\pm}(X, \omega)$ at the same frequencies. Note that linear branches continuously connect to nonlinear branches at the neutral stability boundary. This property is not surprising: at the neutral stability boundary in the (X, k)-plane, the linear branch $k^{\mathrm{l}}(X, \omega)$ is purely real and equals its nonlinear counterpart $k^{\mathrm{nl}}(X, \omega)$.

As discussed in Section 3.2 (Fig. 4), the linear spatial branches are globally defined as $k^{\mathrm{l}+}$ or $k^{\mathrm{l}-}$ for $\omega \succ \{\omega_0(X)\}$. While lowering the frequency, starting from large positive values, the $k^{\mathrm{l}+}$ and/or $k^{\mathrm{l}-}$ branch may cross the k_{r}-axis in the complex k-plane (Fig. 4b–d). As this linear wave number branch moves into the opposite half k-plane, it becomes spatially amplified and gives birth to a nonlinear branch. This corresponds in the (X, k)-plane to the emergence of a k^{nl} branch connected at the boundary of the nonlinear balloon to a $k_{\mathrm{r}}^{\mathrm{l}}$ branch (Fig. 5).

By further lowering the frequency, switching between the nonlinear branches may take place, as implied by the saddle structure of the dashed curves in Fig. 5. When the frequency decreases, pinching between $k^{\mathrm{nl}-}$ and $k^{\mathrm{nl}+}$ will take place for $\omega = \omega_{\mathrm{s}}^{\mathrm{nl}}$ at the saddle point $(X_{\mathrm{s}}^{\mathrm{nl}}, k_{\mathrm{s}}^{\mathrm{nl}})$ of the nonlinear dispersion relation (20) in the (X, k)-plane. Below this saddle point frequency, the nonlinear spatial branches move into the left- and right-hand sectors bounded by the saddle point asymptotes. For a given frequency in this range, nonlinear spatial branches are indeed generated

at the boundary of the nonlinear balloon but they fail to exist in the heart of the nonlinear region surrounding the saddle point. This behavior is provoked by the merging of $k^{\mathrm{nl}+}$ and $k^{\mathrm{nl}-}$ on the steepest descent line (thick dotted line of Fig. 5) and their subsequent disappearance. The implications of such a nonlinear saddle point structure on global mode selection are profound, as discussed in Section 4.6.

4. Globally synchronized structures

Having investigated local instability properties of the spatially developing medium, we now turn to the study of globally synchronized solutions of system (1) and associated bifurcations. Such global modes are defined as stationary time-periodic solutions satisfying

$$\psi\left(x, t + \frac{2\pi}{\omega_{\mathrm{g}}}\right) = \psi(x, t),$$

where ω_{g} is the global real frequency. Selection criteria for self-sustained global oscillations are derived below and the leading-order approximations of their global frequency and spatial structure are obtained. The properties of the medium which dictate the selected global mode type are identified and the ensuing bifurcations are analyzed as global control parameters are varied.

4.1. Boundary conditions and nonlinear eigenvalue problem

To completely determine the global mode problem, proper boundary conditions in connection with Eq. (1) have to be specified. Global modes are defined as intrinsic oscillations which are due to the dynamics of the central region and not to perturbations invading the system from $X = \pm\infty$. Consequently, the boundary conditions must be causal: the solution close to the boundaries is necessarily dictated by the intrinsic oscillations occurring in the central region. Thus, far downstream near $X = +\infty$ the solution is necessarily made up of a $+$ branch caused by the dynamics governing the central region upstream of it. Similarly, the solution necessarily involves a $-$ branch towards $X = -\infty$. Such boundary conditions at $X = \pm\infty$ will be referred to as causal.

When the medium is assumed to be stable in the far downstream and upstream regions, causal boundary conditions are equivalent with decaying ones. Indeed, in the stable regions no nonlinear solutions exist. Causality then requires a linear $k^{\mathrm{l}+}$ ($k^{\mathrm{l}-}$) branch towards $X = +\infty(-\infty)$. Due to stability, $k_{\mathrm{i}}^{\mathrm{l}+} > 0$ and $k_{\mathrm{i}}^{\mathrm{l}-} < 0$, thus the solution necessarily decays towards $X = \pm\infty$.

However, the medium may remain CU up to $X = \pm\infty$. In such instances, decaying boundary conditions are not necessarily fulfilled. However, causality still holds: if the solution remains fully nonlinear down to $X = +\infty$, it is there necessarily made up of the $k^{\mathrm{nl}+}$ branch only. Thus, proper boundary conditions for the global mode problem do not necessarily require exponential decay, provided they satisfy causality.

Since a global mode is a solution over the entire X-axis, it necessarily connects a $-$ branch at $X = -\infty$ to a $+$ branch at $X = +\infty$. This crossover from $-$ to $+$ branches may only be achieved for specific frequencies. The search for global modes is thus a nonlinear eigenvalue problem for the global frequency ω_{g}. The manner in which this crossover takes place in the central region gives rise to different types of global modes as described below.

4.2. Steep global modes

According to Pier et al. [34], the spatial structure of steep global modes is characterized by the presence of a sharp front at the upstream boundary X^{ca} of the AU region. The sketch in Fig. 6a represents the envelope $|\psi|$ and

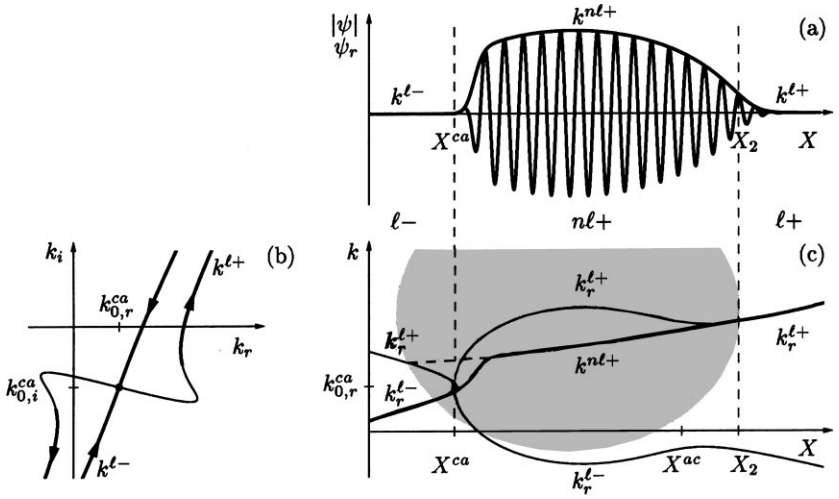

Fig. 6. Structure of steep global mode obtained by direct numerical simulation of CGL equation. (a) Envelope $|\psi|$ and real part ψ_r as functions of downstream distance X. The sharp front located at the upstream boundary X^{ca} of AU region initiates the fully nonlinear development extending down to the neutral station X_2. (b) Analytically computed linear spatial branches $k^{l\pm}(X)$ of steep global frequency ω_0^{ca} in the complex k-plane. Pinching occurs for the absolute wave number k_0^{ca} at $X = X^{ca}$. Thick lines pertain to the stable or CU regions $X < X^{ca}$ and $X > X^{ac}$, thin lines to the central AU region $X^{ca} < X < X^{ac}$. (c) Corresponding linear $k_r^{l\pm}$ (solid) and nonlinear k^{nl+} (dashed) spatial branches in the (X, k)-plane. Local wave number of simulation in (a) follows path indicated by thick line. Three domains are identified: the k^{l-} branch prevails in the upstream linear l− region $X < X^{ca}$; the front at X^{ca} is associated with a jump in wave number, and in its wake the k^{nl-} branch develops in the fully nonlinear nl+ domain $X^{ca} < X < X_2$ extending towards the boundary of the nonlinear balloon (shaded); the k^{l+} branch continuously takes over in the linear l+ region downstream of the neutral station X_2.

real part ψ_r of a steep global mode obtained by direct numerical simulation of the CGL equation (4). The length of the computational domain is $L = 102$. Linear and parabolic variations are, respectively, used for $\omega_{0,r}(X)$ and $\omega_{0,i}(X)$, as in Fig. 3a, so that $\omega_0^{ca} = 0.4$, $\omega_0^{ac} = 0$, $\omega_{0,i}^{max} = 0.5$ and $X^{ca} = \frac{3}{16}L$, $X^{ac} = \frac{11}{16}L$. Other coefficients take the constant values $k_0 = 0.5 - 0.8i$, $\omega_{kk} = 1 - i$ and $\gamma = 0.1 - i$.

The front at the location X^{ca} of marginal absolute instability $[\omega_{0,i}(X^{ca}) = 0]$ is precisely of the type obtained in Section 2.4: it oscillates at the real absolute frequency $\omega_g = 0.42 \sim \omega_0^{ca} = 0.40$ and allows a crossover between the upstream k^{l-} and the downstream k^{nl+} branches. Indeed, in Fig. 6c the numerically obtained local wave number $\mathrm{Re}((-i/\psi)\partial\psi/\partial x)$ represented by a thick line follows the corresponding analytically determined $k_r^{l\pm}(X, \omega_0^{ca})$ (thin solid curves) and $k^{nl+}(X, \omega_0^{ca})$ (thin dashed curve). The exponential decay of the upstream tail of the front is determined by the imaginary part of the corresponding absolute wave number $k_0^{ca} \equiv k_0(X^{ca})$. The upstream $k^{l-}(X, \omega_g)$ branch extending towards $X = -\infty$ is precisely generated at the pinch point $X = X^{ca}$ in the complex k-plane (Fig. 6b). As depicted in the (X, k)-plane of Fig. 6c, nonlinear travelling waves following the k^{nl+} branch prevail in the region $X^{ca} < X < X_2$ extending down to the location X_2 where the k^{nl+} branch meets the boundary of the nonlinear balloon in the (X, k)-plane. At the neutrally stable station X_2 the amplitude of the nonlinear travelling wave vanishes and the linear branch $k^{l+}(X, \omega_g)$ continuously takes over in the downstream linear region $X > X_2$.

The following frequency selection criterion then holds: the steep global frequency ω_g is given by the real absolute frequency ω_0^{ca} prevailing at the front location X^{ca} separating the CU and AU regions. In other words,

$$\omega_g = \omega_0(X^{ca}), \qquad \omega_{0,i}(X^{ca}) = 0. \tag{24}$$

The front at X^{ca} effectively acts as a wave maker for the entire flow. It may be interpreted as a local oscillator inducing the linear upstream − branch and the nonlinear downstream + branch.

4.3. Saddle-node bifurcation to steep global modes

It should be noted that the steep global mode criterion (24) is also fulfilled by the absolute frequency ω_0^{ac} prevailing at the downstream boundary X^{ac} of the AU region. Thus, whenever $\omega_{0,\mathrm{i}}^{\max} > 0$, two steep global modes exist: one of frequency ω_0^{ca} with a front at the upstream boundary X^{ca} of the AU region and one of frequency ω_0^{ac} with a front at its downstream boundary X^{ac} (see Fig. 3a). When $\omega_{0,\mathrm{i}}^{\max} < 0$, no AU region is present and no steep global mode exists. Thus, $\omega_{0,\mathrm{i}}^{\max}$ constitutes the global control parameter governing the existence of steep global modes. When $\omega_{0,\mathrm{i}}^{\max}$ is varied, transition to steep global modes occurs via a saddle-node bifurcation at $\omega_{0,\mathrm{i}}^{\max} = 0$ as demonstrated below.

The spatial structure of a solution with a front at X^{ca} has been detailed in the previous section. The structure of a solution with a front at X^{ac} is similar. Indeed, both linear $k^{\mathrm{l}\pm}(X, \omega_0^{\mathrm{ac}})$ branches equal $k_0^{\mathrm{ac}} \equiv k_0(X^{\mathrm{ac}})$ at $X = X^{\mathrm{ac}}$. Due to the assumption $k_{0,\mathrm{i}} < 0$, the $k^{\mathrm{l}-}$ branch is again exponentially damped while the $k^{\mathrm{l}+}$ branch is amplified. As a result, nonlinear travelling waves $k^{\mathrm{nl}+}$ are only present downstream of the front ($X > X^{\mathrm{ac}}$) and linear damped waves $k^{\mathrm{l}-}$ upstream of the front ($X < X^{\mathrm{ac}}$). Thus, the nonlinear part of such a global mode extends in the downstream CU region, whereas the central AU domain is covered by an exponentially decaying upstream tail.

Let us now show that an upstream front is a stable configuration whereas a downstream front is unstable. Consider a small displacement of the upstream front from its equilibrium location X^{ca} towards $X > X^{\mathrm{ca}}$. The front now experiences a slightly AU medium, hence, according to Dee and Langer [16], the nonlinear part grows and the front propagates towards its decaying edge, i.e., upstream. When this front is displaced towards $X < X^{\mathrm{ca}}$, it penetrates into a CU region and is thus pushed downstream. In any case the front is seen to return to its equilibrium position X^{ca}. Thus, the corresponding steep global mode is an attractor onto which direct numerical simulation converges.

On the contrary, a downstream front displaced from its equilibrium position X^{ac} towards the AU region $X < X^{\mathrm{ac}}$ continues to propagate upstream and completely invades the AU domain. When the front is displaced towards the CU region $X > X^{\mathrm{ac}}$, it is swept away downstream towards $X = +\infty$. A downstream front is therefore unstable.

Thus when $\omega_{0,\mathrm{i}}^{\max} > 0$, a pair of steep global modes exists: the mode with a front at the upstream (resp. downstream) boundary of the AU region is stable (resp. unstable). In the limit $\omega_{0,\mathrm{i}}^{\max} \downarrow 0$, the AU domain shrinks and the front locations move in closer to each other, $X^{\mathrm{ca}} \uparrow X^{\max}$ and $X^{\mathrm{ac}} \downarrow X^{\max}$. When $\omega_{0,\mathrm{i}}^{\max} = 0$ both front frequencies ω_0^{ca} and ω_0^{ac} equal $\omega_0(X^{\max})$, and both steep global modes coincide. When $\omega_{0,\mathrm{i}}^{\max} < 0$, the domain is nowhere AU and no steep global mode exists.

This behavior is typical of a saddle-node bifurcation: while decreasing the bifurcation parameter $\omega_{0,\mathrm{i}}^{\max}$, a stable and an unstable solution meet and disappear at the critical value $\omega_{0,\mathrm{i}}^{\max} = 0$. Note that in general the steep global mode remains fully nonlinear for all $\omega_{0,\mathrm{i}}^{\max} > 0$. Indeed, for $0 < \omega_{0,\mathrm{i}}^{\max} \ll 1$ the extent of the convectively unstable domain remains $\mathcal{O}(1)$ (in terms of X) and so does the nonlinear region where the global mode lives.

4.4. Linear global modes

The linear global instability of the unperturbed $\psi = 0$ state has been studied by Chomaz et al. [7] and Le Dizès et al. [25]. The instability properties were derived from an analytic continuation of the local absolute frequency $\omega_0(X)$ in the complex X-plane, as summarized below.

Linear global modes are assumed to be of the form $\psi(x, t) = \phi(X)\,\mathrm{e}^{-\mathrm{i}\omega_{\mathrm{g}} t}$ of complex global frequency ω_{g}. The spatial function ϕ is defined over the complex X-plane and the local complex wave number then satisfies the linear dispersion relation (19) with complex X. A linear global mode is entirely made up of linear spatial branches $k^{\mathrm{l}\pm}$. Due to causal boundary conditions, the $k^{\mathrm{l}-}$ branch prevailing near $X = -\infty$ must necessarily connect to the $k^{\mathrm{l}+}$ branch near $X = +\infty$. This can be achieved at a saddle point $X_{\mathrm{s}}^{\mathrm{l}}$ of the absolute frequency in the complex

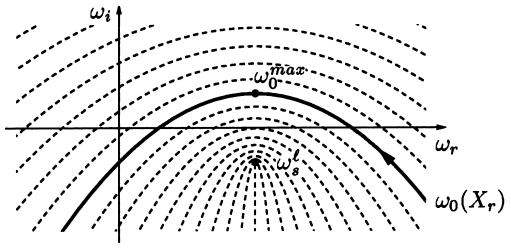

Fig. 7. Curves $\omega_0(X_\mathrm{r} + \mathrm{i}X_\mathrm{i})$ in the complex frequency plane for different values of X_i when X_r varies along the entire real axis. Bold curve pertains to $X_\mathrm{i} = 0$. The linear saddle point frequency $\omega_\mathrm{s}^\mathrm{l}$ is obtained at a cusp of this set of curves and is seen to lie below $\omega_0^{\max}$, towards the center of curvature of the $\omega_0(X_\mathrm{r})$ curve.

X-plane.[1] The frequency of the linear global mode is then equal to the saddle point frequency $\omega_\mathrm{s}^\mathrm{l}$, defined by

$$\omega_\mathrm{s}^\mathrm{l} = \omega_0(X_\mathrm{s}^\mathrm{l}), \qquad \frac{\mathrm{d}\omega_0}{\mathrm{d}X}(X_\mathrm{s}^\mathrm{l}) = 0, \tag{25}$$

or equivalently by

$$\omega_\mathrm{s}^\mathrm{l} = \Omega^\mathrm{l}(k_\mathrm{s}^\mathrm{l}, X_\mathrm{s}^\mathrm{l}), \qquad \frac{\partial\Omega^\mathrm{l}}{\partial k}(k_\mathrm{s}^\mathrm{l}, X_\mathrm{s}^\mathrm{l}) = \frac{\partial\Omega^\mathrm{l}}{\partial X}(k_\mathrm{s}^\mathrm{l}, X_\mathrm{s}^\mathrm{l}) = 0. \tag{26}$$

Linear global instability is determined by the sign of $\omega_{\mathrm{s,i}}^\mathrm{l} \equiv \mathrm{Im}\,\omega_\mathrm{s}^\mathrm{l}$, when $\omega_{\mathrm{s,i}}^\mathrm{l} < 0$ (resp. $\omega_{\mathrm{s,i}}^\mathrm{l} > 0$) the state $\psi = 0$ is linearly stable (resp. unstable).

4.5. Hysteresis

The existence of nonlinear steep global modes is determined by the sign of $\omega_{0,\mathrm{i}}^{\max}$, while the linear global instability of the unperturbed state $\psi = 0$ is dictated by the sign of $\omega_{\mathrm{s,i}}^\mathrm{l}$. It is now shown qualitatively that always $\omega_{0,\mathrm{i}}^{\max} \geq \omega_{\mathrm{s,i}}^\mathrm{l}$, and in general $\omega_{0,\mathrm{i}}^{\max} > \omega_{\mathrm{s,i}}^\mathrm{l}$. Thus, steep global modes may exist in globally linearly stable media (situations where $\omega_{\mathrm{s,i}}^\mathrm{l} < 0 < \omega_{0,\mathrm{i}}^{\max}$), and the saddle-node bifurcation implies hysteretic behavior as $\omega_{0,\mathrm{i}}^{\max}$ is varied.

The relative position of $\omega_{0,\mathrm{i}}^{\max}$ and $\omega_{\mathrm{s,i}}^\mathrm{l}$ is most conveniently illustrated in the complex frequency plane as sketched in Fig. 7. The solid curve represents $\omega_0(X)$ for real X. The AU region corresponds to the X-interval over which $\omega_0(X)$ lies in the $\omega_\mathrm{i} > 0$ half-plane. The maximum $\omega_{0,\mathrm{i}}^{\max}$ is reached at $X = X^{\max}$. Thus, steep global modes exist whenever the curve $\omega_0(X)$ crosses the real ω-axis. The complex frequency $\omega_\mathrm{s}^\mathrm{l}$ is obtained at a saddle point of the analytically continued function $\omega_0(X)$. For most situations of physical interest, $\omega_{0,\mathrm{i}}(X)$ is an increasing–decreasing function on the real X-axis, while $\omega_{0,\mathrm{r}}(X)$ is simply a smooth function. The dashed curves of Fig. 7 represent the loci of $\omega_0(X_\mathrm{r} + \mathrm{i}X_\mathrm{i})$ for different values of X_i when X_r varies along the entire real axis. The saddle point frequency $\omega_\mathrm{s}^\mathrm{l}$ is obtained at a cusp of this set of curves and lies below the $\omega_0(X_\mathrm{r})$ curve, towards its center of curvature. Thus, it follows clearly that $\omega_{0,\mathrm{i}}^{\max} > \omega_{\mathrm{s,i}}^\mathrm{l}$ and one recovers the well-known result that global linear instability requires an AU region of finite extent [7,25].

In the neighborhood of $\omega_0^{\max}$, the absolute frequency $\omega_0(X)$ may be approximated by the Taylor expansion

$$\omega_0(X) \sim \omega_0^{\max} + \omega_{0X}(X - X^{\max}) + \tfrac{1}{2}\omega_{0XX}(X - X^{\max})^2 \tag{27}$$

[1] Only linear global modes with a double turning point are considered here. The reader is referred to Le Dizès et al. [25] for a detailed analysis of linear global modes with two simple turning points.

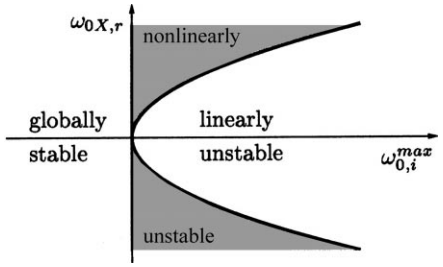

Fig. 8. Global linear and nonlinear stability in the $(\omega_{0,\mathrm{i}}^{\max}, \omega_{0X,\mathrm{r}})$-plane. Global stability is governed by the sign of $\omega_{0,\mathrm{i}}^{\max}$. When $\omega_{0,\mathrm{i}}^{\max} > 0$, the medium is globally nonlinearly unstable although globally linearly stable in the gray region.

with $\omega_{0X,\mathrm{i}} = 0$ and $\omega_{0XX,\mathrm{i}} < 0$. The linear saddle point, solution of (25), is then explicitly given by

$$X_{\mathrm{s}}^{\mathrm{l}} = X^{\max} - \frac{\omega_{0X,\mathrm{r}}}{\omega_{0XX}}, \qquad \omega_{\mathrm{s}}^{\mathrm{l}} = \omega_0^{\max} - \frac{1}{2}\frac{(\omega_{0X,\mathrm{r}})^2}{\omega_{0XX}}, \tag{28}$$

thus

$$\mathrm{Im}\,\omega_{\mathrm{s}}^{\mathrm{l}} = \omega_{0,\mathrm{i}}^{\max} + \frac{1}{2}\frac{(\omega_{0X,\mathrm{r}})^2}{|\omega_{0XX}|^2}\omega_{0XX,\mathrm{i}}.$$

Only if $\mathrm{d}\omega_{0,\mathrm{r}}(X^{\max})/\mathrm{d}X = 0$, does the saddle point $X_{\mathrm{s}}^{\mathrm{l}}$ coincide with $X^{\max}$ on the real X-axis and, under such a condition, $\omega_{\mathrm{s}}^{\mathrm{l}} = \omega_0(X^{\max})$. The difference between $\omega_{0,\mathrm{i}}^{\max}$ and $\omega_{\mathrm{s,i}}^{\mathrm{l}}$ is seen to depend on the magnitude of $\omega_{0X,\mathrm{r}} \equiv \mathrm{d}\omega_{0,\mathrm{r}}(X^{\max})/\mathrm{d}X$ and to scale as $(\omega_{0X,\mathrm{r}})^2$. The influence of the two parameters $\omega_{0,\mathrm{i}}^{\max}$ and $\omega_{0X,\mathrm{r}}$ on global linear and nonlinear instability is illustrated in Fig. 8.

The following scenario holds as the global control parameter $\omega_{0,\mathrm{i}}^{\max}$ is varied at a fixed $\omega_{0X,\mathrm{r}}$ setting. When $\omega_{0,\mathrm{i}}^{\max} < 0$ (left-hand half-plane of Fig. 8), the unperturbed state is stable, no nonlinear global mode exists. When $\omega_{0,\mathrm{i}}^{\max} > 0$ while $\omega_{\mathrm{s,i}}^{\mathrm{l}} < 0$ (shaded region of Fig. 8), a pair of steep global modes exist, one of which is stable, the other unstable. However, the unperturbed state is still linearly globally stable, [2] but nonlinearly unstable. Only for $\omega_{0,\mathrm{i}}^{\max}$ large enough such that $\omega_{\mathrm{s,i}}^{\mathrm{l}} > 0$ (clear region inside parabola of Fig. 8), does the basic state become linearly unstable. Whereas the global saddle-node bifurcation is controlled by $\omega_{0,\mathrm{i}}^{\max}$, the extent of the hysteresis range in $\omega_{0,\mathrm{i}}^{\max}$ is governed by a second control parameter, namely $\omega_{0X,\mathrm{r}}$.

4.6. Soft global modes

The existence of soft global modes has been analyzed in an earlier study [33]. Their structure is now briefly summarized, as well as their relationship to steep global modes. The sketch in Fig. 9a represents the envelope $|\psi|$ and real part ψ_{r} of a soft global mode obtained by direct numerical simulation of the CGL equation (4). The length of the computational domain is $L = 102$. Linear and parabolic variations are, respectively, used for $\omega_{0,\mathrm{r}}(X)$ and $\omega_{0,\mathrm{i}}(X)$ so that $\omega_0^{\mathrm{ca}} = 0.5$, $\omega_0^{\mathrm{ac}} = 0.6$, $\omega_{0,\mathrm{i}}^{\max} = 0.5$ and $X^{\mathrm{ca}} = \frac{1}{5}L$, $X^{\mathrm{ac}} = \frac{4}{5}L$. Other coefficients take the constant values $k_0 = 1.0 - 0.1\mathrm{i}$, $\omega_{kk} = 1 - 0.5\mathrm{i}$ and $\gamma = 0.2 - \mathrm{i}$.

In contrast to steep modes, no front is present and soft modes display an overall smoothly varying envelope and wave number (thick curve in Fig. 9c). The connection between the upstream $-$ branch and the downstream $+$ branch occurs here in the core of the nonlinear region, at a saddle point of the nonlinear dispersion relation (20).

[2] The unperturbed state is, however, locally unstable.

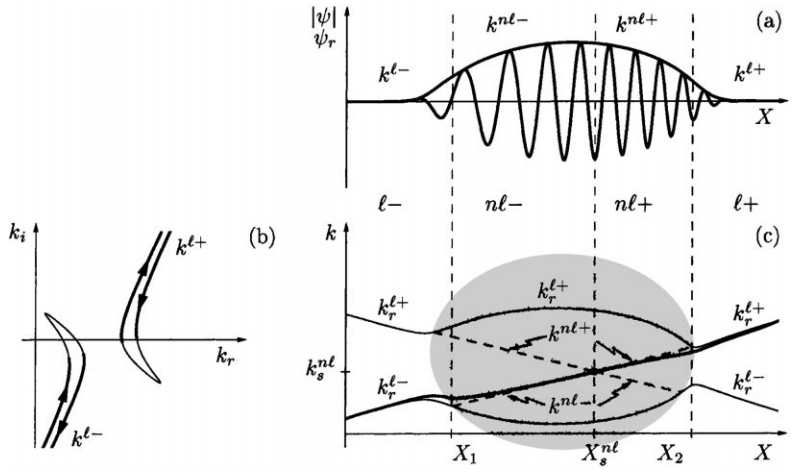

Fig. 9. Structure of soft global mode obtained by direct numerical simulation of CGL equation. (a) Overall smoothly varying envelope $|\psi|$ and real part ψ_r as functions of downstream distance X. (b) Analytically computed linear spatial branches $k^{l\pm}(X)$ of nonlinear saddle point frequency ω_s^{nl} in the complex k-plane. Both linear branches cross the k_r-axis and give birth to their nonlinear counterparts at the respective neutral stations. Thick lines pertain to the stable or CU regions $X < X^{ca}$ and $X > X^{ac}$, thin lines to the central AU region $X^{ca} < X < X^{ac}$. (c) Corresponding linear $k_r^{l\pm}$ (thin solid) and nonlinear $k^{nl\pm}$ (thin dashed) spatial branches in the (X, k)-plane. Pinching of nonlinear branches occurs for k_s^{nl} at $X = X_s^{nl}$ in the core of the nonlinear region. Local wave number of simulation in (a) follows path indicated by thick line. Four domains are identified: the central nonlinear nl− and nl+ regions prevail upstream and downstream of X_s^{nl} where the nonlinear spatial branches k^{nl-} and k^{nl+} meet; at the upstream X_1 and downstream X_2 boundaries of the nonlinear balloon (shaded) the nonlinear spatial branches are continuously connected to their respective linear counterparts $k^{l\pm}$ prevailing in the semi-infinite linear regions l− and l+, respectively.

As already discussed in Section 3.3, the nonlinear branches $k^{nl\pm}(X, \omega)$, formally defined as the level contours $\Omega^{nl}(k, X) = C^{st}$, may display a saddle point (X_s^{nl}, k_s^{nl}) in the (X, k)-plane (solid dot in Fig. 5). More precisely, pinching of the nonlinear branches, defined by the condition

$$k^{nl+}(X_s^{nl}, \omega_s^{nl}) = k^{nl-}(X_s^{nl}, \omega_s^{nl}) = k_s^{nl},$$

then occurs at the real station X_s^{nl} for the real saddle point frequency ω_s^{nl} of Ω^{nl} such that

$$\omega_s^{nl} = \Omega^{nl}(k_s^{nl}, X_s^{nl}), \qquad \frac{\partial \Omega^{nl}}{\partial k}(k_s^{nl}, X_s^{nl}) = \frac{\partial \Omega^{nl}}{\partial X}(k_s^{nl}, X_s^{nl}) = 0 \tag{29}$$

with the saddle condition

$$\left(\frac{\partial^2 \Omega^{nl}}{\partial k \partial X}(k_s^{nl}, X_s^{nl})\right)^2 - \frac{\partial^2 \Omega^{nl}}{\partial k^2}(k_s^{nl}, X_s^{nl}) \frac{\partial^2 \Omega^{nl}}{\partial X^2}(k_s^{nl}, X_s^{nl}) > 0. \tag{30}$$

Note the formal analogy of this nonlinear saddle point criterion (29) with its linear counterpart (26) which involves in general complex values of k_s^l and X_s^l. The upstream $k^{nl-}(X, \omega_s^{nl})$ branch and downstream $k^{nl+}(X, \omega_s^{nl})$ branch are precisely initiated at the nonlinear saddle point X_s^{nl}, as depicted in Fig. 9c. These nonlinear travelling waves prevail in the range $X_1 < X < X_2$, where X_1 and X_2 denote the neutrally stable stations of frequency ω_s^{nl} at the boundary of the nonlinear balloon in the (X, k)-plane. At X_1 and X_2, the amplitudes of the nonlinear travelling waves k^{nl-} and k^{nl+}, respectively, vanish and give way to their linear counterparts k^{l-} and k^{l+}, respectively.

For the CGL equation (4) with $\omega_0(X)$ of the form (27), all other coefficients being kept uniform in X, the nonlinear saddle point location is explicitly obtained as

$$X_{\mathrm{s}}^{\mathrm{nl}} = X^{\max} + \frac{\gamma_{\mathrm{i}}\omega_{0X,\mathrm{r}}}{\mathrm{Im}(\gamma^{\star}\omega_{0XX})}, \tag{31}$$

$$k_{\mathrm{s}}^{\mathrm{nl}} = k_{0,\mathrm{r}} + \frac{\mathrm{Re}(\gamma^{\star}\omega_{kk})}{\mathrm{Im}(\gamma^{\star}\omega_{kk})}k_{0,\mathrm{i}}, \tag{32}$$

and the soft global mode frequency reads

$$\omega_{\mathrm{s}}^{\mathrm{nl}} = \omega_{0,\mathrm{r}}^{\max} - \frac{\gamma_{\mathrm{r}}}{\gamma_{\mathrm{i}}}\omega_{0,\mathrm{i}}^{\max} + \frac{\gamma_{\mathrm{i}}(\omega_{0X,\mathrm{r}})^2}{2\,\mathrm{Im}(\gamma^{\star}\omega_{0XX})} + \frac{|\gamma^{\star}\omega_{kk}|^2}{2\gamma_{\mathrm{i}}\,\mathrm{Im}(\gamma^{\star}\omega_{kk})}k_{0,\mathrm{i}}^2. \tag{33}$$

The numerically obtained global frequency $\omega_{\mathrm{g}} = 0.64$ of Fig. 9 very favorably compares with the analytical prediction (33) of $\omega_{\mathrm{s}}^{\mathrm{nl}} = 0.65$.

Condition (30) requires that $(\mathrm{Im}\,\gamma^{\star}\omega_{kk})(\mathrm{Im}\,\gamma^{\star}\omega_{0XX}) < 0$. It was shown in [33] that in situations where

$$\mathrm{Im}(\gamma^{\star}\omega_{kk}) > 0, \tag{34}$$

the nonlinear branches $k^{\mathrm{nl}\pm}$ exist in the neighborhood of $X_{\mathrm{s}}^{\mathrm{nl}}$ for frequencies such that $\omega > \omega_{\mathrm{s}}^{\mathrm{nl}}$. When $\omega \downarrow \omega_{\mathrm{s}}^{\mathrm{nl}}$, the branches pinch at $k_{\mathrm{s}}^{\mathrm{nl}}$ for $X = X_{\mathrm{s}}^{\mathrm{nl}}$, and for $\omega < \omega_{\mathrm{s}}^{\mathrm{nl}}$, they fail to be defined around $X_{\mathrm{s}}^{\mathrm{nl}}$. In the following it is always assumed that the possible frequencies for the nonlinear spatial branches lie in the range $\omega > \omega_{\mathrm{s}}^{\mathrm{nl}}$. The opposite situation is exactly analogous and applies when $\mathrm{Im}(\gamma^{\star}\omega_{kk}) < 0$.

4.7. Transition between soft and steep global modes

The selection mechanisms governing steep and soft global modes are now compared. The steep criterion (24) only involves the boundary of the AU domain on the physical X-axis, regardless of the characteristics of the regions $X \neq X^{\mathrm{ca}}$. Nevertheless, a steep global mode only exists if the nonlinear $k^{\mathrm{nl}+}(X, \omega_0^{\mathrm{ca}})$ branch can be followed from X^{ca} down to the boundary of the nonlinear balloon and if there it can be continuously connected to the linear branch $k^{\mathrm{l}+}(X, \omega_0^{\mathrm{ca}})$. In contrast, the soft criterion (29) involves a saddle point of the nonlinear dispersion relation. Again, a soft global mode only exists if the nonlinear spatial branches issuing from this nonlinear pinch point may effectively be continued via corresponding linear $k^{\mathrm{l}\pm}$ branches in the respective downstream and upstream linear domains.

Selection of either steep or soft global modes depends not only on the local criteria (24) and (29), but also on the necessity to enforce the boundary conditions. The key argument in the following derivation is based on a careful monitoring of the linear wave number branches in the complex k-plane and of their nonlinear counterparts in the (X, k)-plane as the global frequency is varied. As always, the CGL equation is used to illustrate the different scenarios. The connection between linear and nonlinear spatial branches is shown to crucially depend on the relative magnitude of the characteristic frequencies $\omega_{\mathrm{s}}^{\mathrm{nl}}$ and ω_0^{ca}. In all instances, only one global mode, steep or soft, is capable of continuously converting $k^{\mathrm{l}-}$ at $X = -\infty$ to $k^{\mathrm{l}+}$ at $X = +\infty$, as X is varied. The two main scenarios of interest are illustrated in Figs. 10 and 11, respectively, as discussed below.

Since nonlinear global modes necessarily involve real frequencies, let us focus on frequencies on the real ω-axis. As shown in Section 3.2, for large positive or negative ω the linear spatial branches do not cross the k_{r}-axis in the complex k-plane. Since nonlinear spatial branches are assumed to exist for $\omega > \omega_{\mathrm{s}}^{\mathrm{nl}}$, we start with large positive values of the frequency.

As ω is decreased, the $k^{\mathrm{l}\pm}(X, \omega)$ branches move in closer to each other and one or both cross the k_{r}-axis for finite values of X. A change in sign of $k_{\mathrm{i}}^{\mathrm{l}}$ signifies that the corresponding branch is spatially growing: downstream spatial

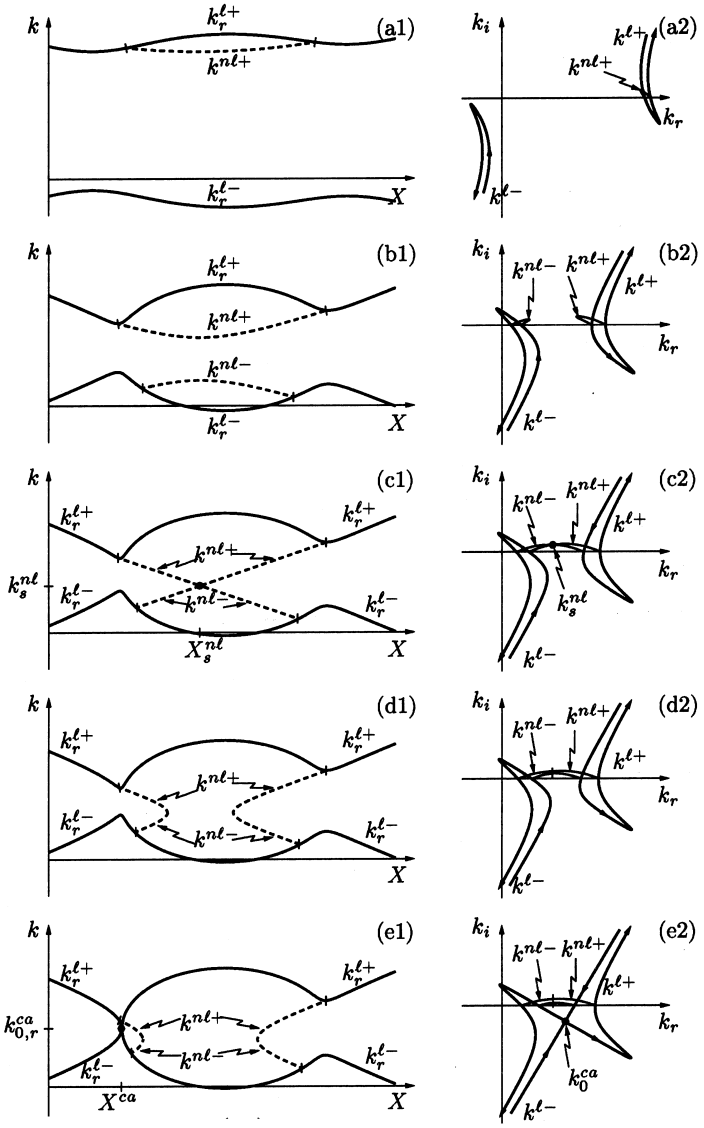

Fig. 10. Evolution of CGL spatial branches with decreasing real frequency in a situation where the soft global mode is selected. The left sequence illustrates the evolution of the real part of linear branches $k_{\mathrm{r}}^{\mathrm{l}\pm}(X,\omega)$ (solid lines) and of nonlinear branches $k^{\mathrm{nl}\pm}(X,\omega)$ (dashed lines) in the (X,k)-plane. Connecting points between linear and nonlinear branches are indicated with tick marks. In the right sequence, corresponding complex linear $k^{\mathrm{l}\pm}(X,\omega)$ branches are sketched in the complex $(k_{\mathrm{r}},k_{\mathrm{i}})$-plane; superimposed on the same graphs are the curves $(k^{\mathrm{nl}\pm},R^2)$ of the nonlinear spatial branches. (a), (b) For frequencies $\omega>\omega_{\mathrm{s}}^{\mathrm{nl}}$ linear $k^{\mathrm{l}\pm}$ spatial branches successively cross the k_{r}-axis in the complex k-plane and give birth to the nonlinear $k^{\mathrm{nl}\pm}$ branches between the corresponding neutral stations. (c) For the nonlinear saddle point frequency $\omega_{\mathrm{s}}^{\mathrm{nl}}$, nonlinear spatial branches pinch at $k_{\mathrm{s}}^{\mathrm{nl}}$ when $X=X_{\mathrm{s}}^{\mathrm{nl}}$. This pinch point joining $k^{\mathrm{nl}-}$ and $k^{\mathrm{nl}+}$ branches gives rise to a soft global mode connecting the $k^{\mathrm{l}-}$ branch near $X=-\infty$ to the $k^{\mathrm{l}+}$ branch prevailing near $X=+\infty$. (d), (e) For frequencies $\omega<\omega_{\mathrm{s}}^{\mathrm{nl}}$, the nonlinear spatial branches fail to exist in the neighborhood of $X_{\mathrm{s}}^{\mathrm{nl}}$, but linear $k^{\mathrm{l}\pm}$ branches are still defined. (e) When $\omega=\omega_0^{\mathrm{ca}}$, the linear branches in turn pinch at $k=k_0^{\mathrm{ca}}$ at the upstream boundary X^{ca} of AU region. However, this pinch point is not associated with a steep global mode since the $k^{\mathrm{nl}+}$ branch prevailing for $X>X^{\mathrm{ca}}$ is not connected to the $k^{\mathrm{l}+}$ branch extending to $X=+\infty$.

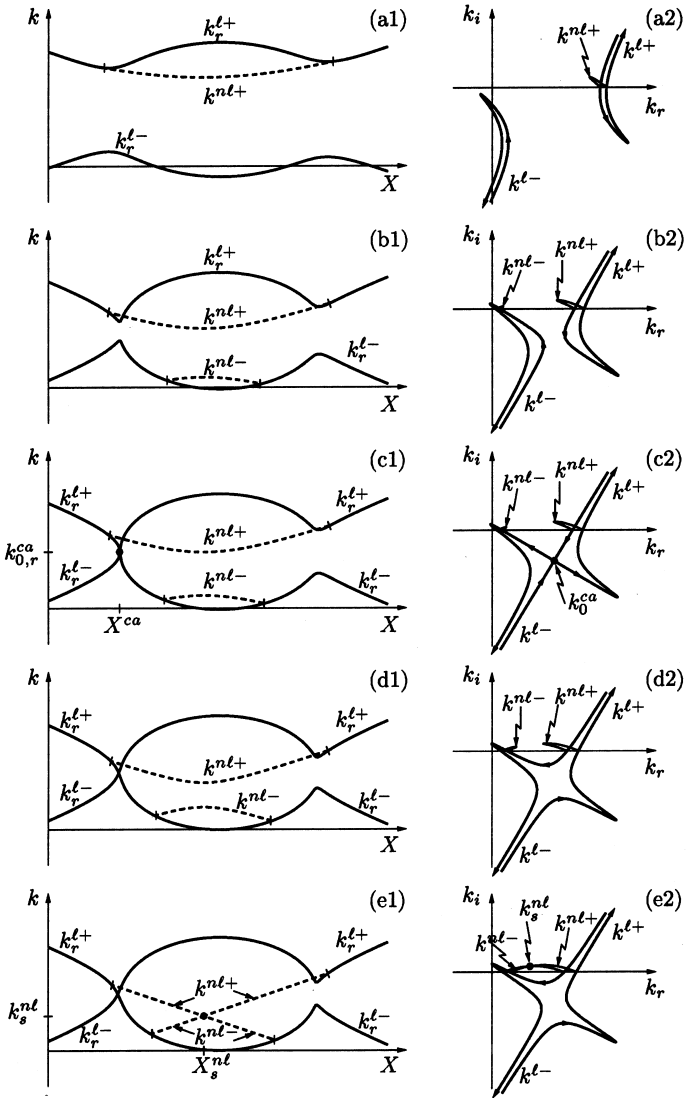

Fig. 11. Evolution of CGL spatial branches with decreasing real frequency in a situation where the steep global mode is selected. The left sequence illustrates the evolution of the real part of linear branches $k_r^{l\pm}(X,\omega)$ (solid lines) and of nonlinear branches $k^{nl\pm}(X,\omega)$ (dashed lines) in the (X,k)-plane. Connecting points between linear and nonlinear branches are indicated with tick marks. In the right sequence, corresponding complex linear $k^{l\pm}(X,\omega)$ branches are sketched in the complex (k_r,k_i)-plane; superimposed on the same graphs are the curves $(k^{nl\pm}, R^2)$ of the nonlinear spatial branches. (a), (b) For frequencies $\omega > \omega_0^{ca}$ linear spatial branches remain separated, nonlinear branches exist between the corresponding neutral stations. (c) For the front frequency ω_0^{ca}, linear spatial branches pinch at k_0^{ca} when $X = X^{ca}$. A sharp front at X^{ca} associated with a wave number jump from k^{l-} to k^{nl+} then gives rise to a global mode connecting the k^{l-} branch near $X = -\infty$ to the k^{l+} branch prevailing near $X = +\infty$. (d), (e) For frequencies $\omega < \omega_0^{ca}$, branch switching between k^{l+} and k^{l-} occurs. (e) When $\omega = \omega_s^{nl}$, the nonlinear branches meet at the nonlinear saddle point location X_s^{nl}. However, this saddle point is not associated with a global mode since no continuous connection to the k^{l-} branch prevailing near $X = -\infty$ exists.

growth for $k_i^{l+} < 0$ and upstream spatial growth for $k_i^{l-} > 0$. As already mentioned (Section 2.3) a spatially growing branch $k^{l\pm}$ gives way to its nonlinear counterpart $k^{nl\pm}$ as a neutrally stable station is crossed in the (X,k)-plane.

Nonlinear k^{nl} branches are by construction always real-valued. However, to illustrate their relationship with the linear k^{l} branches they are also represented in the complex k-planes of Figs. 10 and 11. For clarity their missing

imaginary part is replaced by the square of the amplitude of the corresponding nonlinear solution. This avoids the collapse of the k^{nl} branches onto the k_{r}-axis, and brings to the fore the continuity between linear and nonlinear branches at the neutral stations where $k_{\mathrm{i}}^{\mathrm{l}}$ as well as the nonlinear amplitude vanish.

In the following discussion representations in the (X, k_{r})- and the $(k_{\mathrm{r}}, k_{\mathrm{i}})$-planes are always shown in parallel. Although the $+$ and $-$ superscripts may not be derived from causality considerations in the AU domain, linear as well as nonlinear $+$ and $-$ branches may be defined without ambiguity as long as the linear and nonlinear branches remain distinct (cf. Sections 3.2 and 3.3).

The branch switching scenario as ω decreases depends on the relative values of the characteristic frequencies $\omega_{\mathrm{s}}^{\mathrm{nl}}$ and ω_0^{ca}. The frequency ω_0^{ac} which corresponds to an unstable steep global mode with a front at the downstream boundary of the AU domain does not play an essential part. For clarity assume that $\omega_0^{\mathrm{ca}} > \omega_0^{\mathrm{ac}}$ and $\omega_{\mathrm{s}}^{\mathrm{nl}} > \omega_0^{\mathrm{ac}}$. If these assumptions are not satisfied, the same selection mechanisms as discussed below prevail, although the detailed topology of spatial branches may be different. Two possibilities now arise: $\omega_{\mathrm{s}}^{\mathrm{nl}} > \omega_0^{\mathrm{ca}}$ or $\omega_{\mathrm{s}}^{\mathrm{nl}} < \omega_0^{\mathrm{ca}}$.

The scenario for $\omega_{\mathrm{s}}^{\mathrm{nl}} > \omega_0^{\mathrm{ca}}$ is illustrated in the sequence of Fig. 10. As ω is decreased, the two linear spatial branches successively cross the k_{r}-axis while remaining separated as depicted in Fig. 10a and b. Each crossing gives birth to a corresponding nonlinear branch connected to its linear counterpart at the neutrally stable locations where k^{l} is real. Both linear and nonlinear $+$ and $-$ branches are well identified and separated. When $\omega \downarrow \omega_{\mathrm{s}}^{\mathrm{nl}}$, the nonlinear branches gradually approach each other. For $\omega = \omega_{\mathrm{s}}^{\mathrm{nl}}$ (Fig. 10c), the $k^{\mathrm{nl}+}$ branch meets the $k^{\mathrm{nl}-}$ branch at $k_{\mathrm{s}}^{\mathrm{nl}}$ for $X = X_{\mathrm{s}}^{\mathrm{nl}}$ as determined by (29). This is the soft global mode configuration, where the nonlinear saddle point at $X_{\mathrm{s}}^{\mathrm{nl}}$ connects the nonlinear $k^{\mathrm{nl}-}(X, \omega_{\mathrm{s}}^{\mathrm{nl}})$ in the region $X < X_{\mathrm{s}}^{\mathrm{nl}}$ to the nonlinear $k^{\mathrm{nl}+}(X, \omega_{\mathrm{s}}^{\mathrm{nl}})$ in the region $X > X_{\mathrm{s}}^{\mathrm{nl}}$. Further outward, the nonlinear $k^{\mathrm{nl}\pm}$ branches give way to their respective linear counterparts $k^{\mathrm{l}\pm}$ at the locations of their respective neutral growth. When decreasing the global frequency to values $\omega < \omega_{\mathrm{s}}^{\mathrm{nl}}$, the nonlinear branches fail to exist in the neighborhood of $X_{\mathrm{s}}^{\mathrm{nl}}$ (Fig. 10d). As ω reaches ω_0^{ca} (Fig. 10e), linear spatial branches do pinch at $X = X^{\mathrm{ca}}$, but the nonlinear spatial branch $k^{\mathrm{nl}+}$ prevailing around X^{ca} cannot be continued far downstream towards the $k^{\mathrm{l}+}$ branch extending down to $X = +\infty$; there is no global mode of frequency ω_0^{ca}.

The scenario for $\omega_0^{\mathrm{ca}} > \omega_{\mathrm{s}}^{\mathrm{nl}}$ is sketched in the sequence of Fig. 11. As ω decreases, the first characteristic frequency encountered is now ω_0^{ca}. When $\omega \downarrow \omega_0^{\mathrm{ca}}$ (Fig. 11a–c), the linear branches approach and pinch at k_0^{ca} for $X = X^{\mathrm{ca}}$ determined by (29). Since $k_{0,\mathrm{i}}^{\mathrm{ca}} < 0$, the relevant branches in a neighborhood of X^{ca} are $k^{\mathrm{l}-}$ and $k^{\mathrm{nl}+}$. A front of frequency ω_0^{ca} at X^{ca} allows a discontinuous jump in wave number from $k^{\mathrm{l}-}(X^{\mathrm{ca}}, \omega_0^{\mathrm{ca}}) = k_0^{\mathrm{ca}}$ to $k^{\mathrm{nl}+}(X^{\mathrm{ca}}, \omega_0^{\mathrm{ca}})$. This front performs the connection between $-$ and $+$ branches necessary to obtain a steep global mode: further downstream, the amplitude of the nonlinear $k^{\mathrm{nl}+}$ branch vanishes at a neutrally stable station and there the linear $k^{\mathrm{l}+}$ branch takes over to $X = +\infty$. Note that the $k^{\mathrm{l}+}(X, \omega_0^{\mathrm{ca}})$ branch necessarily crosses the k_{r}-axis; the $k^{\mathrm{l}-}(X, \omega_0^{\mathrm{ca}})$ branch however may or may not cross. For $\omega = \omega_0^{\mathrm{ca}}$, the nonlinear branches, if they both exist, do not meet. Decreasing further ω towards $\omega_{\mathrm{s}}^{\mathrm{nl}}$ (Fig. 11d and e), the nonlinear branches in turn approach and pinch for $\omega = \omega_{\mathrm{s}}^{\mathrm{nl}}$. However, since $\omega_{\mathrm{s}}^{\mathrm{nl}} < \omega_0^{\mathrm{ca}}$, the linear $k^{\mathrm{l}\pm}$ branches have undergone branch switching for $\omega = \omega_0^{\mathrm{ca}}$. As can be seen in Fig. 11e, the nonlinear branches issuing at $k_{\mathrm{s}}^{\mathrm{nl}}$, $X_{\mathrm{s}}^{\mathrm{nl}}$ cannot be continued towards the $k^{\mathrm{l}-}$ branch near $X = -\infty$. In this situation, due to global considerations, no soft mode exists, although the local criterion (29) may be satisfied.

This completes the discussion of the global mode selection mechanism: the type of selected global mode depends on the relative values of the linear pinchpoint frequency ω_0^{ca} and nonlinear pinchpoint frequency $\omega_{\mathrm{s}}^{\mathrm{nl}}$. If

$$\omega_{\mathrm{s}}^{\mathrm{nl}} < \omega_0^{\mathrm{ca}},$$

linear spatial branches meet first as the overall frequency is lowered: the steep criterion (24) yields a global solution on the entire X-axis with a sharp front located at X^{ca}. However, if

$$\omega_0^{\mathrm{ca}} < \omega_{\mathrm{s}}^{\mathrm{nl}},$$

the nonlinear saddle point is encountered first and a soft global mode with overall smoothly varying envelope and wave number prevails. There exists also situations where the nonlinear dispersion relation displays no saddle point in the nonlinear balloon. Then a steep mode is necessarily obtained. The preceding close inspection of spatial linear and nonlinear branches guarantees that the selection criteria for steep and soft global modes are mutually exclusive, and that all situations are accounted for.

According to this discussion, when a global control parameter is continuously varied, the transition mechanism between soft and steep global modes is the following. Starting with a system where a soft mode is selected, i.e., where $\omega_s^{nl} > \omega_0^{ca}$, two possibilities arise if the control parameter is changed:

- The saddle point frequency ω_s^{nl} may equal the front frequency ω_0^{ca} for a critical value of the control parameter. Beyond this value, $\omega_s^{nl} < \omega_0^{ca}$, and a steep mode prevails. The transition to a steep mode of the same frequency takes place when $\omega_s^{nl} = \omega_0^{ca}$.
- The nonlinear saddle point may reach the boundary of the nonlinear balloon and disappear while still $\omega_s^{nl} > \omega_0^{ca}$. Then, transition to a steep mode again occurs, but in this situation the global frequency is discontinuous at transition.

This will be fully justified in Section 4.9, where we map out the domains of existence of soft and steep global modes in an appropriate control parameter space. To identify the relevant control parameters, a discussion of the role of the absolute wave number is first required.

4.8. Role of the absolute wave number

The local instability properties are seen to be essentially controlled by the streamwise evolution of the absolute frequency $\omega_0(X)$ and wave number $k_0(X)$ which in principle can be varied independently. The criterion for steep global modes (24) only depends on the local absolute frequency $\omega_0(X)$ regardless of the local absolute wave number $k_0(X)$. The soft global mode criterion (29), however, depends on $k_0(X)$ through the complete nonlinear dispersion relation. In this section, the role of the absolute wave number is discussed by varying $k_0(X)$ in the CGL equation, all other coefficients remaining fixed.

From expressions (23) for the linear spatial $k^{l\pm}$ branches it is readily seen that a change in $k_0(X)$ by some constant value, say κ, results in a displacement of the $k^{l\pm}$ curves in the complex k-plane. Under this process, the linear pinchpoint properties are not affected. Nonlinear characteristics, however, are closely related to the crossing of the k_r-axis by the $k^{l\pm}$ branches; it follows that changes in $k_{0,i}$ strongly influence the nonlinear properties of the medium, unlike changes of $k_{0,r}$. This calls for two distinct physical interpretations of $k_{0,r}$ and $k_{0,i}$, respectively.

Consider the uniform CGL equation (6) with k_0 replaced by $k_0 - \kappa_r$. Then, under the change of unknown function

$$\psi(x,t) = \phi(x,t)\,\mathrm{e}^{\mathrm{i}\kappa_r x},$$

the original CGL equation (6) is recovered for ϕ. This shows that the only effect of a change in $k_{0,r}$ is a change in wavelength; linear spatial growth or decay rates, frequencies as well as nonlinear amplitudes remain the same. A variation of $k_{0,r}$ results in a change of carrier wave but does not alter the linear or the nonlinear stability properties of the system. In the spatially dependent CGL equation (4), the following change of unknown function

$$\psi(x,t) = \phi(x,t)\exp\left(\frac{\mathrm{i}}{\epsilon}\int^X \kappa_r(u)\,\mathrm{d}u\right)$$

results in modifying the local absolute wave number to $k_0(X) - \kappa_r(X)$. Any slowly modulated carrier wave defined by the real function $\kappa_r(X)$ may thus be used to transform the real part of the absolute local wave number. Under such a transformation, the global mode selection criteria as well as the characteristic frequencies remain unaltered: the function $k_{0,r}(X)$ may then be chosen arbitrarily since it does not affect the local and global dynamics.

In order to bring to the fore the role of $k_{0,\mathrm{i}}(X)$, it is convenient, in the remainder of this section, to select $k_{0,\mathrm{r}}(X)$ so that the function $\omega_{kk}(X)k_0(X)$ appearing in front of the advection term $\partial\psi/\partial x$ in (4) is real [12]. Under such a condition,

$$k_{0,\mathrm{r}}(X) = -\frac{\omega_{kk,\mathrm{r}}(X)}{\omega_{kk,\mathrm{i}}(X)}k_{0,\mathrm{i}}(X),$$

and the CGL equation reads

$$\frac{\partial\psi}{\partial t} + \frac{|\omega_{kk}|^2}{\omega_{kk,\mathrm{i}}}k_{0,\mathrm{i}}\frac{\partial\psi}{\partial x} = -\mathrm{i}\left(\omega_0 + \frac{1}{2}\omega_{kk}k_0^2\right)\psi + \frac{\mathrm{i}}{2}\omega_{kk}\frac{\partial^2\psi}{\partial x^2} - \mathrm{i}\gamma|\psi|^2\psi. \tag{35}$$

The form (35) clearly indicates that the real factor

$$U(X) = \frac{|\omega_{kk}(X)|^2}{\omega_{kk,\mathrm{i}}(X)}k_{0,\mathrm{i}}(X)$$

may be interpreted as an advection velocity. Since causality requires that $\omega_{kk,\mathrm{i}} < 0$, a negative (positive) $k_{0,\mathrm{i}}$ is readily seen to correspond to advection towards $X = +\infty$ ($X = -\infty$). Thus, the sign of $k_{0,\mathrm{i}}$ controls the advection direction whereas its magnitude is directly related to the advection velocity. As stated in Section 1, it is assumed that $U(X) > 0$, i.e., $k_{0,\mathrm{i}}(X) < 0$ in the entire domain. The basic advection is then directed towards $X = +\infty$.

In order to further discuss the role of $k_{0,\mathrm{i}}$ in the selection of global modes, consider, for simplicity, that $k_{0,\mathrm{i}}$ is constant over the entire domain. A change in $k_{0,\mathrm{i}}$ is seen to be associated with a displacement of the $k^{\mathrm{l}\pm}$ curves along the k_{i}-axis in the complex k-plane. Its effect on the nonlinear balloon and nonlinear spatial branches in the (X, k)-plane is outlined in Fig. 12. Since the function $\omega_0(X)$ is kept fixed, a change of $k_{0,\mathrm{i}}$ leaves the extent of the AU

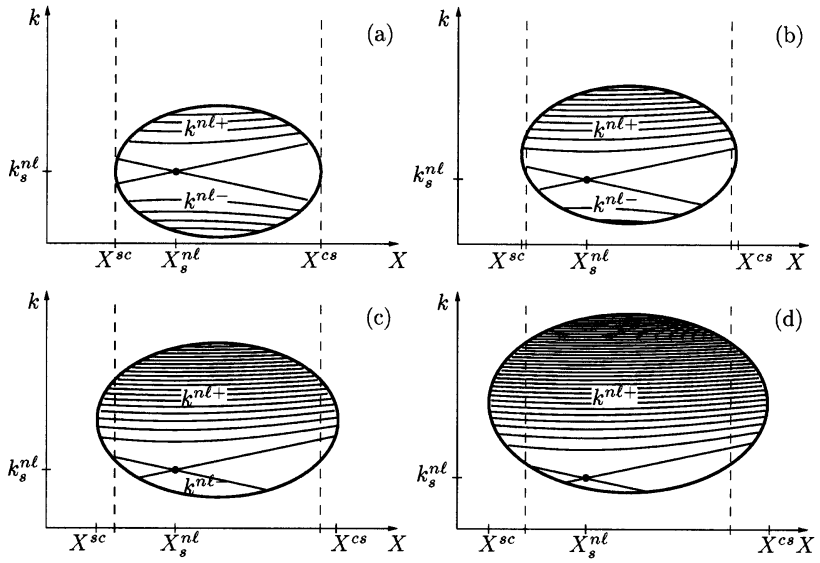

Fig. 12. Evolution of CGL nonlinear balloon and spatial $k^{\mathrm{nl}\pm}$ branches in the (X, k)-plane as the advection towards $X = +\infty$ is increased. Vertical dashed lines indicate AU domain extending over $X^{\mathrm{ca}} < X < X^{\mathrm{ac}}$. (a) Without mean advection ($k_{0,\mathrm{i}} = 0$), spatial branches display symmetry with respect to the nonlinear saddle point wave number $k_{\mathrm{s}}^{\mathrm{nl}}$ and the nonlinear domain exactly spans the AU region, $X^{\mathrm{sc}} = X^{\mathrm{ca}}$ and $X^{\mathrm{ac}} = X^{\mathrm{cs}}$. (b)–(d) With increasing downstream advection $k_{0,\mathrm{i}} < 0$, the nonlinear balloon inflates and extends beyond the AU region, $X^{\mathrm{sc}} < X^{\mathrm{ca}}$ and $X^{\mathrm{ac}} < X^{\mathrm{cs}}$. During this process the fraction of the nonlinear balloon covered by the downstream $k^{\mathrm{nl}+}$ branches increases with respect to the $k^{\mathrm{nl}-}$ branches. Simultaneously, the nonlinear saddle point $(X_{\mathrm{s}}^{\mathrm{nl}}, k_{\mathrm{s}}^{\mathrm{nl}})$ is seen to descend to eventually leave the nonlinear balloon.

range $X^{ca} < X < X^{ac}$ unaltered, as indicated by vertical dashed lines $X = X^{ca}$ and $X = X^{ac}$ in Fig. 12. Without mean advection, $k_{0,i} = 0$ (Fig. 12a), the nonlinear balloon exactly spans the AU region. In this situation, local linear instability coincides with local absolute instability: $X^{sc} = X^{ca}$ and $X^{ac} = X^{cs}$. Nonlinear spatial branches cover the nonlinear balloon symmetrically with respect to $k = k_s^{nl}$. Fig. 12b–d is obtained for increasing negative values of $k_{0,i}$, i.e., increasing advection towards $X = +\infty$. Increasing $|k_{0,i}|$ then shifts the $k^{l\pm}$ branches (23) towards negative k_i in the complex k-plane, thereby enhancing the instability of the downstream k^{l+} branches and reducing the instability of the upstream k^{l-} branches. Under such circumstances, the onset of linear instability no longer coincides with transition to absolute instability: the nonlinear balloon inflates and extends beyond the AU range into the CU regions $X^{sc} < X < X^{ca}$ and $X^{ac} < X < X^{cs}$. The basic flow advection breaks the k^{nl+}/k^{nl-} symmetry, and the part of the nonlinear balloon spanned by the k^{nl+} branches increases to the detriment of the k^{nl-} branches. During this process, the nonlinear saddle point moves towards the lower neutral stability boundary and eventually leaves the nonlinear balloon. The advection velocity, measured by $k_{0,i}$, thus strongly affects the existence of the nonlinear saddle point and hence the existence of smooth global modes.

In the remainder of this section, we temporarily allow advection in the positive or negative direction so that $k_{0,i}$ may change sign. It has been shown in Section 4.2 that among the two stationary fronts at X^{ca} and X^{ac}, only the one located at the upstream boundary of the AU region is stable. Since flow direction is directly related to the sign of $k_{0,i}$, the stable steep global mode frequency is ω_0^{ca} for $k_{0,i} < 0$ and ω_0^{ac} for $k_{0,i} > 0$. These are indeed the fronts at the stations of local marginal absolute instability with their nonlinear wave train covering the AU domain and their exponentially decaying tail extending into the CU region (see also Fig. 13). The soft global mode frequency ω_s^{nl} has been obtained in (33), and, in contrast to the steep global mode frequencies ω_0^{ca} and ω_0^{ac}, it is seen to depend on $k_{0,i}$.

In the previous section, it has been demonstrated that the global mode of largest frequency is selected; thus, the transition scenario between steep and soft global modes as a function of $k_{0,i}$ is derived from the relative values of ω_0^{ca}, ω_0^{ac} and $\omega_s^{nl}(k_{0,i})$, as displayed in Fig. 13. According to (33), the soft frequency ω_s^{nl} is largest for $k_{0,i} = 0$, all other coefficients being kept fixed. Thus, soft modes prevail when advection is small enough, $\omega_s^{nl} > \omega_0^{ca}$ and $\omega_s^{nl} > \omega_0^{ac}$. With increasing downstream advection ($k_{0,i} < 0$), the nonlinear saddle point frequency ω_s^{nl} decreases. When $\omega_s^{nl} < \omega_0^{ca}$, the soft mode is replaced by a steep mode with a sharp front at X^{ca} (left-hand side of Fig. 13). Similarly, if $k_{0,i}$ increases from 0 ($k_{0,i} > 0$), which corresponds to advection towards $X = -\infty$, the nonlinear

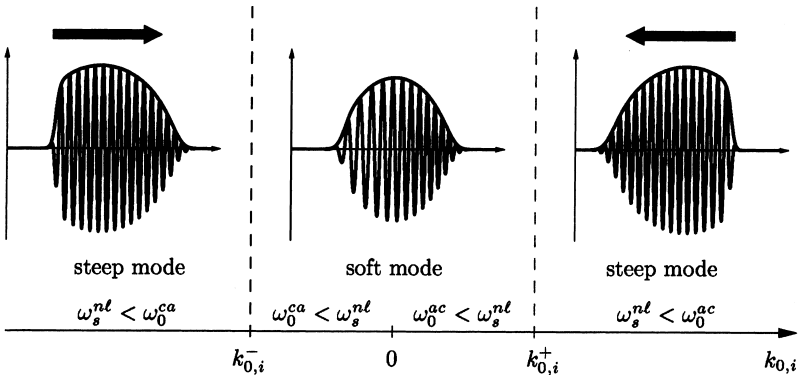

Fig. 13. Transition between steep and soft global modes as a function of $k_{0,i}$ in CGL equation. Black arrows indicate advection direction. For small advection velocities ($k_{0,i}$ small), the saddle point frequency ω_s^{nl} is larger than the front frequencies ω_0^{ca} and ω_0^{ac}, and thus a soft global mode is selected. With increasing advection towards $X = +\infty$ ($k_{0,i} < 0$), the saddle point frequency ω_s^{nl} decreases, and, when $k_{0,i} < k_{0,i}^-$ the soft mode is replaced by a steep global mode with a front at the left boundary of the AU region. Similarly, with increasing advection towards $X = -\infty$ ($k_{0,i} > 0$), the saddle point frequency ω_s^{nl} again decreases, and at $k_{0,i} = k_{0,i}^+$ transition takes place to a steep global mode with a front at the right boundary of the AU region.

saddle point frequency ω_s^{nl} again decreases. When $\omega_s^{nl} < \omega_0^{ac}$, the soft mode is now replaced by a steep mode with a front at $X = X^{ac}$ (right-hand side of Fig. 13). Since $k_{0,i} > 0$, the front at X^{ac} is now the stable one: upstream and downstream directions have been interchanged. In any case, the front location corresponds to the upstream boundary of the AU region. The critical transition values $k_{0,i}^- < 0$ and $k_{0,i}^+ > 0$ between soft and steep global modes are defined by $\omega_0^{ca} = \omega_s^{nl}$ and $\omega_0^{ac} = \omega_s^{nl}$, respectively.

4.9. Domains of existence in control parameter space

Now that the roles of $\omega_{0,i}^{max}$, $\omega_{0X,r}$ and $k_{0,i}$ have been separately discussed, the domains of existence of steep and soft global modes may be obtained in the three-dimensional space of these control parameters (Fig. 14). Consider the CGL equation (4) with $\omega_0(X)$ of the form (27), all other coefficients being assumed uniform in X for simplicity. The front frequencies ω_0^{ca} and ω_0^{ac} then read

$$\omega_0^{ca}, \omega_0^{ac} = \omega_{0,r}^{max} - \frac{\omega_{0XX,r}}{\omega_{0XX,i}}\omega_{0,i}^{max} \mp \omega_{0X,r}\sqrt{\frac{2\omega_{0,i}^{max}}{-\omega_{0XX,i}}}. \tag{36}$$

They exist whenever $\omega_{0,i}^{max} > 0$ and their values are seen to be effectively independent of $k_{0,i}$.

The selected global mode type depends on the relative values of the front frequencies (36) and the nonlinear saddle point frequency ω_s^{nl} (33). However, note that the nonlinear saddle point formally defined by (31) and (32) only exists if (k_s^{nl}, X_s^{nl}) lies in the nonlinear balloon, i.e., if

$$\Omega_i^l(k_s^{nl}, X_s^{nl}) > 0. \tag{37}$$

For the CGL equation under study, one readily obtains

$$\Omega_i^l(k_s^{nl}, X_s^{nl}) = \omega_{0,i}^{max} + \frac{1}{2}\omega_{0XX,i}\left(\frac{\gamma_i}{\mathrm{Im}\,\gamma^\star\omega_{0XX}}\right)^2(\omega_{0X,r})^2 + \frac{|\omega_{kk}|^2\,\mathrm{Im}\,\gamma^2\omega_{kk}^\star}{2(\mathrm{Im}\,\gamma^\star\omega_{kk})^2}(k_{0,i})^2. \tag{38}$$

Whenever $\Omega_i^l(k_s^{nl}, X_s^{nl}) < 0$, the nonlinear saddle point does not exist, and only a steep global mode is obtained. In the control parameter space of Fig. 14, the domain where condition (37) is satisfied is located above the surface labeled $\Omega_i^l(k_s^{nl}, X_s^{nl}) = 0$. According to (38), this surface is a paraboloid entirely contained in the half-space $\omega_{0,i}^{max} \geq 0$ and tangent to the plane $\omega_{0,i}^{max} = 0$ at $\omega_{0X,r} = k_{0,i} = 0$. Below this surface no soft mode may exist and only steep modes are obtained. Above this surface, the soft global frequency ω_s^{nl} must be compared to ω_0^{ca} and ω_0^{ac}. We only consider situations with advection towards $X = +\infty$, i.e., the half-space $k_{0,i} < 0$, so that only ω_0^{ca} comes into consideration for steep modes. Within the region where a nonlinear saddle point exists, transition between soft and steep modes occurs when $\omega_s^{nl} = \omega_0^{ca}$. This transition surface is derived from (33) and (36) and is sketched in Fig. 14. It is seen to meet the surface $\Omega_i^l(k_s^{nl}, X_s^{nl}) = 0$ along a curve in the plane $k_{0,i} = 0$. As may be inferred from these critical surfaces, the parameter space is divided into four regions (Fig. 14):

- (a) Below the global threshold, $\omega_{0,i}^{max} < 0$, no front and no saddle point exists, the unperturbed state $\psi = 0$ remains stable.
- (b) When $\omega_{0,i}^{max} > 0$ and $\Omega_i^l(k_s^{nl}, X_s^{nl}) < 0$, no saddle point exists and a steep global mode prevails.
- (c) When $\Omega_i^l(k_s^{nl}, X_s^{nl}) > 0$ and $\omega_s^{nl} < \omega_0^{ca}$, a saddle point exists but the steep mode is selected.
- (d) When $\Omega_i^l(k_s^{nl}, X_s^{nl}) > 0$ and $\omega_s^{nl} > \omega_0^{ca}$, the soft mode is selected.

Thus, at global mode onset $\omega_{0,i}^{max} = 0$, transition occurs always via a steep global mode except for the triply degenerate case $\omega_{0,i}^{max} = k_{0,i} = \omega_{0X,r} = 0$. With increasing $\omega_{0,i}^{max}$, transition from a steep to a soft mode occurs for finite values of $\omega_{0,i}^{max}$ either as soon as the nonlinear saddle point comes into existence (on the surface $\Omega_i^l(k_s^{nl}, X_s^{nl}) = 0$) or when its frequency reaches the steep frequency (on the surface $\omega_s^{nl} = \omega_0^{ca}$).

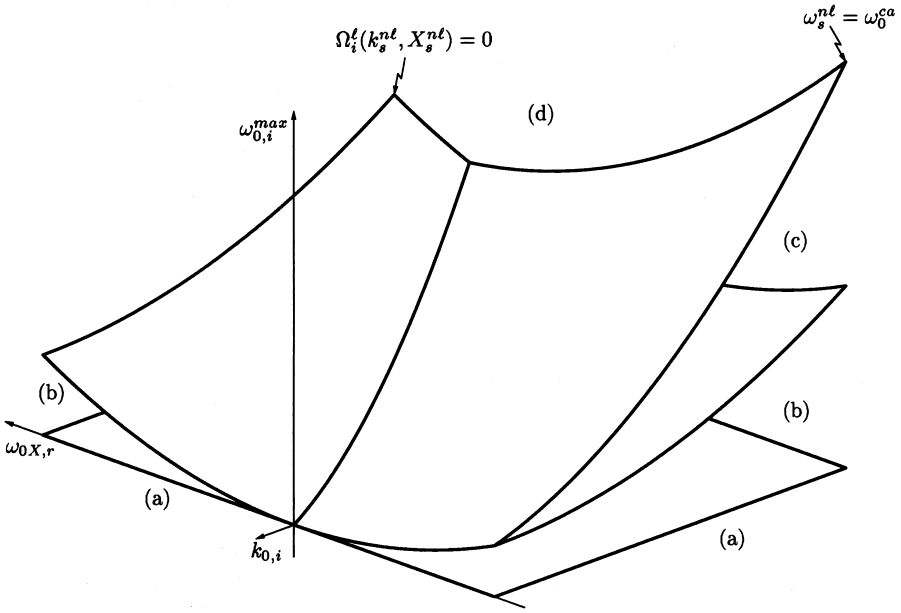

Fig. 14. Domains of existence of steep and soft global modes in the three-dimensional control parameter space $(\omega_{0X,\mathrm{r}}, k_{0,\mathrm{i}}, \omega_{0,\mathrm{i}}^{\max})$ of CGL equation. A nonlinear saddle point exists above the surface $\Omega_{\mathrm{i}}^{\mathrm{l}}(k_{\mathrm{s}}^{\mathrm{nl}}, X_{\mathrm{s}}^{\mathrm{nl}}) = 0$. The associated frequency $\omega_{\mathrm{s}}^{\mathrm{nl}}$ is larger than the front frequency ω_0^{ca} above the surface labeled $\omega_{\mathrm{s}}^{\mathrm{nl}} = \omega_0^{\mathrm{ca}}$. Hence soft global modes prevail in region (d). In region (c), steep modes are selected according to $\omega_{\mathrm{s}}^{\mathrm{nl}} < \omega_0^{\mathrm{ca}}$. In region (b), no nonlinear saddle point exists and only steep modes are obtained. In region (a), below global threshold $\omega_{0,\mathrm{i}}^{\max} < 0$, the unperturbed state is stable.

4.10. Summary of transition mechanisms

The main global mode selection mechanisms have been shown to be governed by three distinct control parameters. The global bifurcation parameter is the maximum absolute growth rate over the entire medium $\omega_{0,\mathrm{i}}^{\max}$. Nonlinear global modes exist whenever a region of absolute instability is present ($\omega_{0,\mathrm{i}}^{\max} > 0$). The transition to a steep global mode occurs discontinuously at $\omega_{0,\mathrm{i}}^{\max} = 0$ through a saddle-node bifurcation. In the absence of absolute instability ($\omega_{0,\mathrm{i}}^{\max} < 0$), no self-sustained global modes exist and the basic state is globally stable.

The basic state remains globally linearly stable up to a finite positive value of $\omega_{0,\mathrm{i}}^{\max}$. The hysteresis width in $\omega_{0,\mathrm{i}}^{\max}$ is governed by $\omega_{0X,\mathrm{r}}$ and scales as $(\omega_{0X,\mathrm{r}})^2$. The advection parameter $k_{0,\mathrm{i}}$ strongly influences transition from steep to soft nonlinear global modes. Soft modes exist for small values of $k_{0,\mathrm{i}}$, whereas for increasing upstream or downstream advection, steep modes prevail. The main global mode properties may be inferred from the three above-mentioned control parameters.

5. Asymptotic spatial structure of global modes

The preceding results have been derived under the assumption that the global mode is, at each station close to the local wave train at the global frequency. This local wave train is governed by the local linear dispersion relation (19) in regions where the amplitude is small, whereas it follows the local nonlinear dispersion relation (20) in finite amplitude domains. These considerations, which only involve the local characteristics of the medium, yield the leading-order WKBJ approximation to the spatial structure. Within this framework, the selection criteria for steep

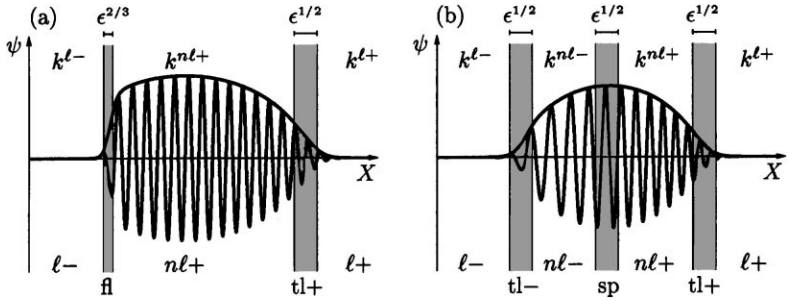

Fig. 15. Spatial structure of (a) steep and (b) soft global modes. (l±) outer semi-infinite linear regions near $X = \pm\infty$ with respective linear spatial $k^{\mathrm{l}\pm}$ branch; (nl±) central nonlinear regions of size $\mathcal{O}(1)$ with respective nonlinear spatial $k^{\mathrm{nl}\pm}$ branch; (tl±) weakly nonlinear transition layers of width $\mathcal{O}(\epsilon^{1/2})$ connecting linear and nonlinear branches of same superscript; (fl) front layer of size $\mathcal{O}(\epsilon^{2/3})$ connecting the $k^{\mathrm{l}-}$ and $k^{\mathrm{nl}+}$ branches and selecting the steep global mode; (sp) saddle point layer of size $\mathcal{O}(\epsilon^{1/2})$ connecting the $k^{\mathrm{nl}\pm}$ branches and selecting the soft global mode.

and soft global modes have been identified and the leading-order steep (24) and soft (29) frequencies have been derived.

The objective of this section is to incorporate the previous results into a consistent WKBJ approximation scheme [2] in order to obtain higher-order correction terms, and to establish that the global mode structures outlined in the preceding sections may effectively be constructed by matching together extended wave packets prevailing in different regions.

The organization of the following sections is motivated by the spatial structure of both steep and soft global modes illustrated in Fig. 15. As already discussed, global modes display nonlinear regions of finite amplitude as well as linear regions of infinitesimal amplitude. In the outer semi-infinite linear regions (l±) extending towards $X = \pm\infty$ (Section 5.1) the respective complex linear spatial branch $k^{\mathrm{l}\pm}$ prevails. The central nonlinear regions (nl±) are of finite extent, i.e., order unity measured in terms of X, and they are dominated by the respective nonlinear spatial branch $k^{\mathrm{nl}\pm}$ as discussed in Section 5.2. These extended regions are connected via three types of narrow *transition layers*:

- The *front layer* (fl) of size $\mathcal{O}(\epsilon^{2/3})$ located at the upstream boundary of the steep global mode nonlinear region connects $k^{\mathrm{l}-}$ and $k^{\mathrm{nl}+}$ branches (Section 5.3).
- The *nonlinear saddle point layer* (sp) of size $\mathcal{O}(\epsilon^{1/2})$ allows crossover between the $k^{\mathrm{nl}\pm}$ branches within the nonlinear soft global mode region (Section 5.4).
- *Weakly nonlinear transition layers* (tl±) of size $\mathcal{O}(\epsilon^{1/2})$ at the downstream end of the steep global mode nonlinear region and at both ends of the soft global mode nonlinear region connect the fully developed nonlinear branches with their linear counterparts (Section 5.5).

Each of these regions is analyzed in turn to obtain a uniformly valid asymptotic approximation over the entire range $-\infty < X < +\infty$. Close inspection of the front layer and the nonlinear saddle point layer yields higher-order corrections of the steep (72) and soft (88) global frequencies, respectively. Since the width of the narrow layers is $\mathcal{O}(\epsilon^{1/2})$ or $\mathcal{O}(\epsilon^{2/3})$ measured in units of X, their characteristic scale is intermediate between the inhomogeneity length scale $\mathcal{O}(1)$ and the instability length scale $\mathcal{O}(\epsilon)$. Thus, although the medium may be considered uniform in the transition layers, they still display many wavelengths, typically $\mathcal{O}(\epsilon^{-1/2})$ or $\mathcal{O}(\epsilon^{-1/3})$.

In the preceding sections, the bifurcation study was largely based on the CGL equation (4) and a complete understanding of the global selection mechanisms was achieved in this context. In this section, the WKBJ approximation scheme is presented in the more general framework of PDE (1).

5.1. Linear WKBJ instability waves

In the semi-infinite linear regions extending towards $X = \pm\infty$ (l$\pm$ in Fig. 15a and b), the global mode amplitude exponentially decays on the fast x-scale. These regions are thus governed by the linear equation (2). Under the slowly varying medium hypothesis (3) a solution of (2) with global frequency ω_{g} may be obtained in terms of WKBJ approximations [2]. The spatial structure is described by a rapidly varying complex phase, accounting for the local wavelength and spatial decay rate, and a slowly varying envelope. For a given value of the frequency ω_{g}, the solution reads

$$\psi(x,t) = A^{\mathrm{l}}(X)\exp\left(\frac{\mathrm{i}}{\epsilon}\int^{X} k^{\mathrm{l}}(u)\,\mathrm{d}u - \mathrm{i}\omega_{\mathrm{g}}t\right) + \text{c.c.}, \tag{39}$$

where $k^{\mathrm{l}}(X)$ is one of the linear spatial branches associated with the frequency ω_{g}. The functions $A^{\mathrm{l}}(X)$ and $k^{\mathrm{l}}(X)$ implicitly depend on ω_{g}; for simplicity their frequency dependence is omitted.

In classical WKBJ fashion, the slowly varying envelope $A^{\mathrm{l}}(X)$ is expanded in powers of ϵ as

$$A^{\mathrm{l}}(X) \sim A^{\mathrm{l}}_0(X) + \epsilon A^{\mathrm{l}}_1(X) + \epsilon^2 A^{\mathrm{l}}_2(X) + \cdots. \tag{40}$$

Thus, spatial differentiation takes the form

$$\frac{\partial\psi}{\partial x} = [(\mathrm{i}k^{\mathrm{l}}(X) + \epsilon\partial_X)A^{\mathrm{l}}(X)]\exp\left(\frac{\mathrm{i}}{\epsilon}\int^{X} k^{\mathrm{l}}(u)\,\mathrm{d}u - \mathrm{i}\omega_{\mathrm{g}}t\right) + \text{c.c.} \tag{41}$$

Upon substituting (39)–(41) into the governing equation (2) and bearing in mind that $\Omega^{\mathrm{l}}(-\mathrm{i}\partial_x) = i\mathcal{L}(\partial_x)$, see (8), one obtains

$$\omega_{\mathrm{g}}(A^{\mathrm{l}}_0 + \epsilon A^{\mathrm{l}}_1 + \cdots) = \Omega^{\mathrm{l}}(k^{\mathrm{l}}(X) - \mathrm{i}\epsilon\partial_X, X)(A^{\mathrm{l}}_0 + \epsilon A^{\mathrm{l}}_1 + \cdots). \tag{42}$$

Note that differentiation with respect to the fast variable, i.e., multiplication by $\mathrm{i}k^{\mathrm{l}}(X)$, does not commute with the slow derivative operator ∂_X. The linear operator appearing in (42) admits the expansion

$$\Omega^{\mathrm{l}}(k^{\mathrm{l}}(X) - \mathrm{i}\epsilon\partial_X, X) = \Omega^{\mathrm{l}}(X) - \mathrm{i}\epsilon(\Omega^{\mathrm{l}}_k(X)\partial_X + \tfrac{1}{2}k^{\mathrm{l}}_X(X)\Omega^{\mathrm{l}}_{kk}(X)) + \mathcal{O}(\epsilon^2) \tag{43}$$

with the notations

$$\Omega^{\mathrm{l}}(X) \equiv \Omega^{\mathrm{l}}(k^{\mathrm{l}}(X), X), \qquad \Omega^{\mathrm{l}}_k(X) \equiv \frac{\partial\Omega^{\mathrm{l}}}{\partial k}(k^{\mathrm{l}}(X), X), \quad \text{etc.}$$

At lowest-order, Eq. (42) reduces to the linear dispersion relation (19), i.e.,

$$\omega_{\mathrm{g}} = \Omega^{\mathrm{l}}(k^{\mathrm{l}}(X), X), \tag{44}$$

which yields the local wave number $k^{\mathrm{l}}(X)$ for a given frequency ω_{g}.

The order ϵ terms read

$$[\omega_{\mathrm{g}} - \Omega^{\mathrm{l}}(k^{\mathrm{l}}(X), X)]A^{\mathrm{l}}_1(X) = -\mathrm{i}\Omega^{\mathrm{l}}_k(X)\frac{\mathrm{d}A^{\mathrm{l}}_0}{\mathrm{d}X} - \frac{\mathrm{i}}{2}\Omega^{\mathrm{l}}_{kk}(X)k^{\mathrm{l}}_X(X)A^{\mathrm{l}}_0(X).$$

By invoking (44), one obtains the obvious solvability condition for $A^{\mathrm{l}}_0(X)$, namely

$$\frac{\mathrm{d}A^{\mathrm{l}}_0}{\mathrm{d}X} = -\frac{1}{2}k^{\mathrm{l}}_X(X)\frac{\Omega^{\mathrm{l}}_{kk}(X)}{\Omega^{\mathrm{l}}_k(X)}A^{\mathrm{l}}_0(X). \tag{45}$$

Thus, the first-order asymptotic approximation to the solution of the linearized equation reads

$$\psi \sim A_0^{\mathrm{l}}(X_1) \exp\left(-\frac{1}{2}\int_{X_1}^{X} k_X^{\mathrm{l}}(u)\frac{\Omega_{kk}^{\mathrm{l}}(u)}{\Omega_k^{\mathrm{l}}(u)}\,\mathrm{d}u\right) \exp\left(\frac{\mathrm{i}}{\epsilon}\int_{X_1}^{X} k^{\mathrm{l}}(u)\,\mathrm{d}u - \mathrm{i}\omega_{\mathrm{g}} t\right) + \text{c.c.}, \tag{46}$$

where X_1 is some arbitrarily specified reference point. In each of the semi-infinite linear regions the respective causal k^{l} branch has to be chosen: $k^{\mathrm{l}-}$ for $X \to -\infty$ and $k^{\mathrm{l}+}$ for $X \to +\infty$.

In the linear region, the nonlinear terms of (1) are seen to be exponentially smaller than the linear ones. Their exact expressions are therefore irrelevant to this work and will not be computed here.

5.2. Nonlinear WKBJ wave trains

In the central nonlinear regions (nl± in Fig. 15a and b), the solution of (1) is obtained in terms of local nonlinear wave trains (10). An asymptotic approximation scheme for nonlinear wave trains is derived in this section, which is formally analogous to linear WKBJ theory.

The fast oscillations of the propagating wave and its slowly varying local wave number and amplitude suggest the following change of variables:

$$\psi(x,t) = \psi(\theta; X),$$

where the real phase function $\theta(x,t)$ is 2π periodic and accounts for propagation on the fast space and time scales, whereas $X = \epsilon x$ allows for slow spatial modulation. Local frequency and wave number are defined as

$$\omega = -\partial_t \theta, \qquad k = \partial_x \theta.$$

For a synchronized global solution, the frequency $\omega = \omega_{\mathrm{g}}$ is constant, whereas the local wave number $k = k^{\mathrm{nl}}(X)$ depends on the slow space variable.

Upon expanding the derivative operators according to

$$\partial_x = k^{\mathrm{nl}}(X)\partial_\theta + \epsilon\partial_X, \qquad \partial_t = -\omega_{\mathrm{g}}\partial_\theta,$$

the governing equation (1) is recast in the form

$$\omega_{\mathrm{g}}\partial_\theta\psi + \mathcal{F}(k^{\mathrm{nl}}(X)\partial_\theta + \epsilon\partial_X; X)[\psi] = 0. \tag{47}$$

Again note that differentiation of $\psi(\theta; X)$ with respect to the fast variable does not commute with ∂_X since $k^{\mathrm{nl}}(X)$ depends on X. Next ψ is expanded according to

$$\psi \sim \psi_0 + \epsilon\psi_1 + \epsilon^2\psi_2 + \cdots,$$

and substituted into (47).

The lowest-order in ϵ yields the local equation

$$\omega\partial_\theta\psi + \mathcal{F}(k\partial_\theta; X)[\psi] = 0, \tag{48}$$

where X acts as an external parameter. When X is considered frozen, the family of local nonlinear wave trains $\Psi(\theta; k, X)$ is recovered. This equation admits solutions only if $\omega = \Omega^{\mathrm{nl}}(k, X)$. In other words, for a global frequency ω_{g}, the nonlinear spatial branch $k^{\mathrm{nl}}(X)$ is derived from the local nonlinear dispersion relation (20) as

$$\omega_{\mathrm{g}} = \Omega^{\mathrm{nl}}(k^{\mathrm{nl}}(X), X), \tag{49}$$

and the leading-order solution ψ_0 then reads

$$\psi_0 = \Psi(\theta; k^{\mathrm{nl}}(X), X). \tag{50}$$

The function Ψ is 2π periodic in the phase variable θ which accounts for the fast propagation through

$$\theta = \frac{1}{\epsilon}\int^X k^{\mathrm{nl}}(u)\,\mathrm{d}u - \omega_{\mathrm{g}} t + \theta_0(X). \tag{51}$$

The so far undetermined slowly drifting phase function $\theta_0(X)$ obeys a solvability condition to be obtained at next order.

The $\mathcal{O}(\epsilon)$ terms in (47) require some care. For clarity of presentation, assume that spatial differentiation only occurs in the linear operator,

$$\mathcal{F}(\partial_x; X)[\psi] = \mathcal{L}(\partial_x; X)[\psi] + \mathcal{N}(X)[\psi].$$

The linear terms are expanded as

$$\begin{aligned}\mathcal{L}(k^{\mathrm{nl}}(X)\partial_\theta\ &+\epsilon\partial_X; X)[\psi_0(\theta; X) + \epsilon\psi_1(\theta; X) + \cdots] \\ &+ \sim \mathcal{L}(X)[\psi_0]\epsilon\left(\mathcal{L}(X)[\psi_1] + \mathcal{L}'(X)[\partial_X\psi_0] + \frac{1}{2}\frac{\mathrm{d}k^{\mathrm{nl}}}{\mathrm{d}X}\mathcal{L}''(X)[\partial_\theta\psi_0]\right) + \mathcal{O}(\epsilon^2),\end{aligned}$$

where the notation $\mathcal{L}(X)$ is shorthand for $\mathcal{L}(k^{\mathrm{nl}}(X)\partial_\theta; X)$ and the primes denote differentiation of $\mathcal{L}(\partial_x; X)$ with respect to its first argument. The nonlinear terms are expanded as

$$\mathcal{N}(X)[\psi_0 + \epsilon\psi_1 + \cdots] = \mathcal{N}(X)[\psi_0] + \epsilon\frac{\partial\mathcal{N}(X)[\psi_0]}{\partial\psi}\psi_1 + \mathcal{O}(\epsilon^2).$$

Thus (47) yields at $\mathcal{O}(\epsilon)$,

$$L[\psi_1] = -\mathcal{L}'(X)[\partial_X\psi_0] - \frac{1}{2}\frac{\mathrm{d}k^{\mathrm{nl}}}{\mathrm{d}X}\mathcal{L}''(X)[\partial_\theta\psi_0], \tag{52}$$

where the linear differential operator L on the left-hand side is defined as

$$L \equiv \omega_{\mathrm{g}}\partial_\theta + \mathcal{L}(X) + \frac{\partial\mathcal{N}(X)[\psi_0]}{\partial\psi}. \tag{53}$$

Thus, ψ_1 satisfies a linear differential equation with respect to θ with X-dependent coefficients. The operator L is singular since one may readily verify that

$$L[\Psi_\theta] = 0 \quad \text{with} \quad \Psi_\theta \equiv \partial_\theta\Psi(\theta; k^{\mathrm{nl}}(X), X).$$

Thus (52) admits solutions for ψ_1 only if its right-hand side satisfies a solvability condition.

Let us introduce an inner product for 2π periodic functions of θ defined by

$$\langle\phi, \psi\rangle = \frac{1}{2\pi}\int_0^{2\pi}\phi(\theta)\psi(\theta)\,\mathrm{d}\theta. \tag{54}$$

The adjoint operator $L^\dagger$ of L is then obtained via successive integration by parts through the relation $\langle\phi, L\psi\rangle = \langle L^\dagger\phi, \psi\rangle$, and it reads

$$L^\dagger = -\omega_{\mathrm{g}}\partial_\theta + \mathcal{L}(-k^{\mathrm{nl}}(X)\partial_\theta; X) + \frac{\partial\mathcal{N}(X)[\psi_0]}{\partial\psi}. \tag{55}$$

Let $\Psi_\theta^\dagger$ be the adjoint eigenfunction of Ψ_θ. Taking the inner product of (52) with $\Psi_\theta^\dagger$ and substituting

$$\partial_X \psi_0 = \frac{\mathrm{d}\theta_0}{\mathrm{d}X}\Psi_\theta + \frac{\mathrm{d}k^{\mathrm{nl}}}{\mathrm{d}X}\Psi_k + \Psi_X,$$

yields the following solvability condition for $\theta_0(X)$,

$$\frac{\mathrm{d}\theta_0}{\mathrm{d}X}\langle \Psi_\theta^\dagger, \mathcal{L}'\Psi_\theta\rangle + \frac{1}{2}\frac{\mathrm{d}k^{\mathrm{nl}}}{\mathrm{d}X}\langle \Psi_\theta^\dagger, 2\mathcal{L}'\Psi_k + \mathcal{L}''\Psi_\theta\rangle + \langle \Psi_\theta^\dagger, \mathcal{L}'\Psi_X\rangle = 0. \tag{56}$$

This entirely specifies the leading-order approximation to the global nonlinear solution

$$\psi(x,t) \sim \Psi\left(\frac{1}{\epsilon}\int^X k^{\mathrm{nl}}(u)\,\mathrm{d}u - \omega_{\mathrm{g}}t + \theta_0(X); k^{\mathrm{nl}}(X), X\right), \tag{57}$$

where the parametric dependence of $k^{\mathrm{nl}}(X)$ on the global frequency ω_{g} is entirely determined by (49).

5.3. Front layer

According to Section 4.2, the front of steep global modes is located at the station of local marginal absolute instability X^{ca} and it is associated with a wave number jump from the $k^{\mathrm{l}-}$ to the $k^{\mathrm{nl}+}$ branch. On the slow scale X, the front discontinuously connects the linear solution (46) of wave number $k^{\mathrm{l}-}$ prevailing in the upstream domain $X < X^{\mathrm{ca}}$ to the nonlinear solution (57) of wave number $k^{\mathrm{nl}+}$ on the downstream side of the front $X > X^{\mathrm{ca}}$. In this section, the linear solution is shown to match to the nonlinear solution through a narrow front layer (fl) as depicted in Fig. 15a. The formulation essentially follows the same approach as in the asymptotic description of the front boundary layer arising in nonlinear dynamo waves developed by Bassom et al. [1] and is based on linear turning point theory [48].

The envelope of the outer linear solution is governed by the amplitude equation (45) which is singular at a turning point X_0 of the dispersion relation (44) defined by

$$\omega_0(X_0) = \omega_{\mathrm{g}}. \tag{58}$$

For $\omega_{\mathrm{g}} = \omega_0^{\mathrm{ca}}$, the turning point is at $X_0 = X^{\mathrm{ca}}$. However, it is to be anticipated that the global frequency does not exactly equal ω_0^{ca}. As outlined below, it is convenient to implement a matching procedure in the turning point region for an arbitrary complex global frequency ω_{g}. Thus, consider the linear governing equation (2) for complex X. The results of Section 5.1 pertaining to linear instability waves remain valid in the complex X-plane, provided that $\Omega^{\mathrm{l}}(k, X)$ and hence $\omega_0(X)$ are analytically continued for complex values of X. Then (58) associates to a frequency ω_{g} the turning point $X_0(\omega_{\mathrm{g}})$ in the complex X-plane.

Expansion of the dispersion relation (44) in the neighborhood of the turning point X_0 yields

$$0 = \tfrac{1}{2}\Omega^{\mathrm{l}}_{kk,0}(k^{\mathrm{l}}(X) - k_0)^2 + \Omega^{\mathrm{l}}_{X,0}(X - X_0) + \text{h.o.t.}, \tag{59}$$

where k_0 is the associated absolute wave number $k_0 \equiv k_0(X_0)$ and the subscript 0 denotes evaluation at (k_0, X_0). By definition of the turning point, $\Omega^{\mathrm{l}}_{k,0} = 0$, and under the assumption that the turning point is simple, $\Omega^{\mathrm{l}}_{X,0} \neq 0$. Thus

$$k^{\mathrm{l}}(X) \sim k_0 \pm \sqrt{\frac{-2\Omega^{\mathrm{l}}_{X,0}}{\Omega^{\mathrm{l}}_{kk,0}}}(X - X_0)^{1/2}.$$

The linear amplitude equation (45) then reduces to

$$\frac{\mathrm{d}A_0}{\mathrm{d}X} \sim -\frac{A_0(X)}{4(X-X_0)}.$$

Hence $A_0(X) \sim C^{\mathrm{st}}(X-X_0)^{-1/4}$ as $X \to X_0$, and the complete behavior of the outer linear solution (46) as $X \to X_0$ reads

$$\psi \sim C^{\mathrm{st}}(X-X_0)^{-1/4} \exp\left[\frac{2\mathrm{i}}{3\epsilon}\sqrt{\frac{-2\Omega^{\mathrm{l}}_{X,0}}{\Omega^{\mathrm{l}}_{kk,0}}(X-X_0)^3}\right] \mathrm{e}^{\mathrm{i}(k_0 x-\omega_{\mathrm{g}} t)} + \text{c.c.} \tag{60}$$

Here it is assumed that the square root branch cut is chosen so that the wave number $k^{\mathrm{l}-}$ prevailing in the domain $X \to -\infty$ is recovered.

It is seen that in the neighborhood of the turning point X_0, the amplitude A_0 becomes singular. Balance of dominant terms, as shown below, yields an inner turning point region of size $\mathcal{O}(\epsilon^{2/3})$. Thus, define an inner variable $\tilde{X}$ by

$$X = X_0 + \epsilon^{2/3}\tilde{X}, \tag{61}$$

and expand ψ as

$$\psi = \tilde{A}(\tilde{X})\,\mathrm{e}^{\mathrm{i}(k_0 x-\omega_{\mathrm{g}} t)} + \text{c.c.} \tag{62}$$

with

$$\tilde{A}(\tilde{X}) = \tilde{C}^{\mathrm{st}}[\tilde{A}_0(\tilde{X}) + \epsilon^{2/3}\tilde{A}_{2/3}(\tilde{X}) + \cdots], \tag{63}$$

where $\tilde{A}_0(\tilde{X})$ is $\mathcal{O}(\epsilon^0)$. Spatial differentiation now becomes $\partial_x = \mathrm{i}k_0 + \epsilon^{1/3}\partial_{\tilde{X}}$. In this inner transition layer, the leading-order wave number is constant and equal to k_0, thus $\partial_{\tilde{X}}$ and $\mathrm{i}k_0$ now commute. The governing equation (2) then yields

$$\omega_{\mathrm{g}}\tilde{A}(\tilde{X}) = \Omega^{\mathrm{l}}(k_0 - \mathrm{i}\epsilon^{1/3}\partial_{\tilde{X}}, X_0 + \epsilon^{2/3}\tilde{X})\tilde{A}(\tilde{X}) \sim [\Omega^{\mathrm{l}}(k_0, X_0) + \epsilon^{2/3}(\tilde{X}\Omega^{\mathrm{l}}_{X,0} - \tfrac{1}{2}\Omega^{\mathrm{l}}_{kk,0}\partial_{\tilde{X}\tilde{X}})]\tilde{A}(\tilde{X}),$$

where $\omega_{\mathrm{g}} = \Omega^{\mathrm{l}}(k_0, X_0)$. The scaling $X - X_0 \sim \epsilon^{2/3}\tilde{X}$ and $x \sim \epsilon^{-1/3}\tilde{X}$ guarantees the balance of dominant terms at order $\mathcal{O}(\epsilon^{2/3})$ in the previous equation and leads to the following Airy equation for the leading-order amplitude:

$$\tfrac{1}{2}\Omega^{\mathrm{l}}_{kk,0}\frac{\mathrm{d}^2\tilde{A}_0}{\mathrm{d}\tilde{X}^2} = \tilde{X}\Omega^{\mathrm{l}}_{X,0}\tilde{A}_0(\tilde{X}). \tag{64}$$

Thus, $\tilde{A}_0(\tilde{X})$ is a linear superposition of the Airy functions $Ai(-\lambda\tilde{X})$ and $Bi(-\lambda\tilde{X})$ with

$$\lambda^3 = -\frac{2\Omega^{\mathrm{l}}_{X,0}}{\Omega^{\mathrm{l}}_{kk,0}}.$$

Upon choosing for λ the solution with $|\mathrm{Arg}\,\lambda| < \pi/3$, the *Bi* component exponentially grows whereas the *Ai* component decays according to

$$Ai(-\lambda\tilde{X}) \sim \frac{1}{2\sqrt{\pi}}(-\lambda\tilde{X})^{-1/4}\exp\left[\frac{2\mathrm{i}}{3}\sqrt{\frac{-2\Omega^{\mathrm{l}}_{X,0}}{\Omega^{\mathrm{l}}_{kk,0}}\tilde{X}^3}\right], \tag{65}$$

as $\tilde{X} \to -\infty$ [2]. Expressing the outer solution (60) in terms of the inner variable $\tilde{X}$, shows that it matches with the inner solution (62) provided that

$$\tilde{A}(\tilde{X}) = \tilde{C}^{\mathrm{st}}[Ai(-\lambda\tilde{X}) + \mathcal{O}(\epsilon^{2/3})] \tag{66}$$

with $C^{\mathrm{st}} = \epsilon^{1/6}((-\lambda)^{-1/4}/2\sqrt{\pi})\tilde{C}^{\mathrm{st}}$.

Thus, for any frequency ω_{g}, linear instability waves are governed by the Airy equation (64) in a region of size $\mathcal{O}(\epsilon^{2/3})$ located at the turning point of the linear local dispersion relation. The location of the turning point in the complex X-plane depends on ω_{g}. For frequencies $\omega_{\mathrm{g}} = \omega_0^{\mathrm{ca}} + \delta\omega$, close to the marginal absolute frequency, the turning point is located at

$$X_0 \sim X^{\mathrm{ca}} + \frac{\delta\omega}{\omega_{0,X}(X^{\mathrm{ca}})}.$$

For $\mathcal{O}(\epsilon^{2/3})$ frequency corrections, $\delta\omega = \epsilon^{2/3}\omega_{2/3}$, the inner Airy region in the complex X-plane contains in its neighborhood the point X^{ca} on the real X-axis.

Before analyzing in more detail the properties of the Airy solutions on the $\tilde{X}$-scale, let us turn to the front structure. As discussed in Section 5.3, a uniform medium at the transition between convective and absolute instability admits stationary front solutions oscillating at its real absolute frequency. Thus, the original nonlinear governing equation (1) rewritten at $X = X^{\mathrm{ca}}$ as

$$\omega_0^{\mathrm{ca}}\frac{\partial\psi}{\partial\theta} + \mathcal{F}(\partial_x; X^{\mathrm{ca}})[\psi] = 0, \tag{67}$$

admits the front solution $\Psi_{\mathrm{f}}(x,\theta)$, which is 2π periodic in the phase function $\theta = \omega_0^{\mathrm{ca}}t$. Towards $x = +\infty$, this solution approaches a fully nonlinear wave train of the form (50). Thus,

$$\Psi_{\mathrm{f}}(x,\omega_0^{\mathrm{ca}}t) \sim \Psi[k^{\mathrm{nl}+}(X^{\mathrm{ca}},\omega_0^{\mathrm{ca}})x - \omega_0^{\mathrm{ca}}t; k^{\mathrm{nl}+}(X^{\mathrm{ca}},\omega_0^{\mathrm{ca}}), X^{\mathrm{ca}}] \quad \text{as } x \to +\infty.$$

Towards $x = -\infty$, the exponential decay rate is dictated by the absolute wave number $k_0^{\mathrm{ca}} = k_0(X^{\mathrm{ca}})$ and the front solution reads

$$\Psi_{\mathrm{f}}(x,\omega_0^{\mathrm{ca}}t) \sim (c_0^{\mathrm{st}} + c_1^{\mathrm{st}}x)\,\mathrm{e}^{\mathrm{i}(k_0^{\mathrm{ca}}x - \omega_0^{\mathrm{ca}}t)} + \mathrm{c.c.}, \tag{68}$$

where the secular term is due to the double root $k^{\mathrm{l}+} = k^{\mathrm{l}-} = k_0^{\mathrm{ca}}$ of the linear dispersion relation. In the uniform medium, the front has no preferred location. A translation of Δx only changes the phase by $k^{\mathrm{nl}+}(\omega_0^{\mathrm{ca}})\Delta x$ in the asymptotic behavior towards the nonlinear side $x = +\infty$ and leads to an additional factor $\mathrm{e}^{\mathrm{i}k_0^{\mathrm{ca}}\Delta x}$ in the upstream exponentially decaying tail.

The exponentially decaying tail (68) has to be matched with (62) in the Airy region. Due to the secular term in (68), matching with (62) is only possible at the zeroes of the Airy function. The Airy function Ai appearing in (66) admits real negative zeros a_i. Thus, the zeros of $\tilde{A}_0$ are located at $\tilde{X}_{\mathrm{i}} = -a_i/\lambda$. In terms of the outer variable X these occur at

$$X_{\mathrm{i}} \equiv X_0(\omega_{\mathrm{g}}) + \epsilon^{2/3}\tilde{X}_{\mathrm{i}} = X^{\mathrm{ca}} + \epsilon^{2/3}\left(\frac{\omega_{2/3}}{\omega_{0,X}} - \frac{a_i}{\lambda}\right) + \mathcal{O}(\epsilon^{4/3}). \tag{69}$$

Whereas the linear WKBJ approximations as well as the turning point region may be investigated in the complex X-plane, the front involves a nonlinear wave train and is thus necessarily restricted to the real X-axis. Requiring that the ith zero (69) of the Airy function is on the real X-axis yields the frequency correction term

$$\omega_{2/3} = a_i\frac{|\omega_{0,X}|^2}{|\lambda|^2}\frac{\mathrm{Im}\,\lambda}{\mathrm{Im}\,\omega_{0,X}}$$

for a zero located at

$$X_{\mathrm{i}} \sim X^{\mathrm{ca}} + \epsilon^{2/3} \frac{a_i}{|\lambda|^2} \frac{\mathrm{Im}(\omega_{0,X}^{\star}\lambda)}{\mathrm{Im}\,\omega_{0,X}}.$$

Since X^{ca} is the transition location from convective to absolute instability, $\mathrm{Im}\,\omega_{0,X}$ is positive. Under the slightly more restrictive assumption that $\pi/3 < \mathrm{Arg}\,\omega_{0,X} < 2\pi/3$, we are guaranteed that $\mathrm{Im}(\omega_{0,X}^{\star}\lambda) < 0$. In most situations of physical interest, variations of $\omega_{0,\mathrm{r}}$ are small compared to those of $\omega_{0,\mathrm{i}}$ and thus the condition on $\mathrm{Arg}\,\omega_{0,X}$ is readily fulfilled.

So far the matching conditions yield a countable set of frequencies

$$\omega_{\mathrm{g}} \sim \omega_0^{\mathrm{ca}} + \epsilon^{2/3} a_i \Omega_{2/3} \quad \text{with} \quad \Omega_{2/3} = \frac{|\omega_{0,X}|^2}{|\lambda|^2} \frac{\mathrm{Im}\,\lambda}{\mathrm{Im}\,\omega_{0,X}}, \tag{70}$$

each being associated with the ith zero $a_i < 0$ of the Airy function. The corresponding fronts are located at

$$X \sim X^{\mathrm{ca}} - \epsilon^{2/3} a_i X_{2/3} \quad \text{with} \quad X_{2/3} = \frac{-\mathrm{Im}(\omega_{0,X}^{\star}\lambda)}{|\lambda|^2\,\mathrm{Im}\,\omega_{0,X}} > 0. \tag{71}$$

Since $X_{2/3} > 0$, higher-order global modes display a front located further downstream in the AU domain. These situations are likely to be unstable since the exponentially decaying tail of the front partly penetrates into the AU domain. Such a higher-order front prevailing in a slightly AU medium tends to move upstream, until it reaches the most upstream possible station associated with a_0. Thus we argue, although we have not proven the result, that the only stable global mode solution is obtained for the first zero indexed by a_0. Up to $\mathcal{O}(\epsilon^{2/3})$, the global frequency and the front location therefore, respectively, read

$$\omega_{\mathrm{g}} \sim \omega_0^{\mathrm{ca}} + \epsilon^{2/3} a_0 \Omega_{2/3}, \qquad X \sim X^{\mathrm{ca}} - \epsilon^{2/3} a_0 X_{2/3} \tag{72}$$

with

$$a_0 = -2.3381\ldots.$$

This completes the investigation of the detailed structure of the front region.

5.4. *Fully nonlinear saddle point layer*

The nonlinear saddle point is defined as the location $X_{\mathrm{s}}^{\mathrm{nl}}$ where the two nonlinear wave number branches meet. The saddle point frequency $\omega_{\mathrm{s}}^{\mathrm{nl}}$ is given by the criterion (29). In the nonlinear regions surrounding the saddle location $X_{\mathrm{s}}^{\mathrm{nl}}$ the asymptotic approximation of the global solution is of the form (57) and the slowly drifting phase function $\theta_0(X)$ is governed by the solvability condition (56).

At the saddle point, the first-order differential equation (56) for θ_0 becomes singular since $\langle \Psi_\theta^{\dagger}, \mathcal{L}'\Psi_\theta \rangle = 0$ at $X_{\mathrm{s}}^{\mathrm{nl}}$ (cf. Eq. (90)). Thus, the nonlinear WKBJ approximation worked out in Section 5.2 is no longer valid in the neighborhood of $X_{\mathrm{s}}^{\mathrm{nl}}$, because θ_0 varies there on a spatial scale which is faster than X. In this section, a nonlinear saddle point layer at $X_{\mathrm{s}}^{\mathrm{nl}}$ is introduced, (sp) in Fig. 15b, and a second-order differential equation for the phase θ_0 is derived after rescaling the spatial variable in the neighborhood of $X_{\mathrm{s}}^{\mathrm{nl}}$. This inner solution in the saddle point region allows a smooth crossover between the WKBJ wave trains in both nonlinear regions.

Let us introduce an inner local space variable $\tilde{X}$ in the saddle point region defined as

$$X = X_{\mathrm{s}}^{\mathrm{nl}} + \epsilon^{1/2}\tilde{X},$$

and expand ψ according to

$$\psi \sim \tilde{\psi}_0 + \epsilon^{1/2}\tilde{\psi}_{1/2} + \epsilon\tilde{\psi}_1 + \cdots . \tag{73}$$

The subsequent analysis yields the higher-order corrections to the global frequency as

$$\omega_{\mathrm{g}} \sim \omega_{\mathrm{s}}^{\mathrm{nl}} + \epsilon^{1/2}\omega_{1/2} + \epsilon\omega_1 + \cdots . \tag{74}$$

Replacing the spatial derivative ∂_x in the inner region by $k_{\mathrm{s}}^{\mathrm{nl}}\partial_\theta + \epsilon^{1/2}\partial_{\tilde{X}}$, the linear operator expands as [3]

$$\begin{aligned}\mathcal{L}(k_{\mathrm{s}}^{\mathrm{nl}}\partial_\theta + \epsilon^{1/2}\partial_{\tilde{X}}, X_{\mathrm{s}}^{\mathrm{nl}} + \epsilon^{1/2}\tilde{X}) &= \mathcal{L}_{\mathrm{s}} + \epsilon^{1/2}(\mathcal{L}'_{\mathrm{s}}\partial_{\tilde{X}} + \tilde{X}\mathcal{L}_{X,\mathrm{s}}) \\ &\quad + \tfrac{1}{2}\epsilon(\mathcal{L}''_{\mathrm{s}}\partial_{\tilde{X}\tilde{X}} + 2\tilde{X}\mathcal{L}'_{X,\mathrm{s}}\partial_{\tilde{X}} + \tilde{X}^2\mathcal{L}_{XX,\mathrm{s}}) + \mathcal{O}(\epsilon^{3/2}).\end{aligned} \tag{75}$$

Substituting the expansions (73)–(75) into the governing equation (1), one recovers at leading order

$$\omega_{\mathrm{s}}^{\mathrm{nl}}\partial_\theta\tilde{\psi}_0 + \mathcal{L}(k_{\mathrm{s}}^{\mathrm{nl}}\partial_\theta, X_{\mathrm{s}}^{\mathrm{nl}})\tilde{\psi}_0 + \mathcal{N}(X_{\mathrm{s}}^{\mathrm{nl}})[\tilde{\psi}_0] = 0.$$

Thus,

$$\tilde{\psi}_0 = \Psi_{\mathrm{s}} \equiv \Psi(\theta + \tilde{\theta}_0(\tilde{X}); k_{\mathrm{s}}^{\mathrm{nl}}, X_{\mathrm{s}}^{\mathrm{nl}}), \tag{76}$$

where the fast phase function in the inner saddle point layer reads $\theta = k_{\mathrm{s}}^{\mathrm{nl}}x - \omega_{\mathrm{s}}^{\mathrm{nl}}t$ and the slow phase $\tilde{\theta}_0(\tilde{X})$ is a so far an undetermined function varying on the intermediate length scale $\tilde{X}$.

The nonlinear term is expanded as

$$\begin{aligned}\mathcal{N}(X_{\mathrm{s}}^{\mathrm{nl}} + \epsilon^{1/2}\tilde{X})[\Psi_{\mathrm{s}} + \epsilon^{1/2}\tilde{\psi}_{1/2} + \epsilon\tilde{\psi}_1 + \mathcal{O}(\epsilon^{3/2})] &= \mathcal{N}_{\mathrm{s}} + \epsilon^{1/2}(\tilde{X}\mathcal{N}_{X,\mathrm{s}} + \mathcal{N}_{\psi,\mathrm{s}}\tilde{\psi}_{1/2}) \\ &\quad + \epsilon(\tfrac{1}{2}\tilde{X}^2\mathcal{N}_{XX,\mathrm{s}} + \tilde{X}\mathcal{N}_{X\psi,\mathrm{s}}\tilde{\psi}_{1/2} + \tfrac{1}{2}\mathcal{N}_{\psi\psi,\mathrm{s}}\tilde{\psi}_{1/2}^2 + \mathcal{N}_{\psi,\mathrm{s}}\tilde{\psi}_1) + \mathcal{O}(\epsilon^{3/2}),\end{aligned} \tag{77}$$

where

$$\mathcal{N}_{\mathrm{s}} \equiv \mathcal{N}(X_{\mathrm{s}}^{\mathrm{nl}})[\Psi_{\mathrm{s}}], \qquad \mathcal{N}_{\psi,\mathrm{s}} \equiv \partial_\psi\mathcal{N}(X_{\mathrm{s}}^{\mathrm{nl}})[\Psi_{\mathrm{s}}], \qquad \mathcal{N}_{X,\mathrm{s}} \equiv \partial_X\mathcal{N}(X_{\mathrm{s}}^{\mathrm{nl}})[\Psi_{\mathrm{s}}], \quad \text{etc.}$$

The order $\epsilon^{1/2}$ problem reads

$$L_{\mathrm{s}}\tilde{\psi}_{1/2} + \omega_{1/2}\Psi_{\theta,\mathrm{s}} + \frac{\mathrm{d}\tilde{\theta}_0}{\mathrm{d}\tilde{X}}\mathcal{L}'_{\mathrm{s}}\Psi_{\theta,\mathrm{s}} + \tilde{X}(\mathcal{L}_{X,\mathrm{s}}\Psi_{\mathrm{s}} + \mathcal{N}_{X,\mathrm{s}}) = 0, \tag{78}$$

where

$$L_{\mathrm{s}} \equiv \omega_{\mathrm{s}}^{\mathrm{nl}}\partial_\theta + \mathcal{L}_{\mathrm{s}} + \mathcal{N}_{\psi,\mathrm{s}}.$$

Let $\Psi_{\theta,\mathrm{s}}^\dagger$ be the adjoint eigenfunction of $\Psi_{\theta,\mathrm{s}}$. Eq. (78) admits solutions for $\tilde{\psi}_{1/2}$ if the following solvability condition is met:

$$\omega_{1/2}\langle\Psi_{\theta,\mathrm{s}}^\dagger, \Psi_{\theta,\mathrm{s}}\rangle + \frac{\mathrm{d}\tilde{\theta}_0}{\mathrm{d}\tilde{X}}\langle\Psi_{\theta,\mathrm{s}}^\dagger, \mathcal{L}'_{\mathrm{s}}\Psi_{\theta,\mathrm{s}}\rangle + \tilde{X}\langle\Psi_{\theta,\mathrm{s}}^\dagger, \mathcal{L}_{X,\mathrm{s}}\Psi_{\mathrm{s}} + \mathcal{N}_{X,\mathrm{s}}\rangle = 0.$$

In Section 5.4.1 below, the last two terms of this equation are shown to vanish (90) and (91). Thus, the solvability condition requires that

$$\omega_{1/2} = 0.$$

There is no correction to the global frequency at order $\epsilon^{1/2}$ and no equation for $\tilde{\theta}_0$ is obtained at this order.

[3] Subscript "s" always denotes evaluation at $\partial_x = k_{\mathrm{s}}^{\mathrm{nl}}\partial_\theta$, $X = X_{\mathrm{s}}^{\mathrm{nl}}$, $k = k_{\mathrm{s}}^{\mathrm{nl}}$.

With $\omega_{1/2} = 0$ and using (92) and (93), the general solution of the linear inhomogeneous equation (78) is obtained as

$$\tilde{\psi}_{1/2} = \tilde{X}\Psi_{X,\mathrm{s}} + \frac{\mathrm{d}\tilde{\theta}_0}{\mathrm{d}\tilde{X}}\Psi_{k,\mathrm{s}} + \tilde{A}(\tilde{X})\Psi_{\theta,\mathrm{s}}, \tag{79}$$

where $\tilde{A}(\tilde{X})$ is an arbitrary real amplitude function.

At order ϵ, the following inhomogeneous equation for $\tilde{\psi}_1$ is obtained

$$\begin{aligned} L_{\mathrm{s}}\tilde{\psi}_1 &+\frac{1}{2}\frac{\mathrm{d}^2\tilde{\theta}_0}{\mathrm{d}\tilde{X}^2}(2\mathcal{L}'_{\mathrm{s}}\Psi_{k,\mathrm{s}} + \mathcal{L}''_{\mathrm{s}}\Psi_{\theta,\mathrm{s}}) + \frac{1}{2}\left(\frac{\mathrm{d}\tilde{\theta}_0}{\mathrm{d}\tilde{X}}\right)^2(2\mathcal{L}'_{\mathrm{s}}\Psi_{\theta k,\mathrm{s}} + \mathcal{L}''_{\mathrm{s}}\Psi_{\theta\theta,\mathrm{s}} + \mathcal{N}_{\psi\psi,\mathrm{s}}(\Psi_{k,\mathrm{s}})^2) \\ &+\tilde{X}\frac{\mathrm{d}\tilde{\theta}_0}{\mathrm{d}\tilde{X}}((\mathcal{L}_{X,\mathrm{s}} + \mathcal{N}_{X\psi,\mathrm{s}})\Psi_{k,\mathrm{s}} + \mathcal{L}'_{X,\mathrm{s}}\Psi_{\theta,\mathrm{s}} + \mathcal{L}'_{\mathrm{s}}\Psi_{\theta X,\mathrm{s}} + \mathcal{N}_{\psi\psi,\mathrm{s}}\Psi_{k,\mathrm{s}}\Psi_{X,\mathrm{s}}) \\ &+\frac{1}{2}\tilde{X}^2(2(\mathcal{L}_{X,\mathrm{s}} + \mathcal{N}_{X\psi,\mathrm{s}})\Psi_{X,\mathrm{s}} + \mathcal{L}_{XX,\mathrm{s}}\Psi_{\mathrm{s}} + \mathcal{N}_{XX,\mathrm{s}} + \mathcal{N}_{\psi\psi,\mathrm{s}}(\Psi_{X,\mathrm{s}})^2) \\ &+\frac{\mathrm{d}\tilde{\theta}_0}{\mathrm{d}\tilde{X}}\tilde{A}(\tilde{X})(\mathcal{L}'_{\mathrm{s}}\Psi_{\theta\theta,\mathrm{s}} + \mathcal{N}_{\psi\psi,\mathrm{s}}\Psi_{\theta,\mathrm{s}}\Psi_{k,\mathrm{s}}) + \tilde{X}\tilde{A}(\tilde{X})((\mathcal{L}_{X,\mathrm{s}} + \mathcal{N}_{\psi X,\mathrm{s}})\Psi_{\theta,\mathrm{s}} + \mathcal{N}_{\psi\psi,\mathrm{s}}\Psi_{\theta,\mathrm{s}}\Psi_{X,s}) \\ &+\frac{\mathrm{d}\tilde{A}}{\mathrm{d}\tilde{X}}\mathcal{L}'_{\mathrm{s}}\Psi_{\theta,\mathrm{s}} + \frac{1}{2}\tilde{A}(\tilde{X})^2\mathcal{N}_{\psi\psi,\mathrm{s}}(\Psi_{\theta,\mathrm{s}})^2 + \mathcal{L}'_{\mathrm{s}}\Psi_{X,\mathrm{s}} + \omega_1\Psi_{\theta,\mathrm{s}} = 0. \end{aligned} \tag{80}$$

This equation admits solutions for $\tilde{\psi}_1$ if the inner product of the forcing terms (everything except $L_{\mathrm{s}}\tilde{\psi}_1$) with $\Psi^{\dagger}_{\theta,\mathrm{s}}$ vanishes. The different inner products are computed in Section 5.4.1. From (94)–(96), it follows that all the terms involving the function $\tilde{A}(\tilde{X})$ vanish: this function remains undetermined at this order. Using (97)–(99), the solvability condition for $\tilde{\theta}_0$ reads

$$A\frac{\mathrm{d}^2\tilde{\theta}_0}{\mathrm{d}\tilde{X}^2} = B\left(\frac{\mathrm{d}\tilde{\theta}_0}{\mathrm{d}\tilde{X}}\right)^2 + 2C\tilde{X}\frac{\mathrm{d}\tilde{\theta}_0}{\mathrm{d}\tilde{X}} + D\tilde{X}^2 - E - 2\omega_1, \tag{81}$$

where

$$A = \frac{\langle\Psi^{\dagger}_{\theta,\mathrm{s}}, 2\mathcal{L}'_{\mathrm{s}}\Psi_{k,\mathrm{s}} + \mathcal{L}''_{\mathrm{s}}\Psi_{\theta,\mathrm{s}}\rangle}{\langle\Psi^{\dagger}_{\theta,\mathrm{s}}, \Psi_{\theta,\mathrm{s}}\rangle}, \qquad B = \Omega^{\mathrm{nl}}_{kk,\mathrm{s}}, \qquad C = \Omega^{\mathrm{nl}}_{kX,\mathrm{s}}, \qquad D = \Omega^{\mathrm{nl}}_{XX,\mathrm{s}}, \qquad E = \frac{\langle\Psi^{\dagger}_{\theta,\mathrm{s}}, \mathcal{L}'_{\mathrm{s}}\Psi_{X,\mathrm{s}}\rangle}{\langle\Psi^{\dagger}_{\theta,\mathrm{s}}, \Psi_{\theta,\mathrm{s}}\rangle}.$$

Let

$$\Theta(\tilde{X}) = \exp\left[-\frac{B}{A}\tilde{\theta}(\alpha\tilde{X}) - \frac{C\alpha^2}{2A}\tilde{X}^2\right] \tag{82}$$

with

$$\alpha^4 = \frac{A^2}{4(C^2 - BD)}. \tag{83}$$

Note that $C^2 - BD > 0$ since $(k^{\mathrm{nl}}_{\mathrm{s}}, X^{\mathrm{nl}}_{\mathrm{s}})$ is a saddle point of $\Omega^{\mathrm{nl}}(k, X)$. Rewriting the solvability condition (81) in terms of Θ yields the parabolic cylinder equation [2]

$$\frac{\mathrm{d}^2\Theta}{\mathrm{d}\tilde{X}^2} = \left(\frac{1}{4}\tilde{X}^2 - \nu - \frac{1}{2}\right)\Theta, \tag{84}$$

where

$$\nu + \frac{1}{2} = \frac{1}{2}\frac{AC - B(E + 2\omega_1)}{\sqrt{A^2(C^2 - BD)}}.$$

This solution in the inner saddle point layer needs to be matched with the wave trains (57) in the outer nonlinear regions. In terms of the inner variable $\tilde{X}$, the phase of the outer nonlinear solutions (57) expands as

$$\frac{1}{\epsilon}\int_{X_s^{nl}}^{X_s^{nl}+\epsilon^{1/2}\tilde{X}} k^{nl}(u)\,du - \omega_g t + \theta_0(X) = (k_s^{nl}x - \omega_s^{nl}t) + \frac{1}{2}k_{X,s}^{nl}\tilde{X}^2 + \mathcal{O}(\epsilon^{1/2}). \tag{85}$$

Matching to the phase $k_s^{nl}x - \omega_s^{nl}t + \tilde{\theta}_0(\tilde{X})$ of the inner solution (76) when $\tilde{X} \to \pm\infty$ requires that

$$\tilde{\theta}_0(\tilde{X}) \sim \tfrac{1}{2}k_{X,s}^{nl}\tilde{X}^2 \quad \text{when} \quad \tilde{X} \to \pm\infty. \tag{86}$$

At the saddle point, the derivative of the wave number reads

$$k_{X,s}^{nl} = \frac{-\Omega_{kX,s}^{nl} + \sqrt{(\Omega_{kX,s}^{nl})^2 - \Omega_{kk,s}^{nl}\Omega_{XX,s}^{nl}}}{\Omega_{kk,s}^{nl}} = \frac{-C + \sqrt{C^2 - BD}}{B}. \tag{87}$$

Using (86) with (87) in (82) shows that the function $\Theta(\tilde{X})$ behaves asymptotically as

$$\ln\Theta(\tilde{X}) \sim -\tfrac{1}{4}\tilde{X}^2,$$

when $\tilde{X} \to \pm\infty$. The only solution of (84) satisfying this asymptotic behavior and taking only non-negative values is obtained for $\nu = 0$ and simply reads

$$\Theta(\tilde{X}) = \exp(-\tfrac{1}{4}\tilde{X}^2).$$

Thus, the asymptotic expansion (86) is exact for all $\tilde{X}$. Then the soft global mode frequency reads to $\mathcal{O}(\epsilon)$

$$\omega_g \sim \omega_s^{nl} + \epsilon\omega_1 \tag{88}$$

with

$$\omega_1 = \frac{1}{2B}(AC - BE - \sqrt{A^2(C^2 - BD)}).$$

5.4.1. Computation of inner products

The values of the inner products used in the previous analysis are obtained from

$$\Omega^{nl}(k, X)\partial_\theta\Psi + \mathcal{L}(k\partial_\theta, X)\Psi + \mathcal{N}(X)[\Psi] = 0. \tag{89}$$

Differentiating (89) separately with respect to θ, k and X, taking the inner product of the three results with $\Psi_\theta^\dagger$, and exploiting the fact that the derivatives Ω_k^{nl} and Ω_X^{nl} vanish at the saddle point (k_s^{nl}, X_s^{nl}), yields

$$\langle\Psi_{\theta,s}^\dagger, \mathcal{L}_s'\Psi_{\theta,s}\rangle = 0, \tag{90}$$

$$\langle\Psi_{\theta,s}^\dagger, \mathcal{L}_{X,s}\Psi_s + \mathcal{N}_{X,s}\rangle = 0. \tag{91}$$

$$L_s\Psi_{k,s} = -\mathcal{L}_s'\Psi_{\theta,s}, \tag{92}$$

$$L_s\Psi_{X,s} = -\mathcal{L}_{X,s}\Psi_{\theta,s} - \mathcal{N}_{X,s}. \tag{93}$$

From these identities, the particular solution (79) to Eq. (78) follows.

The order ϵ problem in the saddle point region specified by (80) requires to compute inner products by double differentiation. Differentiating (89) separately with respect to $\theta\theta$, θk and θX, and taking the inner product of the three results with $\Psi_\theta^\dagger$ at the saddle point, one obtains

$$\langle \Psi_{\theta,\mathrm{s}}^\dagger, \mathcal{N}_{\psi\psi,\mathrm{s}}(\Psi_{\theta,\mathrm{s}})^2\rangle = 0, \tag{94}$$

$$\langle \Psi_{\theta,\mathrm{s}}^\dagger, \mathcal{L}'_{\mathrm{s}}\Psi_{\theta\theta,\mathrm{s}} + \mathcal{N}_{\psi\psi,\mathrm{s}}\Psi_{\theta,\mathrm{s}}\Psi_{k,\mathrm{s}}\rangle = 0, \tag{95}$$

$$\langle \Psi_{\theta,\mathrm{s}}^\dagger, (\mathcal{L}_{X,\mathrm{s}} + \mathcal{N}_{X\psi,\mathrm{s}})\Psi_{\theta,\mathrm{s}} + \mathcal{N}_{\psi\psi,\mathrm{s}}\Psi_{\theta,\mathrm{s}}\Psi_{X,\mathrm{s}}\rangle = 0. \tag{96}$$

Differentiating (89) separately with respect to *kk*, *kX* and *XX* similarly yields at the saddle point

$$\langle \Psi_{\theta,\mathrm{s}}^\dagger, 2\mathcal{L}'_{\mathrm{s}}\Psi_{\theta k,\mathrm{s}} + \mathcal{L}''_{\mathrm{s}}\Psi_{\theta\theta,\mathrm{s}} + \mathcal{N}_{\psi\psi,\mathrm{s}}(\Psi_{k,\mathrm{s}})^2\rangle = -\Omega^{\mathrm{nl}}_{kk,\mathrm{s}}\langle \Psi_{\theta,\mathrm{s}}^\dagger, \Psi_{\theta,\mathrm{s}}\rangle, \tag{97}$$

$$\langle \Psi_{\theta,\mathrm{s}}^\dagger, (\mathcal{L}_{X,\mathrm{s}} + \mathcal{N}_{X\psi,\mathrm{s}})\Psi_{k,\mathrm{s}} + \mathcal{L}'_{X,\mathrm{s}}\Psi_{\theta,\mathrm{s}} + \mathcal{L}'_{\mathrm{s}}\Psi_{\theta X,\mathrm{s}} + \mathcal{N}_{\psi\psi,\mathrm{s}}\Psi_{k,\mathrm{s}}\Psi_{X,\mathrm{s}}\rangle = -\Omega^{\mathrm{nl}}_{kX,\mathrm{s}}\langle \Psi_{\theta,\mathrm{s}}^\dagger, \Psi_{\theta,\mathrm{s}}\rangle, \tag{98}$$

$$\langle \Psi_{\theta,\mathrm{s}}^\dagger, 2(\mathcal{L}_{X,\mathrm{s}} + \mathcal{N}_{X\psi,\mathrm{s}})\Psi_{X,\mathrm{s}} + \mathcal{L}_{XX,\mathrm{s}}\Psi_{\mathrm{s}} + \mathcal{N}_{XX,\mathrm{s}} + \mathcal{N}_{\psi\psi,\mathrm{s}}(\Psi_{X,\mathrm{s}})^2\rangle = -\Omega^{\mathrm{nl}}_{XX,\mathrm{s}}\langle \Psi_{\theta,\mathrm{s}}^\dagger, \Psi_{\theta,\mathrm{s}}\rangle. \tag{99}$$

Results (94)–(99) are invoked to cast the phase evolution equation in its final form (81).

5.5. *Weakly nonlinear transition layers*

Frequency corrections for steep and soft global modes have been derived by performing a detailed asymptotic analysis of the corresponding narrow transition layers where their respective frequency selection mechanism takes place: the front layer for steep modes and the nonlinear saddle point layer for soft modes. The only type of layer that remains to be investigated in order to obtain uniformly valid asymptotic approximations for global modes is the weakly nonlinear transition layer. This layer applies to the downstream end of the steep mode nonlinear region (tl+ in Fig. 15a) and to both ends of the soft mode nonlinear region (tl± in Fig. 15b). It should be emphasized that these layers are slaved to the dynamics imposed by the front or the nonlinear saddle point frequency.

A smooth transition between nonlinear and linear solutions occurs at the boundary of the nonlinear balloon (Figs. 3 and 5) in the (X, k)-plane. Consider a global solution of frequency ω_{g}. Its local linear and nonlinear wave number branches $k^{\mathrm{l}}(X, \omega_{\mathrm{g}})$ and $k^{\mathrm{nl}}(X, \omega_{\mathrm{g}})$ are derived, respectively, from the curves $\Omega^{\mathrm{l}}(k, X) = \omega_{\mathrm{g}}$ and $\Omega^{\mathrm{nl}}(k, X) = \omega_{\mathrm{g}}$. A $k^{\mathrm{nl}}(X, \omega_{\mathrm{g}})$ branch is connected at the border of the nonlinear balloon to the corresponding linear $k^{\mathrm{l}}(X, \omega_{\mathrm{g}})$ branch at the particular station $X = X_t(\omega_{\mathrm{g}})$ for $k = k_t(\omega_{\mathrm{g}})$ where the pair (k_t, X_t) is defined by

$$\omega_{\mathrm{g}} = \Omega^{\mathrm{l}}(k_t, X_t) = \Omega^{\mathrm{nl}}(k_t, X_t). \tag{100}$$

As demonstrated in Sections 4.2 and 4.6, a continuous transition between linear and nonlinear wave number branches occurs at the downstream boundary of the nonlinear region of a steep global mode and at both downstream and upstream boundaries of the nonlinear region of a soft global mode. At a downstream boundary, the $k^{\mathrm{nl}+}$ branch prevailing in the region $X < X_t$ is continuously connected to the $k^{\mathrm{l}+}$ branch for $X > X_t$. At an upstream boundary, transition from $k^{\mathrm{l}-}$ for $X < X_t$ to $k^{\mathrm{nl}-}$ for $X > X_t$ occurs.

When $X \to X_t$ from within the nonlinear region, the amplitude of the nonlinear wave train decays, nonlinearities weaken, higher harmonics become slaved to the fundamental, and eventually a linear instability wave takes over. In the present section, we show how the connection between linear and nonlinear solutions is achieved across a narrow transition layer located at X_t.

Let us focus on an upstream transition layer (tl−), i.e., the solution is fully nonlinear for $X > X_t$ and decays exponentially for $X < X_t$. The same analysis applies in the downstream transition layer (tl+). The asymptotic behavior of the nonlinear wave trains $\Psi(\theta; k, X)$ is first derived as (k, X) approaches the neutral stability boundary of the nonlinear balloon (Section 5.5.1). This result is then used along the particular path $(k^{\mathrm{nl}}(X), X)$ to derive expansions for the modulus (Section 5.5.2) and phase (Section 5.5.3) of the global mode as $X \downarrow X_t$. This outer expansion is shown in Section 5.5.4 to match with the inner solution prevailing in the transition layer. Finally, the inner solution is matched in Section 5.5.5 to the outer linear WKBJ approximation prevailing in the region $X < X_t$.

5.5.1. Weakly nonlinear behavior

In the nonlinear balloon of the (X, k)-plane characterized by $\Omega_{\mathrm{i}}^{\mathrm{l}}(k, X) > 0$, the governing equation (1) admits local solutions of the form (50). Let us first study the behavior of the periodic functions $\Psi(\theta; k, X)$ in the (k, X)-plane as (k, X) approaches the boundary of the nonlinear balloon, i.e., $\Omega_{\mathrm{i}}^{\mathrm{l}}(k, X) \downarrow 0$.

The nonlinear operator $\mathcal{F}[\psi]$ in (1) is expanded in powers of ψ so as to read

$$\frac{\partial \psi}{\partial t} = \mathcal{L}(\partial_x, X)[\psi] + \sum_{r=2}^{\infty} \mathcal{N}_r(\partial_x, X)[\psi], \tag{101}$$

where the operators $\mathcal{N}_r$ are of rth order in ψ. In all generality, each $\mathcal{N}_r$ depends on ∂_x, but to simplify the subsequent computations, it is assumed that the $\mathcal{N}_r$'s do not involve spatial derivation, i.e.,

$$\mathcal{N}_r(\partial_x, X)[\psi] = N_r(X)\psi^r. \tag{102}$$

The results would remain valid for any nonlinear operator with spatial derivatives, but the notation and results become unwieldy in more general cases. The method is easily extended to specific examples.

The 2π periodic function Ψ is expanded as the Fourier series

$$\Psi(\theta; k, X) = \sum_n \Psi^{(n)}(k, X)\, \mathrm{e}^{\mathrm{i}n\theta}, \tag{103}$$

where $\Psi^{(-n)} = (\Psi^{(n)})^\star$. Due to the invariance of the governing equation under the transformation $\theta \to \theta + C^{\mathrm{st}}$, $\Psi^{(1)}(k, X)$ may be chosen to be real for each (k, X).

Substituting (102) and (103) into (101) yields the equations for the harmonic components of Ψ,

$$\Delta^{(n)}(k, X)\Psi^{(n)}(k, X) = \mathrm{i}\sum_{r=2}^{\infty} N_r(X) \sum_{n_1+\cdots+n_r=n} \Psi^{(n_1)}(k, X) \cdots \Psi^{(n_r)}(k, X) \tag{104}$$

with the definition

$$\Delta^{(n)}(k, X) = n\Omega^{\mathrm{nl}}(k, X) - \Omega^{\mathrm{l}}(nk, X).$$

When $\Omega_{\mathrm{i}}^{\mathrm{l}}(k, X) \downarrow 0$, the term $\Delta^{(1)}(k, X)$ vanishes, whereas the $\Delta^{(n)}(k, X)$ remain finite for $|n| \neq 1$. Thus, in this limit, the components with $|n| \neq 1$ are slaved to the fundamental $n = \pm 1$ and scale as

$$\Psi^{(n)}(k, X) = \begin{cases} \mathcal{O}[(\Psi^{(1)}(k, X))^{|n|}] & \text{if } n \neq 0, \\ \mathcal{O}[(\Psi^{(1)}(k, X))^2] & \text{if } n = 0, \end{cases} \tag{105}$$

when $\Omega_{\mathrm{i}}^{\mathrm{l}}(k, X) \downarrow 0$. The dominant terms of (104) for $n = 2$ read

$$\Delta^{(2)}(k, X)\Psi^{(2)}(k, X) = \mathrm{i}N_2(X)[\Psi^{(1)}(k, X)]^2 + \mathcal{O}[(\Psi^{(1)})^4], \tag{106}$$

and for $n = 0$,

$$\Delta^{(0)}(k, X)\Psi^{(0)}(k, X) = 2\mathrm{i}N_2(X)\Psi^{(1)}(k, X)\Psi^{(-1)}(k, X) + \mathcal{O}[(\Psi^{(1)})^4]. \tag{107}$$

For $n = 1$, Eq. (104) yields

$$\begin{aligned}\Delta^{(1)}(k, X)\Psi^{(1)}(k, X) &= 2\mathrm{i}N_2(X)[\Psi^{(2)}(k, X)\Psi^{(-1)}(k, X) + \Psi^{(1)}(k, X)\Psi^{(0)}(k, X)] \\ &\quad +3\mathrm{i}N_3(X)|\Psi^{(1)}(k, X)|^2\Psi^{(1)}(k, X) + \mathcal{O}[(\Psi^{(1)})^5].\end{aligned} \tag{108}$$

Substituting (106) and (107) into (108) yields the leading-order expression for $\Psi^{(1)}$

$$|\Psi^{(1)}(k, X)|^2 \sim \frac{\Delta^{(1)}(k, X)}{3\mathrm{i}N_3(X) - 2N_2(X)^2((1/\Delta^{(2)}(k, X)) + (2/\Delta^{(0)}(k, X)))}. \tag{109}$$

Thus,

$$|\Psi^{(1)}(k, X)|^2 = \mathcal{O}[\Delta^{(1)}(k, X)],$$

and

$$\Psi^{(1)}(k, X) = \mathcal{O}[\sqrt{\Omega_{\mathrm{i}}^1(k, X)}]. \tag{110}$$

5.5.2. Asymptotic amplitude decay of outer nonlinear wave trains

The preceding results, valid for any (k, X) when $\Omega_{\mathrm{i}}^1(k, X) \downarrow 0$ are now used to derive the asymptotic behavior of the nonlinear wave train (57) of specific frequency ω_{g} as $X \downarrow X_t$. Let us expand the nonlinear solution (57) into harmonic components as follows:

$$\Psi(\theta; k^{\mathrm{nl}}(X), X) = \sum_n (\psi_0^{(n)}(X) + \epsilon\psi_1^{(n)}(X) + \cdots) \exp\left\{\mathrm{i}n\left(\frac{1}{\epsilon}\int^X k^{\mathrm{nl}}(u)\,\mathrm{d}u - \omega_{\mathrm{g}}t\right)\right\}. \tag{111}$$

Then, according to (103),

$$\psi_0^{(n)}(X) = \Psi^{(n)}(k^{\mathrm{nl}}(X), X)\,\mathrm{e}^{\mathrm{i}n\theta_0(X)}.$$

From (105) and (110) with $\Omega_{\mathrm{i}}^1(k^{\mathrm{nl}}(X), X) = \mathcal{O}(X - X_t)$, it follows that, for each $n \neq 0$,

$$\psi_0^{(n)}(X) = \mathcal{O}[(X - X_t)^{|n|/2}] \quad \text{as} \quad X \downarrow X_t. \tag{112}$$

The asymptotic behavior of $\psi_0^{(1)}(X)$ for $X \downarrow X_t$ is derived from (109) as

$$\psi_0^{(1)}(X) \sim \Psi_0^{(1)}\,\mathrm{e}^{\mathrm{i}\theta_0(X)}(X - X_t)^{1/2} \tag{113}$$

with

$$|\hat{\Psi}_0^{(1)}|^2 = \frac{\Delta_{X,t}^{(1)}}{3\mathrm{i}N_{3,t} - 2(N_{2,t})^2(1/\Delta_t^{(2)} + 2/\Delta_t^{(0)})}, \tag{114}$$

where subscript t means evaluation at $X = X_t$ and $k = k_t = k^{\mathrm{nl}}(X_t)$, and

$$\Delta_{X,t}^{(1)} = \frac{\mathrm{d}}{\mathrm{d}X}\Delta^{(1)}(k^{\mathrm{nl}}(X), X)\bigg|_{X=X_t}.$$

In the same fashion one obtains for the second harmonic

$$\psi_0^{(2)}(X) \sim \hat{\Psi}_0^{(2)}\, \mathrm{e}^{\mathrm{i}2\theta_0(X)}(X - X_t) \tag{115}$$

with, according to (106),

$$\hat{\Psi}_0^{(2)} = \frac{N_{2,t}}{\Delta_t^{(2)}}(\Psi_0^{(1)})^2. \tag{116}$$

In the bulk of the nonlinear region the harmonic spectrum is fully developed but towards the neutral stability boundary the higher-order harmonics become slaved to the fundamental. Since the higher-order harmonics decay faster than $\Psi^{(1)}$ as the neutral stability boundary is approached, the nonlinear solution is approximated by a purely sinusoidal wave of vanishing amplitude. Matching to a linear solution in the region $X < X_t$ therefore becomes possible.

5.5.3. Diverging slow phase of outer nonlinear wave trains

So far only the behavior of the amplitude as $X \downarrow X_t$ has been obtained. In this section the asymptotic behavior of the slow phase $\theta_0(X)$ near the neutral stability boundary of the nonlinear region is computed.

Let us write the phase solvability condition (56) as

$$0 = \frac{\mathrm{d}\theta_0}{\mathrm{d}X}\langle \Psi_\theta^\dagger, \mathcal{L}'\Psi_\theta\rangle + \frac{1}{2}\frac{\mathrm{d}k^{\mathrm{nl}}}{\mathrm{d}X}\langle \Psi_\theta^\dagger, \mathcal{L}''\Psi_\theta\rangle + \left\langle \Psi_\theta^\dagger, \mathcal{L}'\left(\frac{\mathrm{d}k^{\mathrm{nl}}}{\mathrm{d}X}\Psi_k + \Psi_X\right)\right\rangle. \tag{117}$$

According to (103) the nonlinear solution Ψ admits the expansion

$$\Psi(\theta + \theta_0(X); k^{\mathrm{nl}}(X), X) = \sum_n \Psi^{(n)}(k^{\mathrm{nl}}(X), X)\, \mathrm{e}^{\mathrm{i}n\theta_0(X)}\, \mathrm{e}^{\mathrm{i}n\theta}.$$

Tedious but straightforward calculations [35] based on this Fourier expansion lead to the asymptotic behavior of the various inner products appearing in (117). One ultimately finds that

$$\begin{aligned}
\langle \Psi_\theta^\dagger, \mathcal{L}'\Psi_\theta\rangle &= (X - X_t)[\mathcal{L}'(\mathrm{i}k_t; X_t) + \text{c.c.}]|\hat{\Psi}_0^{(1)}|^2 + \mathcal{O}[(X - X_t)^2],\\
\langle \Psi_\theta^\dagger, \mathcal{L}''\Psi_\theta\rangle &= (X - X_t)[\mathcal{L}''(\mathrm{i}k_t; X_t) + \text{c.c.}]|\hat{\Psi}_0^{(1)}|^2 + \mathcal{O}[(X - X_t)^2],\\
\langle \Psi_\theta^\dagger, \mathcal{L}'(k_X^{\mathrm{nl}}\Psi_k + \Psi_X)\rangle &= \tfrac{1}{2}[\mathrm{i}\mathcal{L}'(\mathrm{i}k_t; X_t) + \text{c.c.}]|\hat{\Psi}_0^{(1)}|^2 + \mathcal{O}[X - X_t].
\end{aligned}$$

Upon substituting these results into (117), the governing equation for the slow phase at the boundary of the nonlinear region becomes

$$\frac{\mathrm{d}\theta_0}{\mathrm{d}X} = -\frac{1}{2}\frac{1}{X - X_t}\frac{\operatorname{Im}\mathcal{L}'(\mathrm{i}k_t; X_t)}{\operatorname{Re}\mathcal{L}'(\mathrm{i}k_t; X_t)} + \mathcal{O}[(X - X_t)^0].$$

Hence, θ_0 diverges logarithmically as

$$\theta_0(X) = -\frac{1}{2}\frac{\operatorname{Im}\mathcal{L}'(\mathrm{i}k_t; X_t)}{\operatorname{Re}\mathcal{L}'(\mathrm{i}k_t; X_t)}\ln(X - X_t) + \mathrm{C}^{\mathrm{st}} + \mathcal{O}[X - X_t], \tag{118}$$

when $X \downarrow X_t$.

5.5.4. Inner transition layer solution

The asymptotic matching of a finite amplitude nonlinear wave train to an exponentially decaying linear solution takes place via a narrow inner transition layer at X_t between the nonlinear and linear regions.

Define an inner variable $\tilde{X}$ in the neighborhood of X_t by $X = X_t + \epsilon^{1/2}\tilde{X}$. The outer solution obtained in the previous section is rewritten in terms of this inner variable. The fast phase θ reads

$$\theta \equiv \frac{1}{\epsilon}\int^{X_t+\epsilon^{1/2}\tilde{X}} k^{\mathrm{nl}}(u)\,\mathrm{d}u - \omega_{\mathrm{g}}t = (k_t x - \omega_{\mathrm{g}}t) + \frac{1}{2}k^{\mathrm{nl}}_{X,t}\tilde{X}^2 + \mathcal{O}(\epsilon^{1/2}), \tag{119}$$

whereas the slow phase θ_0 of Eq. (118) is expanded as

$$\theta_0 \sim -\frac{1}{2}\frac{\operatorname{Im}\mathcal{L}'(\mathrm{i}k_t; X_t)}{\operatorname{Re}\mathcal{L}'(\mathrm{i}k_t; X_t)}\ln\tilde{X} + \mathrm{C}^{\mathrm{st}}. \tag{120}$$

Thus, as $X \downarrow X_t$, keeping only the leading-order terms in the harmonics $|n| \leq 2$ of the outer solution given by (111) yields the following expansion:

$$\psi \sim \epsilon^{1/4}\tilde{X}^{1/2}[\hat{\psi}_0^{(1)}\,\mathrm{e}^{\mathrm{i}(\theta+\theta_0)} + \mathrm{c.c.}] + \epsilon^{1/2}\tilde{X}\left(\frac{\mathrm{i}N_{2,t}}{\Delta_t^{(2)}}[(\hat{\psi}_0^{(1)})^2\,\mathrm{e}^{2\mathrm{i}(\theta+\theta_0)} + \mathrm{c.c.}] + \frac{\mathrm{i}N_{2,t}}{\Delta_t^{(0)}}2|\hat{\psi}_0^{(1)}|^2\right) + \mathcal{O}(\epsilon^{3/4}). \tag{121}$$

This behavior of the outer solution in terms of the inner variable $\tilde{X}$ suggests to expand the harmonic components of the inner solution as

$$\psi \sim \sum_n \epsilon^{n/4}(\tilde{\psi}_0^{(n)}(x,\tilde{X}) + \epsilon^{1/2}\tilde{\psi}_{1/2}^{(n)}(x,\tilde{X}) + \cdots)\,\mathrm{e}^{-\mathrm{i}n\omega_{\mathrm{g}}t} \tag{122}$$

with $\tilde{\psi}_0^{(0)} = 0$ since $\psi^{(0)} = \mathcal{O}(|\psi^{(1)}|^2)$. Each component of the inner expansion has to be matched for $\tilde{X} \to +\infty$ with the corresponding component of the outer expansion in the nonlinear region. Due to the presence of slow and fast spatial scales $\tilde{X}$ and x, the spatial derivative in the governing equation (1) now reads $\partial_x + \epsilon^{1/2}\partial_{\tilde{X}}$.

For $n = 1$, the leading-order problem reads

$$\omega_{\mathrm{g}}\tilde{\psi}_0^{(1)} = \mathrm{i}\mathcal{L}(\partial_x; X_t)[\tilde{\psi}_0^{(1)}].$$

Hence

$$\tilde{\psi}_0^{(1)} = \tilde{A}_0^{(1)}(\tilde{X})\,\mathrm{e}^{\mathrm{i}k_t x}, \tag{123}$$

where $\tilde{A}_0^{(1)}(\tilde{X})$ is a slowly varying amplitude. For $n = 2$, the leading-order problem reads

$$2\omega_{\mathrm{g}}\tilde{\psi}_0^{(2)} - \mathrm{i}\mathcal{L}(\partial_x; X_t)[\tilde{\psi}_0^{(2)}] = \mathrm{i}N_{2,t}\tilde{\psi}_0^{(1)}\tilde{\psi}_0^{(1)}, \tag{124}$$

which yields the solution

$$\tilde{\psi}_0^{(2)} = \frac{\mathrm{i}N_{2,t}}{\Delta_t^{(2)}}[\tilde{A}_0^{(1)}(\tilde{X})]^2\,\mathrm{e}^{2\mathrm{i}k_t x}. \tag{125}$$

For $n = 0$, the order $\epsilon^{1/2}$ problem

$$0 = \mathcal{L}(\partial_x; X_t)[\tilde{\psi}_{1/2}^{(0)}] + 2N_{2,t}|\tilde{\psi}_0^{(1)}|^2$$

yields

$$\tilde{\psi}_{1/2}^{(0)} = \frac{2\mathrm{i}N_{2,t}}{\Delta_t^{(0)}}|\tilde{A}_0^{(1)}(\tilde{X})|^2. \tag{126}$$

For $n = 1$, the order $\epsilon^{1/2}$ terms read

$$0 = \mathrm{i}\omega_{\mathrm{g}}\tilde{\psi}_{1/2}^{(1)} + \mathcal{L}(\partial_x; X_t)[\tilde{\psi}_{1/2}^{(1)}] + [\mathcal{L}'(\partial_x; X_t)\partial_{\tilde{X}} + \tilde{X}\mathcal{L}_X(\partial_x; X_t)]\tilde{\psi}_0^{(1)} + 3N_{3,t}|\tilde{\psi}_0^{(1)}|^2\tilde{\psi}_0^{(1)} + 2N_{2,t}[\tilde{\psi}_0^{(2)}\tilde{\psi}_0^{(-1)} + \tilde{\psi}_{1/2}^{(0)}\tilde{\psi}_0^{(1)}]. \tag{127}$$

This inhomogeneous differential equation in x admits solutions for $\tilde{\psi}_{1/2}^{(1)}$ only if the resonant part in $\mathrm{e}^{\mathrm{i}k_t x}$ of the forcing terms vanishes. Upon using (123), (125) and (126) in (127), this leads to the solvability condition

$$0 = \mathcal{L}'(\mathrm{i}k_t; X_t)\frac{\mathrm{d}\tilde{A}_0^{(1)}}{\mathrm{d}\tilde{X}} + \mathcal{L}_X(\mathrm{i}k_t; X_t)\tilde{X}\tilde{A}_0^{(1)}(\tilde{X}) + \left(3N_{3,t} + 2\mathrm{i}(N_{2,t})^2\left(\frac{1}{\Delta_t^{(2)}} + \frac{2}{\Delta_t^{(0)}}\right)\right)|\tilde{A}_0^{(1)}(\tilde{X})|^2\tilde{A}_0^{(1)}(\tilde{X}). \tag{128}$$

This amplitude equation for $\tilde{A}_0^{(1)}(\tilde{X})$ is of the form

$$\frac{\mathrm{d}\tilde{A}_0^{(1)}}{\mathrm{d}\tilde{X}} + ((a_r + \mathrm{i}a_i)\tilde{X} + (b_r + \mathrm{i}b_i)|\tilde{A}_0^{(1)}(\tilde{X})|^2)\tilde{A}_0^{(1)}(\tilde{X}) = 0, \tag{129}$$

and its solutions are

$$\frac{\tilde{A}_0^{(1)}(\tilde{X})}{\tilde{A}_0^{(1)}(0)} = \frac{\exp[-\frac{1}{2}(a_r + \mathrm{i}a_i)\tilde{X}^2 - \frac{1}{2}\mathrm{i}(b_i/b_r)\ln(1 + 2b_r|\tilde{A}_0^{(1)}(0)|^2\int_0^{\tilde{X}}\mathrm{e}^{-a_r u^2}\,\mathrm{d}u)]}{\sqrt{1 + 2b_r|\tilde{A}_0^{(1)}(0)|^2\int_0^{\tilde{X}}\mathrm{e}^{-a_r u^2}\mathrm{d}u}}, \tag{130}$$

where $\tilde{A}_0^{(1)}(0)$ is the integration constant. Matching of the inner solution $\tilde{\psi}_0^{(1)}$ to the outer nonlinear solution $\psi_0^{(1)}$ of (113) requires that $|\tilde{A}_0^{(1)}(\tilde{X})| \sim \sqrt{\tilde{X}}$ as $\tilde{X} \to +\infty$. This implies that

$$1 + 2b_r|\tilde{A}_0^{(1)}(0)|^2\int_0^{+\infty}\mathrm{e}^{-a_r u^2}\,\mathrm{d}u = 0, \quad |\tilde{A}_0^{(1)}(0)|^2 = \frac{-1}{b_r}\sqrt{\frac{a_r}{\pi}}.$$

With this value for $|\tilde{A}_0^{(1)}(0)|$ the inner solution (130) admits for $\tilde{X} \to +\infty$ the asymptotic expansion

$$\tilde{A}_0^{(1)}(\tilde{X}) \sim \sqrt{-\frac{a_r}{b_r}\tilde{X}}\exp\frac{\mathrm{i}}{2}\left[\left(\frac{b_i}{b_r}a_r - a_i\right)\tilde{X}^2 + \frac{b_i}{b_r}\ln\tilde{X} + \mathrm{C}^{\mathrm{st}}\right]. \tag{131}$$

Comparison of (128) and (129) yields

$$a_r + \mathrm{i}a_i = \frac{\mathcal{L}_X(\mathrm{i}k_t; X_t)}{\mathcal{L}'(\mathrm{i}k_t; X_t)} = -\mathrm{i}k_{X,t}^{\mathrm{l}}, \qquad b_r + \mathrm{i}b_i = |\hat{\Psi}_0^{(1)}|^{-2}\frac{\Delta_{X,t}^{(1)}}{\mathrm{i}\mathcal{L}'(\mathrm{i}k_t; X_t)} = -|\hat{\Psi}_0^{(1)}|^{-2}\left(\mathrm{i}k_{X,t}^{\mathrm{nl}} + \frac{\mathcal{L}_X(\mathrm{i}k_t; X_t)}{\mathcal{L}'(\mathrm{i}k_t; X_t)}\right)$$

with $|\hat{\Psi}_0^{(1)}|^2$ obtained in (114). Thus,

$$-\frac{a_r}{b_r} = |\hat{\Psi}_0^{(1)}|^2, \qquad \frac{b_i}{b_r}a_r - a_i = k_{X,t}^{\mathrm{nl}}, \qquad -\frac{b_i}{b_r} = \frac{\mathrm{Im}\,\mathcal{L}'(\mathrm{i}k_t, X_t)}{\mathrm{Re}\,\mathcal{L}'(\mathrm{i}k_t, X_t)}.$$

This completes the proof that the fundamental component of the outer nonlinear solution given by Eq. (121) completely matches the fundamental component of the inner weakly nonlinear solution $\epsilon^{1/4}\tilde{A}_0^{(1)}(\tilde{X})\,\mathrm{e}^{\mathrm{i}(k_t x - \omega_{\mathrm{g}} t)}$, where $\tilde{A}_0^{(1)}(\tilde{X})$ is given by (130).

5.5.5. Matching to the outer linear solution

As $X \uparrow X_t$, the outer linear WKBJ approximation (39) reads, at leading order,

$$\psi \sim A_0^{\mathrm{l}}(X_t)\,\mathrm{e}^{\mathrm{i}(k_t x-\omega_{\mathrm{g}} t)}\exp\left(\frac{\mathrm{i}}{2}k_{X,t}^{\mathrm{l}}\tilde{X}^2\right)+\text{c.c.}, \tag{132}$$

when expressed in terms of the inner variable $\tilde{X}$. Using (130), the asymptotic behavior of the inner solution as $\tilde{X}\to-\infty$ yields

$$\psi \sim \epsilon^{1/4}\frac{\tilde{A}_0^{(1)}(0)}{\sqrt{2}}\,\mathrm{e}^{\mathrm{i}(k_t x-\omega_{\mathrm{g}} t)}\exp\left(-\frac{a_r+\mathrm{i}a_i}{2}\tilde{X}^2-\frac{\mathrm{i}}{2}\frac{b_i}{b_r}\ln 2\right)+\text{c.c.} \tag{133}$$

Since $a_r+\mathrm{i}a_i=-\mathrm{i}k_{X,t}^{\mathrm{l}}$, both expansions (132) and (133) asymptotically match provided that

$$A_0^{\mathrm{l}}(X_t)=\epsilon^{1/4}\frac{\tilde{A}_0^{(1)}(0)}{\sqrt{2}}\,\mathrm{e}^{-\mathrm{i}b_i(\ln 2)/2b_r}.$$

Thus, at leading order, the weakly nonlinear inner expansion (133) exactly matches the outer linear WKBJ approximation (39). In the inner transition layer the slaved higher-order harmonics scale as $\epsilon^{|n|/4}$ and automatically match their slaved counterparts in the outer linear region.

6. Conclusions

It has been demonstrated that a wide class of one-dimensional nonlinear evolution equations with spatially varying coefficients may support two types of fully nonlinear self-sustained global modes in a doubly infinite domain. Steep global modes are triggered by the presence of a sharp stationary front located at the upstream transition point between local convective and absolute instability. This front acts as a source and imposes its real absolute frequency to the entire medium. Soft global modes are due to the presence of a saddle point of the local nonlinear dispersion relation which again acts as a source and imposes its frequency to the entire medium, as given by saddle point conditions.

A necessary condition for the occurrence of either of these modes is the existence of a region of local absolute instability. Recall that linearly unstable global modes given by a complex saddle point of the local linear dispersion relation [7,25,30] also require a range of local absolute instability. But, this range must in general be of finite extent whereas nonlinear global modes exist, however small the AU domain. The relationship between linear global instability and the existence of fully nonlinear global modes is non-trivial: in the generic case, nonlinear global instability does not coincide with linear global instability. The nature of the various global bifurcation scenarios constitute the major result of the present investigation. Steep global modes occur right at local absolute instability onset below the linear global instability threshold, via a saddle-node bifurcation, while the medium is still linearly globally stable.

Soft global modes generically do not appear at local absolute instability onset but only for a sufficiently large domain of local absolute instability. Furthermore, they are more likely to be observed in systems with weak advection. It is essential to note that steep and soft global modes are mutually exclusive, as dictated by the relative magnitude of their respective frequencies. The existence and selection of either kind of global modes has been confirmed by direct numerical simulations of the CGL equation with varying coefficients for small but finite values of ϵ. As a word of caution, it should be stated that soft global modes are likely to be more fragile than their steep counterparts. They may become unstable whenever the region of local absolute instability protrudes beyond the central nonlinear regions, in the tails of the extended wave packet. This lack of robustness is all the more acute as the WKBJ limit $\epsilon=0$ is approached.

In several physical systems [1,37] linear and nonlinear global instabilities have been found to occur at the same value of the global control parameter. This peculiar feature takes place in situations where the entire spatial dependence is accounted for in a single real spatially varying parameter, say $R(X)$, which displays an extremum at a real position $X^{\max}$ such that $\mathrm{d}R(X^{\max})/\mathrm{d}X = 0$. Under these circumstances, the local linear dispersion relation is necessarily of the form $\Omega^{\mathrm{l}}(k, X) = \Omega^{\mathrm{l}}_{\star}[k, R(X)]$ and the local absolute frequency is readily obtained as $\omega_0(X) = \omega_{0\star}[R(X)]$. The real station $X^{\max}$ is then simultaneously associated with a maximum of $\omega_{0,\mathrm{i}}(X)$ and with a saddle point $X^{\mathrm{l}}_{\mathrm{s}}$ of $\omega_0(X)$.

The analytical structure underlying the spatial distribution of steep and soft global modes has been systematically derived in the WKBJ approximation $\epsilon \ll 1$. It has been shown that for a wide class of one-dimensional evolution equations the various inner layers and outer regions may be matched together to arrive at a consistent description valid over the entire spatial domain. In particular, higher-order frequency corrections have been obtained.

It should be emphasized that the different transition scenarios depend on the precise form of the linear and nonlinear dispersion relations. Due to the number of parameters required to specify the spatial variations of the medium, only situations of physical significance have been presented and a comprehensive survey of all possible configurations has not been attempted.

This study has been undertaken in order to understand the nature of synchronized structures in real slowly varying open shear flows. In the latter framework, the local linear dispersion relation is obtained from the Rayleigh or the Orr–Sommerfeld equation, whereas the local nonlinear dispersion relation requires the computation of finite amplitude structures in a streamwise periodic interval. In this context, steep global modes may be constructed as reported elsewhere [35,36].

Acknowledgements

The authors have benefited from many enlightening and fruitful discussions with Arnaud Couairon.

References

[1] A.P. Bassom, K.M. Kuzanyan, A.M. Soward, A nonlinear dynamo wave riding on a spatially varying background, Proc. R. Soc. London A 455 (1999) 1443–1481.
[2] C.M. Bender, S.A. Orszag, Advanced Mathematical Methods for Scientists and Engineers, McGraw-Hill, New York, 1978.
[3] A. Bers, Space–time evolution of plasma instabilities — absolute and convective, in: M.N. Rosenbluth, R.Z. Sagdeev (Eds.), Handbook of Plasma Physics, North–Holland, Amsterdam, 1983, pp. 451–517.
[4] R.J. Briggs, Electron-stream Interaction with Plasmas, MIT Press, Cambridge, MA, 1964.
[5] P. Büchel, M. Lücke, D. Roth, R. Schmitz, Pattern selection in the absolutely unstable regime as a nonlinear eigenvalue problem: Taylor vortices in axial flow, Phys. Rev. E 53 (1996) 4764–4777.
[6] J.-M. Chomaz, P. Huerre, L.G. Redekopp, The effect of nonlinearity and forcing on global modes, in: P. Coullet, P. Huerre (Eds.), New Trends in Nonlinear Dynamics and Pattern Forming Phenomena, Plenum Press, New York, 1990, pp. 259–274.
[7] J.-M. Chomaz, P. Huerre, L.G. Redekopp, A frequency selection criterion in spatially developing flows, Stud. Appl. Math. 84 (1991) 119–144.
[8] J.-M. Chomaz, Absolute and convective instabilities in nonlinear systems, Phys. Rev. Lett. 69 (1992) 1931–1934.
[9] J.-M. Chomaz, A. Couairon, Against the wind, Phys. Fluids 11 (1999) 2977–2983.
[10] A. Couairon, J.-M. Chomaz, Global instability in fully nonlinear systems, Phys. Rev. Lett. 77 (1996) 4015–4018.
[11] A. Couairon, Modes globaux fortement nonlinéaires dans les écoulements ouverts, Ph.D. Thesis, École Polytechnique, 1997.
[12] A. Couairon, J.-M. Chomaz, Absolute and convective instabilities, front velocities and global modes in nonlinear systems, Physica D 108 (1997) 236–276.
[13] A. Couairon, J.-M. Chomaz, Pattern selection in the presence of cross flow, Phys. Rev. Lett. 79 (1997) 2666–2669.
[14] A. Couairon, J.-M. Chomaz, Fully nonlinear global modes in slowly varying flows, Phys. Fluids 11 (1999) 3688–3703 .
[15] M.C. Cross, P.C. Hohenberg, Pattern formation outside of equilibrium, Rev. Mod. Phys. 65 (1993) 851–1112.
[16] G.T. Dee, J.S. Langer, Propagating pattern selection, Phys. Rev. Lett. 50 (1983) 383–386.

[17] T.M. DelSole, B.F. Farrell, Nonlinear equilibrium of localized instabilities on a baroclinic jet, J. Atmos. Sci. 51 (1994) 2270–2284.
[18] K. Hannemann, H. Oertel Jr., Numerical simulation of the absolutely and convectively unstable wake, J. Fluid Mech. 199 (1989) 55–88.
[19] D.A. Hammond, L.G. Redekopp, Global dynamics of symmetric and asymmetric wakes, J. Fluid Mech. 331 (1997) 231–260.
[20] P. Huerre, P.A. Monkewitz, Local and global instabilities in spatially developing flows, Ann. Rev. Fluid Mech. 22 (1990) 473–537.
[21] P. Huerre, M. Rossi, Hydrodynamic instabilities in open flows, in: C. Godrèche, P. Manneville (Eds.), Hydrodynamics and Nonlinear Instabilities, Cambridge University Press, Cambridge, 1998, pp. 81–294.
[22] P. Huerre, Open shear flow instabilities, in: G.K. Batchelor, H.K. Moffatt, M.G. Worster (Eds.), Developments in Fluid Mechanics: A Collection for the Millenium, Cambridge University Press, Cambridge, 2000.
[23] R.E. Hunt, D.G. Crighton, Instability of flows in spatially developing media, Proc. R. Soc. London A 435 (1991) 109–128.
[24] S. Le Dizès, P. Huerre, J.-M. Chomaz, P.A. Monkewitz, Nonlinear stability analysis of slowly diverging flows: limitations of the weakly nonlinear approach, in: H. Eckelmann, J.M.R. Graham, P. Huerre, P.A. Monkewitz (Eds.), Proceedings of the IUTAM Symposium on Bluff Body Wakes, Dynamics and Instabilities, Springer, Berlin, 1993, pp. 147–152.
[25] S. Le Dizès, P. Huerre, J.-M. Chomaz, P.A. Monkewitz, Linear global modes in spatially developing media, Phil. Trans. R. Soc. London A 354 (1996) 169–212.
[26] P. Manneville, Structures Dissipatives, Chaos et Turbulence, Aléa, Saclay, 1991.
[27] C. Mathis, M. Provansal, L. Boyer, The Bénard–von Karman instability: an experimental study near the threshold, J. Phys. Paris Lett. 45 (1984) L83–L491.
[28] N. Meunier, M.R.E. Proctor, D.D. Sokoloff, A.M. Soward, S.M. Tobias, Asymptotic properties of a nonlinear $\alpha\omega$-dynamo wave: period, amplitude and latitude dependence, Geophys. Astrophys. Fluid Dyn. 86 (1997) 249–285.
[29] P.A. Monkewitz, D.W. Bechert, B. Barsikowr, B. Lehmann, Self-excited oscillations and mixing in heated round jets, J. Fluid Mech. 213 (1990) 611–639.
[30] P.A. Monkewitz, P. Huerre, J.M. Chomaz, Global linear stability analysis of weakly non-parallel shear flows, J. Fluid Mech. 251 (1993) 1–20.
[31] H.W. Müller, M. Lücke, M. Kamps, Transversal convection patterns in horizontal shear flow, Phys. Rev. A 45 (1992) 3714–3726.
[32] A.C. Newell, T. Passot, J. Lega, Order parameter equations for patterns, Ann. Rev. Fluid Mech. 25 (1993) 399–453.
[33] B. Pier, P. Huerre, Fully nonlinear global modes in spatially developing media, Physica D 97 (1996) 206–222.
[34] B. Pier, P. Huerre, J.-M. Chomaz, A. Couairon, Steep nonlinear global modes in spatially developing media, Phys. Fluids 10 (1998) 2433–2435.
[35] B. Pier, Comportement non linéaire synchronisé dans les écoulements cisaillés, Ph.D. Thesis, École Polytechnique, 91128 Palaiseau, France, 1999.
[36] B. Pier, P. Huerre, Nonlinear self-sustained structures and fronts in spatially developing wake flows, J. Fluid Mech., submitted for publication.
[37] R.T. Pierrehumbert, Local and global baroclinic instability of zonally varying flow, J. Atmos. Sci. 41 (1984) 2141–2162.
[38] M. Provansal, C. Mathis, L. Boyer, Bénard–von Kármán instability: transient and forced regimes, J. Fluid Mech. 182 (1987) 1–22.
[39] W. van Saarloos, Dynamical velocity selection: marginal stability, Phys. Rev. Lett. 58 (1987) 2571–2574.
[40] W. van Saarloos, Front propagation into unstable states: marginal stability as a dynamical mechanism for velocity selection, Phys. Rev. A 37 (1988) 211–229.
[41] W. van Saarloos, Front propagation into unstable states. II. Linear versus nonlinear marginal stability and rate of convergence, Phys. Rev. A 39 (1989) 6367–6390.
[42] W. van Saarloos, P.C. Hohenberg, Fronts, pulses, sources and sinks in generalized complex Ginzburg–Landau equations, Physica D 56 (1992) 303–367.
[43] A.M. Soward, C.A. Jones, The linear stability of the flow in the narrow gap between two concentric rotating spheres, Q. J. Mech. Appl. Math. 36 (1983) 19–42.
[44] K.R. Sreenivasan, S. Raghu, D. Kyle, Absolute instability in variable density round jets, Exp. Fluids 7 (1989) 309–317.
[45] K.R. Sreenivasan, P.J. Strykowski, D.J. Olinger, On the Hopf bifurcation and the Landau–Stuart constants associated with vortex "shedding" behind circular cylinders, unpublished, 1990.
[46] P.J. Strykowski, D.L. Niccum, The stability of countercurrent mixing layers in circular jets, J. Fluid Mech. 227 (1991) 309–343.
[47] S. Tobias, M.R.E. Proctor, E. Knobloch, Convective and absolute instabilities of fluid flows in finite geometry, Physica D 113 (1998) 43–72.
[48] W. Wasow, Linear Turning Point Theory, Springer, New York, 1985.
[49] B.M. Woodley, N. Peake, Global linear stability analysis of thin aerofoil wakes, J. Fluid. Mech. 339 (1997) 239–260.